



UNITED STATES ENVIRONMENTAL PROTECTION AGENCY
WASHINGTON, D.C. 20460

COPY

FEB - 3 2009

OFFICE OF
AIR AND RADIATION

David C. Moody, Ph.D.
Manager, Carlsbad Field Office
U.S. Department of Energy
P.O. Box 3090
Carlsbad, NM 88221

Dear Dr. Moody:

Attached you will find the U.S. Environmental Protection Agency's (EPA's) report, entitled *Verification of the Waste Isolation Pilot Plant Chemical Conceptual Models*. This report details our extensive review of the WIPP performance assessment chemical conceptual models. There are four models included in this report – gas generation, chemical conditions, dissolved actinide source term, and colloidal actinide source term models.

EPA believed these performance assessment chemical conceptual models required independent review and verification by the Agency as a result of our review of the Department of Energy's (DOE's) 2006 planned change request to decrease the amount of magnesium oxide in the WIPP repository. It appeared that reaction-path calculations and documents supplied by DOE may have suggested new aspects to the existing performance assessment chemical conceptual models approved and peer reviewed during the original certification. Most notably, there appeared to be no assumption of brine equilibrium in the models, as well as insufficient anhydrite sulfate available in the calculations (to ensure lower pH in the repository and maintain lower radioactive material solubility values, which are included in the present chemistry conceptual model).

EPA has completed its review and determined that the chemical conceptual models used in the certification have had only minor changes and refinements and that they are still adequate for use in the WIPP performance assessment calculations. EPA considers the chemical conceptual models list and corresponding details in Appendix 2 of our report as the present baseline for these conceptual models. This information will be used by the Agency in reviewing any change request proposed by DOE in the future.

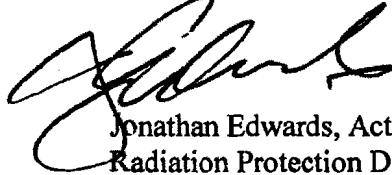
As a result of this review, EPA also recommends that it is necessary and appropriate to include all water balance considerations in the performance assessment calculations. Presently, only water consumed by anoxic corrosion of iron is included;

See list on the back
2/3/09
5-1007-5
200209

water balance effects may be positive or negative related to performance. In addition, the Agency recommends that a more accurate representation of plastic and rubber rate degradation be included in the performance assessment calculations, as this effect may be presently overstated.

If you have any questions regarding this request, please contact Chuck Byrum at (214) 665-7555.

Sincerely,

A handwritten signature in black ink, appearing to read 'Jonathan Edwards', is written over the typed name.

Jonathan Edwards, Acting Director
Radiation Protection Division

cc: Russ Patterson, DOE/CBFO
George Basabilvaso, DOE/WIPP
Alton Harris, DOE/HQ
Steve Zappe, NMED
EPA WIPP Team
EPA Docket



Final Report

Verification of the Waste Isolation Pilot Plant Chemistry Conceptual Models

**Contract Number EP-D-05-002
Work Assignment No. 4-02**

Prepared for:

U.S. Environmental Protection Agency
Office of Radiation and Indoor Air
1310 L Street N.W.
Washington, DC 20005

Charles O. Byrum
Work Assignment Manager

Prepared by:

S. Cohen & Associates
1608 Spring Hill Road
Suite 400
Vienna, Virginia 22182

September 19, 2008

TABLE OF CONTENTS

Acronym List	v
Executive Summary	vii
1.0 Introduction.....	1-1
2.0 Repository Chemistry Conceptual Models	2-1
2.1 Geologic Setting, Hydrologic Setting, and Repository Characteristics.....	2-1
2.2 Gas Generation Conceptual Model.....	2-2
2.2.1 CCA and PAVT Gas Generation Conceptual Model	2-3
2.2.2 Effects of AMWTP Waste Review on Gas Generation Conceptual Model	2-4
2.2.3 CRA-2004 PA and PABC Gas Generation Conceptual Model	2-7
2.3 Chemical Conditions Conceptual Model.....	2-10
2.3.1 CCA and PAVT Chemical Conditions Conceptual Model.....	2-10
2.3.2 Effects of AMWTP Waste Review on Chemical Conditions Conceptual Model.....	2-13
2.3.3 CRA-2004 and PABC Chemical Conditions Conceptual Model	2-15
2.3.4 Recent Chemical Conditions Conceptual Model Revisions	2-16
2.4 Dissolved Actinide Source Term Conceptual Model	2-17
2.4.1 CCA and PAVT Dissolved Actinide Source Term Conceptual Model	2-17
2.4.2 Effects of AMWTP Waste Review on Dissolved Actinide Source Term Conceptual Model	2-19
2.4.3 CRA-2004 and PABC Dissolved Actinide Source Term Conceptual Model	2-19
3.0 MgO Planned Change Request	3-1
3.1 Sandia National Laboratories EQ3/6 Modeling of Calcite Precipitation Effects	3-2
3.2 Wolery and Sassani (2007)	3-7
3.2.1 CPR Degradation Without Iron	3-7
3.2.2 CPR Degradation with Iron Corrosion	3-11
3.3 Lichtner (2007)	3-13
3.4 October 2007 EPA/DOE Technical Exchange Meeting.....	3-14
4.0 EPA EQ3/6 Modeling Calculations	4-1
4.1 Conceptual Model Considerations.....	4-1
4.2 GWB Calculations	4-7
4.3 ERDA-6 Calculations	4-14
4.4 Modeling Results Summary.....	4-16
5.0 Water Balance Considerations.....	5-1
5.1 Brine Consumption by Reaction with MgO	5-1
5.2 Effects of CPR Degradation on Water Balance.....	5-2
6.0 Effects of Mineral Volume Changes.....	6-1
7.0 Adequacy of Chemistry Conceptual Models	7-1

8.0	Conclusions and Recommendations	8-1
9.0	References.....	9-1

LIST OF APPENDICES

- Appendix A: Final Chemistry-Related Conceptual Models
- Appendix B: Wolery and Sassani (2007) EQ6 Modeling Results
- Appendix C: Availability of Sulfate to Support Microbial Degradation

LIST OF TABLES

Table 3-1.	EQ3/6 Modeling Calculations Using GWB Brine, Brush et al. (2006).....	3-4
Table 3-2.	EQ3/6 Modeling Calculations Using ERDA-6 Brine, Brush et al. (2006).....	3-5
Table 3-3.	Wolery EQ6 Calculations Using GWB Brine to Assess Effects of Including Sulfide and Iron ^a	3-9
Table 3-4.	Wolery EQ6 Calculations Using GWB Brine to Evaluate the Effects of Different Cellulose and Iron Reaction Rates ^a	3-10
Table 4-1.	Stein (1985) Salado Core Sample Data	4-3
Table 4-2.	Amounts of Salado Minerals Calculated for EQ3/6 Input Files, Equivalent to 100% of the DRZ; Scaled to 1 kg Water in Brine	4-7
Table 4-3.	Results of EQ3/6 Modeling Calculations with 1,045 m ³ GWB Brine Performed for the Present Investigation	4-9
Table 4-4.	Results of EQ3/6 Modeling Calculations with GWB Brine: Effects of Magnesite Formation, Organic Ligands, Calcite Suppression, and Increased GWB Brine Volume	4-11
Table 4-5.	Results of EQ3/6 Modeling Calculations with GWB Brine: Effects of Polyhalite, Iron Corrosion Rates, and CPR Degradation Rate	4-13
Table 4-6.	Results of EQ3/6 Modeling Calculations with ERDA-6 Brine	4-15
Table 4-7.	Effects of CPR Degradation and Iron Corrosion Reactions on Brine Compositions	4-18
Table 5-1.	GWB Brine Volumes Associated with Repository Chemical Processes and Modeled Cumulative Brine Inflow for the Undisturbed PABC Scenario	5-5
Table 6-1.	Volume Changes Predicted Using Results of Selected EQ3/6 Reaction Path Simulations; All Simulations Assumed 100% of the DRZ Minerals Were Available for Reaction	6-2

LIST OF FIGURES

Figure 4-1.	Titration Calculation with 1,045 m ³ GWB Brine, 49% of the DRZ Salado Minerals, Magnesite Reaction Product	4-19
Figure 4-2.	Titration Calculation, Iron and Sulfide Species Included, 1,045 m ³ GWB brine, 100% of the DRZ Salado Minerals, Hydromagnesite Reaction Product	4-20
Figure 4-3.	Cellulose Calculation, Iron and Sulfide Species Included, 1,045 m ³ GWB brine, 100% of the DRZ Salado Minerals, Hydromagnesite Reaction Product	4-21
Figure 4-4.	Cellulose Calculation, Iron and Sulfide Species Included, 1,045 m ³ GWB brine, 49% of the DRZ Salado Minerals, Hydromagnesite Reaction Product...	4-22
Figure 4-5.	Cellulose Calculation, Iron and Sulfide Species Included, 1,045 m ³ GWB brine, 25% of the DRZ Salado Minerals, Hydromagnesite Reaction Product...	4-23
Figure 4-6.	Cellulose Calculation, Iron and Sulfide Species Included, 7,763 m ³ GWB brine, 100% of the DRZ Salado Minerals, Hydromagnesite Reaction Product	4-24
Figure 4-7.	Cellulose Calculation, Iron and Sulfide Species Included, 7,763 m ³ GWB brine, 25% of the DRZ Salado Minerals, Hydromagnesite Reaction Product...	4-25

ACRONYM LIST

amsl	Above mean sea level
AMWTP	Advanced Mixed Waste Treatment Project
atm	Atmospheres
CaSO ₄	Anhydrite
CCA	Compliance Certification Application
CH ₄	Methane
CO ₂	Carbon dioxide
CPR	Cellulosics, plastics, and rubber
CRA-2004	Compliance Recertification Application- 2004
DBR	Direct Brine Release
DOE	Department of Energy
DRZ	Disturbed rock zone
E1	Performance assessment scenario with one drilling intrusion through a waste panel that also penetrates pressurized brine in the Castile Formation
E1E2	Performance assessment scenario defined as two drilling intrusions through excavated areas of the repository, with the first intrusion not penetrating pressurized brine and the second intrusion penetrating pressurized brine in the Castile Formation
E2	Performance assessment scenario in which a waste panel is inadvertently penetrated by drilling, with this intrusion not penetrating pressurized brine in the Castile Formation
EDTA	Ethylenediaminetetraacetic Acid
EF	Excess Factor (equal to the Safety Factor)
EPA	Environmental Protection Agency
ERDA-6	Energy Research and Development Administration, simulated Castile brine formulation
Fe(OH) ₂	Ferrous iron hydroxide
FeS	Iron sulfide
GWB	Generic Weep Brine, simulated Salado brine formulation
H ⁺	Hydrogen ion
H ₂	Hydrogen
H ₂ S	Hydrogen sulfide
HS ⁻	Bisulfide ion

INEEL	Idaho National Engineering and Environmental Laboratory
m	Molal (moles/kg solvent water)
M	Molar (moles/liter)
MB	Marker bed
MgO	Magnesium oxide; also the chemical formula for the mineral periclase, the reactive mineral in the MgO backfill
N ₂	Nitrogen
PA	Performance assessment
PABC	Performance Assessment Baseline Characterization
PAVT	Performance Assessment Verification Test
pH	-log ₁₀ of the hydrogen ion activity (NBS pH scale)
pmH	-log ₁₀ of the hydrogen ion molality (Mesmer pH scale)
S1	Specific scenario, undisturbed
S2	Specific scenario, E1 intrusion at 350 years
TRU	Transuranic
XRD	X-ray diffraction
WIPP	Waste Isolation Pilot Plant

EXECUTIVE SUMMARY

The Waste Isolation Pilot Plant (WIPP) is operated by the U.S. Department of Energy (DOE) under the oversight of the U.S. Environmental Protection Agency (EPA). EPA's assessment of WIPP's ability to comply with containment requirements specified in 40 CFR § 191.13 is based on performance assessment (PA) calculations. WIPP PA calculations are carried out by DOE using linked computer models that calculate the probabilities of cumulative radionuclide releases from the disposal system during the 10,000 years following closure. These computer models and many of the parameters included in the calculations are based on conceptual models that describe the expected performance of the disposal system. Peer review of all conceptual models is required by 40 CFR § 194.27; the original conceptual models used in the Compliance Certification Application (CCA) were peer reviewed at the time of the CCA by the Conceptual Models Peer Review Panel. This panel determined that the chemistry-related conceptual models were adequate for use in PA (Wilson et al. 1996a, 1996b, 1997a, and 1997b). Since the reviews conducted by the panel in 1996 and 1997, additional peer review has not been performed on any of the conceptual models related to repository chemistry.

The repository chemistry conceptual models include the Gas Generation, Chemical Conditions, Dissolved Actinide Source Term, and Colloidal Actinide Source Term conceptual models. Since the Conceptual Models Peer Review, DOE has continued studying some of the processes related to WIPP repository chemistry. Consequently, additional information has become available regarding actinide solubilities, reactivity of the MgO backfill, and the probability and rates of microbial gas generation in the repository. Some of this new information was incorporated into the Gas Generation, Chemical Conditions, and Dissolved Actinide Source Term conceptual models for the Performance Assessment Baseline Characterization (PABC). Because of this evolution of the conceptual models, it is important to assess these changes and determine whether they are of sufficient magnitude to require peer review of the revised conceptual models.

During a review of information submitted by DOE in support of a planned change in the amounts of MgO backfill placed in the repository (Moody 2006), EPA identified information that could potentially affect the repository chemistry conceptual models. One issue identified by EPA was that some geochemical reaction-path modeling calculations carried out to simulate microbial degradation of cellulose, plastics, and rubber (CPR) resulted in relatively high pH values and evolution of the WIPP brine composition away from a sodium-chloride ± magnesium composition toward a magnesium-sulfide composition. Such high pH, magnesium-sulfide brine compositions differ from the brine compositions assumed in the Dissolved Actinide Source Term conceptual model and might result in actinide solubilities that are significantly different from those used in the PABC. In addition, DOE has stated that insufficient anhydrite [CaSO_4] will be present in the repository system to maintain saturation of the brine with respect to this sulfate-bearing phase (Kanney et al. 2004). Because equilibrium with Salado minerals such as anhydrite is included in the Chemical Conditions conceptual model, this issue must be evaluated to determine if the Chemical Conditions conceptual model should be revised.

Review of the reaction-path modeling to simulate CPR degradation performed by Brush et al. (2006), Wolery and Sassani (2007), and Lichtner (2007) indicated that most of these calculations were inconsistent with the Chemical Conditions conceptual model, because the brines did not remain in equilibrium with anhydrite. Consequently, additional reaction-path calculations were

performed using assumptions more consistent with the Gas Generation and Chemical Conditions conceptual models. The possible diffusive transport of sulfate for microbial degradation of CPR was also evaluated. The results of this evaluation indicate that adequate sulfate will be available to maintain relatively moderate pH values under conditions with sufficient water for a direct brine release, as previously believed.

Based on a review of the existing information, it was determined that the chemistry-related conceptual models have changed slightly since the initial peer review. The current chemistry-related conceptual models appear to be consistent with the available experimental data and repository information, and all changes to the conceptual models since the last peer review have been relatively minor refinements made in response to the availability of additional data. Consequently, there appears to be no need for additional peer review and the chemistry-related conceptual models appear to remain adequately supported for use in PA. However, there may be some areas where implementation of the current chemistry-related conceptual models in WIPP PA could be improved. One area of possible implementation improvement is related to the water balance within the repository, including accounting for the corrosion of iron by FeS formation instead of Fe(OH)₂, consumption of water by MgO hydration, release of this water by magnesite formation, and production of water by CPR degradation. Another area of potential improvement would be reconsideration of the rates of plastic and rubber degradation. Additional evaluation would be required to determine whether such changes in the repository water balance and implementation of the plastics and rubber degradation rate are advisable.

1.0 INTRODUCTION

The Waste Isolation Pilot Plant (WIPP) is an underground transuranic (TRU) waste disposal facility operated by the U.S. Department of Energy (DOE). The WIPP Land Withdrawal Act (Public Law 102-579) required certification by the U.S. Environmental Protection Agency (EPA) that WIPP operations would comply with EPA's disposal regulations before DOE could begin accepting TRU waste for disposal at WIPP. The WIPP Land Withdrawal Act also required recertification of WIPP five years after the initial receipt of TRU waste for disposal, and every five years thereafter until the end of the decommissioning phase (Public Law 102-579).

DOE submitted the Compliance Certification Application (CCA) to EPA in 1996. EPA reviewed the CCA and supporting materials, and required a number of changes to parameters used in the CCA Performance Assessment (PA); the resulting PA was the Performance Assessment Verification Test (PAVT). Based on their review of the CCA, additional information provided to EPA by DOE, and results of the PAVT, EPA certified WIPP in late 1998. WIPP subsequently began accepting TRU waste for disposal in March 1999. In March 2004, DOE submitted the Compliance Recertification Application (CRA-2004) to EPA. After reviewing the CRA-2004, EPA requested additional information from DOE and also required changes to a number of PA parameters, resulting in the Performance Assessment Baseline Characterization (PABC). Based on their review of the information provided by DOE, EPA recertified WIPP operations in March 2006.

Assessment of WIPP's ability to comply with containment requirements specified in 40 CFR § 191.13 is based on PA calculations. WIPP PA calculations are carried out by DOE using linked computer models that calculate the probabilities of cumulative radionuclide releases from the disposal system during the 10,000 years following closure. These computer models and many of the parameters included in the calculations are based on conceptual models that describe the expected performance of the disposal system. Peer review of all conceptual models is required by 40 CFR § 194.27, and the conceptual models used in the PA were originally peer reviewed at the time of the CCA by the Conceptual Models Peer Review Panel. This panel ultimately determined that all of the conceptual models were adequate, with the exception of the Spallings conceptual model (Wilson et al. 1996a, 1996b, 1997a, and 1997b). Although the panel did not find the Spallings conceptual model to be adequate, the panel determined that the predicted spallings volumes were reasonable. Since the reviews conducted by the panel in 1996 and 1997, additional peer review has not been performed on any of the conceptual models related to repository chemistry.

The repository chemistry conceptual models include the Gas Generation, Chemical Conditions, Dissolved Actinide Source Term, and Colloidal Actinide Source Term conceptual models. Since the Conceptual Models Peer Review, DOE has continued studying some of the processes related to WIPP repository chemistry. Consequently, additional information has become available regarding actinide solubilities, reactivity of the MgO backfill, and the probability and rates of microbial gas generation in the repository. Some of this new information was incorporated into the Gas Generation, Chemical Conditions, and Dissolved Actinide Source Term conceptual models for the PABC. Because of this evolution of the conceptual models, it is important to assess these changes and determine their relative importance. If the conceptual model changes are relatively minor and do not significantly affect the conceptualization of repository chemical

processes, additional peer review of the conceptual models is unlikely to be necessary. On the other hand, if the cumulative effects of these changes result in a significantly revised conceptualization of repository chemical processes, peer review of the revised conceptual models may be required.

DOE submitted a Planned Change Request to EPA to decrease the proportions of MgO backfill placed in the repository to control chemical conditions (Moody 2006). During review of the information submitted by DOE in support of the Planned Change Request, EPA identified information that could potentially affect the repository chemistry conceptual models. One issue identified by EPA was that some geochemical reaction-path modeling calculations carried out to simulate microbial degradation of cellulose, plastics, and rubber (CPR) resulted in relatively high pH values and evolution of the WIPP brine composition away from a sodium-chloride or sodium-magnesium-chloride composition toward a magnesium-sulfide composition. Such high pH, magnesium-sulfide brine compositions differ from the brine compositions assumed in the Dissolved Actinide Source Term conceptual model and might result in actinide solubilities that are significantly different from those used in the PABC. In addition, DOE has stated that insufficient anhydrite (CaSO_4) will be present in the repository system to maintain saturation of the brine with respect to this sulfate-bearing phase (Kanney et al. 2004). This assertion was previously reviewed by an EPA contractor and found to be inadequately justified (TEA 2004). However, DOE has continued to maintain that limited anhydrite may be available for equilibration with brine (e.g., Brush et al. 2006). Because equilibrium with Salado minerals such as anhydrite was assumed in the Chemical Conditions conceptual model, this assertion by DOE must be evaluated to determine if the Chemical Conditions conceptual model should be revised.

The potential effects of additional information and the reaction-path modeling results on the repository chemistry conceptual models are reviewed in this report. The repository chemistry conceptual models that were reviewed and approved by the Conceptual Models Peer Review Panel, as updated and implemented for the PAVT, CRA-2004 PA, and the PABC, are summarized in Section 2.0. The results of geochemical reaction-path modeling calculations provided by DOE that may affect the validity of these conceptual models are reviewed in Section 3.0. Review of the reaction-path modeling to simulate CPR degradation performed by Brush et al. (2006), Wolery and Sassani (2007), and Lichtner (2007) indicated that most of these calculations were not consistent with the Chemical Conditions conceptual model, because the brines did not remain in equilibrium with anhydrite. Consequently, additional reaction-path calculations were performed using assumptions more consistent with the Gas Generation and Chemical Conditions conceptual models (Section 4.0). The likely availability of sulfate for microbial degradation of CPR was also evaluated. The results of these revised calculations indicate that CPR degradation via sulfate reduction and concurrent iron corrosion are not expected to cause WIPP brine pH values higher than the assumed values in the chemistry-related conceptual models. Based on the revised geochemical modeling calculations, a review of the possible effects of water either released or consumed by reactions in the repository is provided in Section 5.0, with an evaluation of possible mineral volume changes included in Section 6.0.

Based on a review of the existing information, it was determined that the chemistry-related conceptual models have changed slightly since the initial peer review because of the availability of additional information (Section 7.0). These changes have been relatively minor improvements

to the conceptual models rather than significant changes to the conceptualization of the expected chemistry-related processes in the repository.

The results of this evaluation of the chemistry-related conceptual models are summarized in Section 8.0. The current chemistry-related conceptual models appear to be consistent with the available experimental data and repository information, and all changes to the conceptual models since the last peer review have been relatively minor refinements made in response to the availability of additional data. Consequently, there appears to be no need for additional peer review at this time, and the conceptual models appear to remain adequately supported for use in PA. However, there are some areas where implementation of the current chemistry-related conceptual models in WIPP PA could be improved. These possible implementation improvements are related to the water balance within the repository, including accounting for the corrosion of iron by FeS formation instead of Fe(OH)₂, consumption of water by MgO hydration, release of this water by magnesite formation, and production of water by CPR degradation. In addition, it is assumed there is a 25% probability that plastics and rubber will degrade in the repository. The rates of plastics and rubber degradation in this case are assumed to equal the rate of cellulose degradation. Such an assumption may overestimate the rates of plastics and rubber degradation. Additional evaluation would be required to determine whether changes to the implementation of the repository water balance and assumed plastics and rubber degradation rates are warranted.

2.0 REPOSITORY CHEMISTRY CONCEPTUAL MODELS

The important geologic and hydrologic features of the WIPP site and WIPP repository characteristics are reviewed in this section to provide a context for the discussion of the repository chemistry conceptual models. The summaries of each repository chemistry conceptual model include the important features of the models used in the CCA PA and PAVT, which were reviewed and accepted by the Conceptual Models Peer Review Panel (Wilson et al. 1996a, 1996b, 1997a, and 1997b) and EPA (1997a, 1997c, 1998a, and 1998b). Subsequent minor revisions made to the chemistry conceptual models used for the CRA-2004 PA, the CRA-2004 PABC, and subsequent to the PABC are also summarized for each conceptual model.

2.1 GEOLOGIC SETTING, HYDROLOGIC SETTING, AND REPOSITORY CHARACTERISTICS

The WIPP repository is located 2,150 ft below ground surface in the Salado Formation. In the area around WIPP, the Salado Formation is a relatively thick bedded salt, composed mainly of layers of impure halite [NaCl] with interbedded layers of anhydrite, polyhalite [$K_2MgCa_2(SO_4)_4 \cdot 2H_2O$], and mudstone (Lambert 1992). These sulfate-bearing interbeds are called Marker Beds (MB); within the Salado Formation, these beds are labeled using numbers that range from MB 100 near the top of the formation to MB 144 near the bottom (DOE 2004, Chapter 2). Intergranular brine has been observed in the Salado Formation. Two formulations of these brines have been used in WIPP laboratory experiments and in PA calculations: Brine A and Generic Weep Brine (GWB) (Snider 2003). The low permeability of the Salado Formation surrounding the WIPP repository provides a significant hydrologic barrier between the repository and other, more transmissive water-bearing strata. A more permeable, transitory region forms within the Salado around the repository in response to the disturbance in the stress field caused by repository excavation; this region is called the Disturbed Rock Zone (DRZ) (DOE 2004, Chapter 6). However, the DRZ is relatively small compared to the thickness of the Salado Formation surrounding the repository (DOE 2004, Chapter 6).

The Salado Formation is underlain by the Castile Formation. The Castile Formation is mainly composed of thick beds of high-purity halite alternating with thick beds of interlaminated carbonate and anhydrite (DOE 2004, Chapter 2). The Castile Formation has been significantly deformed in some areas around WIPP, with pressurized brines associated with the deformed areas. Borehole ERDA-6 encountered both deformation and pressurized brine in the Castile Formation; the composition of this ERDA-6 brine has been used to represent the likely composition of Castile Brine in laboratory experiments and PA calculations.

The Salado Formation is overlain by the Rustler Formation (DOE 2004, Chapter 2). This formation is composed of evaporite layers called, from bottom to top, the Los Medaños Member, the Culebra Dolomite Member, the Tamarisk Member, the Magenta Dolomite Member, and the Forty-Niner Member. The Culebra Dolomite is mostly composed of dolomite, with small amounts of anhydrite or gypsum [$CaSO_4 \cdot 2H_2O$] (Lambert 1992). The Culebra Dolomite is the most transmissive continuously saturated unit above the WIPP facility. It therefore provides the most direct pathway from the repository to the accessible environment, apart from releases directly to the surface (DOE 2004, Chapter 2). As a consequence, this aquifer has been studied more extensively than other portions of the Rustler Formation (Lambert 1992; DOE 2004,

Chapter 2). The Magenta Dolomite has lower transmissivity than the Culebra Dolomite, and is unfractured at the WIPP site (DOE 2004, Chapter 2).

The presence of water in the WIPP repository is important to the chemistry conceptual models and to PA modeling of radionuclide releases. For example, water in the form of brine (inundated conditions) or water vapor (humid conditions) is necessary for microbial degradation of CPR. The increase in gas pressure that may result from microbial gas generation can influence releases from the repository through spallings, in which high gas pressures force waste material into an intruding borehole. Another potential release mechanism affected by the presence of water in the repository is direct brine release (DBR), wherein repository brine carrying radionuclides flows to the surface through an intruding borehole.

There are a number of ways in which water could enter the repository waste region. Although the permeability of the undisturbed Salado Formation is low, excavation of the repository has affected both the hydraulic gradient and permeability of the DRZ, resulting in a low flow of interstitial brine from the halite to the anhydrite marker beds and into the repository. As a result, small brine seeps have been observed in the underground workings at WIPP (DOE 2004, Chapter 6). The waste emplaced in the repository cannot have more than 1% free liquid by volume (DOE 2004, Appendix TRUWASTE), so free liquid in the waste is not expected to be a significant source of water in the repository. Microbial degradation of CPR could result in the release of water. On the other hand, anoxic corrosion of steel in the repository or hydration of MgO in the repository backfill will consume water.

In the future, after active institutional control at WIPP has ended, intrusions into the repository might occur during drilling for natural resources such as oil or natural gas and could be a possible source of large volumes of water. An intruding borehole could increase the amount of brine in the repository if the borehole passed through the repository and continued into a pressurized brine region in the Castile; in this case, Castile brine could flow up the borehole into the repository. In WIPP PA, it is assumed that repository brine will have the composition of Salado brine in the undisturbed repository. The repository brine is also expected to have the composition of Salado brine if an intruding borehole does not encounter pressurized Castile brine (scenario E2). However, for scenarios that include intrusion through a waste panel and into pressurized Castile brine (scenarios E1 and E1E2), the repository brine composition is assumed to be equivalent to Castile brine because of the potentially large quantities of brine that could flow into the repository (DOE 2004, Chapter 6).

2.2 GAS GENERATION CONCEPTUAL MODEL

The Gas Generation conceptual model includes gas generation by anoxic corrosion of ferrous metals and by microbial degradation of CPR; this conceptual model also includes removal of carbon dioxide [CO₂] by reaction with the MgO backfill (Wilson et al. 1996a). The Gas Generation conceptual model used in WIPP PA is called the average stoichiometry model, to differentiate it from alternative gas generation conceptual models considered for the CCA (Wilson et al. 1996a). Information used to develop this conceptual model included the quantities and compositions of WIPP waste, observation of brine seepage into excavated salt, Salado and Castile brine compositions, observation of halophilic microbes in brine seepage and salt lakes near the WIPP site, experimental investigation of steel corrosion rates, experimental

investigation of microbial degradation of CPR materials, and measured rates of radiolytic gas generation from water and plastics (Wilson et al. 1996a).

2.2.1 CCA and PAVT Gas Generation Conceptual Model

The Gas Generation Conceptual Model developed for the CCA and considered by the Conceptual Models Peer Review Panel included the following assumptions (DOE 1996 Appendix MASS and Appendix SOTERM, Wilson et al. 1996a and 1996b). This conceptual model was accepted by the Conceptual Models Peer Review Panel (Wilson et al. 1996b) and by EPA (1997a, 1997c, 1998a, 1998b).

- A small amount of oxygen will be trapped in the repository immediately after closure. This oxygen is assumed to be quickly consumed by oxic corrosion or aerobic microbial degradation of CPR and these processes will not generate significant amounts of gas.
- Anoxic corrosion can occur in the repository as soon as the shafts are sealed.
- Anoxic corrosion of steel in the waste and waste containers produces hydrogen (H₂); the chemical reaction that represents the stoichiometry of anoxic corrosion of steel is $\text{Fe} + 2 \text{H}_2\text{O} \rightarrow \text{Fe}(\text{OH})_2 + \text{H}_2$.
- The amounts of aluminum in the waste and steel contained in rockbolts, netting, and equipment that will be left underground after closure are too small to cause significant gas generation.
- Anoxic corrosion cannot occur unless brine is present in the repository and in contact with the steel; anoxic corrosion consumes brine and the corrosion rate is a function of brine saturation.
- Anoxic corrosion is a function of the surface area of steel in the repository and it consumes steel, so the reaction may be limited by the amount of steel in the repository; however, the rate of anoxic corrosion is more likely to be limited by the available amount of brine.
- The rate of anoxic corrosion of steel is the principal control on the total quantity of gas generated in the repository.
- Microbial degradation of CPR in the waste and waste emplacement materials may produce CO₂, nitrogen (N₂), hydrogen sulfide (H₂S), and methane (CH₄); natural analogue data indicate that CPR degradation processes will occur in the sequence: denitrification → sulfate reduction → methanogenesis.
- CPR degradation is represented by a zero-order reaction rate, so the microbial gas generation rate is independent of the CPR concentration.

- CO₂ will be removed from the repository brines and gas phase by reaction with the MgO backfill, so CO₂ generated from CPR degradation will not significantly affect repository gas pressures.
- The most important CPR degradation reaction is expected to be C₆H₁₀O₅ (cellulose monomer) + H₂O → 3 CH₄ + 3 CO₂ (methanogenesis) because of the limited amounts of nitrate and sulfate in the waste; consequently the quantities of N₂ and H₂S produced by microbial degradation of CPR will be negligible.
- CO₂ and H₂S generated by microbial degradation of CPR will not passivate steel because of the small quantities of H₂S produced by CPR degradation and because CO₂ will be consumed by reaction with the MgO backfill.
- The probability that significant microbial degradation of CPR will not occur is 50%, there is a 25% probability that only cellulosic materials will be significantly degraded by microbes, and there is a 25% probability that cellulose, plastics, and rubber will be significantly degraded by microbes.
- The effects of CPR degradation on the amount of brine in the repository are uncertain, so they are not accounted for in PA.
- Gas generation will take place homogeneously throughout the repository because of the assumed homogeneous distribution of waste.
- Radiolysis of water in the waste and brine and radiation of plastics and rubber in the waste will not have significant effects on the amounts of gas generated.

2.2.2 Effects of AMWTP Waste Review on Gas Generation Conceptual Model

In 2002, DOE requested approval from EPA to accept super-compacted waste from the Advanced Mixed Waste Treatment Project (AMWTP) at Idaho National Engineering and Environmental Laboratory (INEEL) for disposal at WIPP (Triay 2002). This compressed waste was expected to have higher densities of CPR and metals than was assumed for wastes in the CCA PA and PAVT inventories. An additional issue associated with the AMWTP compressed waste was the increased inventory of CPR that would be emplaced in the repository. At the time of the CCA, INEEL planned to thermally treat waste with higher CPR densities, which would have removed CPR from this waste and, consequently, from the WIPP inventory. However, INEEL subsequently planned to supercompact this waste, resulting in a much higher total CPR inventory (Leigh et al. 2005b).

At the time of the CCA, it was assumed that waste would be randomly placed in the repository. However, data collected since waste emplacement began in 1999 indicated that large-scale clustering of waste types could occur in the repository as different generator sites shipped waste to WIPP. Because of the distinctive characteristics of the AMWTP waste and the possibility that the waste could be placed in a limited number of panels in the repository, DOE's request to emplace the compressed waste raised questions regarding the potential effects of this waste on PA results.

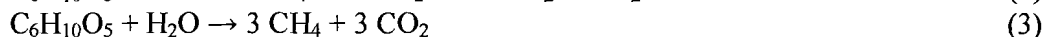
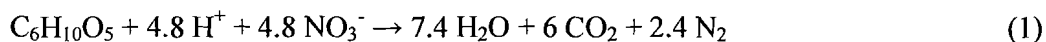
The potential effects of the unique characteristics of the AMWTP waste on PA were evaluated by DOE (Hansen et al. 2003a, 2003b), and the results of DOE's analysis were reviewed by EPA. This review also included an assessment of pipe overpack waste from the Rocky Flats Environmental Technology Site; these pipe overpacks are stainless steel cylinders that were predominantly placed in Panel 1 of the repository. EPA and its technical contractor reviewed the issues related to AMWTP and pipe overpack waste, evaluating DOE's conclusion that the PA assumptions used in the PAVT remained appropriate despite the differences caused by the AMWTP and pipe overpack waste and other information developed since the PAVT (TEA 2004). This report covered a number of potential effects of AMWTP waste and heterogeneous waste emplacement on PA. TEA (2004) concluded that AMWTP waste disposal in the repository was unlikely to have a significant impact on overall repository performance.

During EPA's review of the AMWTP waste disposal request, the most significant issues related to the Gas Generation conceptual model were whether anoxic corrosion gas generation rates would increase because of the relatively large amounts of metal in the AMWTP and pipe overpack waste, the reactions by which CPR degradation would be likely to occur, and whether sufficient MgO backfill would be available to react with the CO₂ generated by CPR degradation.

At EPA's request, DOE performed a series of PA calculations to evaluate the effects of increased iron surface area on the predicted releases from the repository. Increased iron surface area was found to increase repository pressure at early times and reduce repository pressure at later times (Hansen et al. 2003a, 2003b). EPA agreed with the conclusion that total repository releases would not significantly increase because of increased iron surface areas and might decrease because of lower long-term pressures and brine saturations (EPA 2004, TEA 2004). This evaluation of the effects of increased iron surface area in the AMWTP did not result in any changes to the Gas Generation conceptual model.

However, evaluation of the effects of higher CPR densities in the AMWTP waste did result in a change to the Gas Generation conceptual model. EPA (1997c, 2001) calculated the MgO Safety Factor to determine whether sufficient MgO is present in the repository to maintain the required chemical conditions. The Safety Factor is defined as the moles of MgO in the backfill divided by the total moles of CPR carbon in the repository (EPA 1997c). This Safety Factor (also called the Excess Factor or EF by DOE) originally was equal to 1.95 (EPA 1997c). The EF decreased to 1.67 when the MgO minisacks were no longer placed with the waste (EPA 2001). As part of the AMWTP review, EPA evaluated whether emplacing higher CPR densities in the repository would significantly affect the EF (EPA 2004, TEA 2004).

In the Gas Generation conceptual model developed for the CCA (Section 2.2.1), the major pathways for microbial degradation of CPR are the reactions:



CPR degradation by denitrification and sulfate reduction (reactions 1 and 2, respectively) produces one mole of CO₂ for each mole of CPR carbon. On the other hand, methanogenesis (reaction 3) produces only 0.5 moles of CO₂ per mole of CPR carbon. Consequently, if

methanogenesis is the dominant CPR degradation reaction in the repository, much smaller amounts of CO₂ will be expected to be produced per mole of CPR carbon. In the Gas Generation conceptual model, these reactions are believed to occur in sequence, as first nitrate and then sulfate in the waste are consumed. Because of limited inventories of nitrate and sulfate in the waste, DOE maintained that the majority of CPR degradation will take place via reaction (3), and that the maximum amount of CO₂ produced will be slightly more than half of the total CPR carbon inventory (DOE 1996 Appendix SOTERM).

EPA (1997c, 2001) calculated the EF by dividing the moles of MgO in the backfill by the total moles of carbon in the waste inventory. However, DOE modified the EF calculation for the AMWTP evaluation by dividing the moles of MgO in the backfill by the moles of CO₂ predicted to be produced by CPR degradation (Hansen et al. 2003a, 2003b). This modification increased the EF, because DOE assumed that limited amounts of nitrate and sulfate in the waste would cause most CO₂ production to occur by methanogenesis (reaction 3). However, EPA (2004) questioned the assumption that methanogenesis would be the most important CPR degradation reaction because of the abundant sulfate minerals in the Salado Formation, such as anhydrite and gypsum. EPA observed that sulfate reduction could cause dissolution of Salado sulfate minerals, and the amount of sulfate released may cause the major CPR degradation reaction to be sulfate reduction. If sufficient sulfate is produced by dissolution of Salado sulfate minerals, all CPR carbon could be degraded to form CO₂. Consequently, EPA (2004) required DOE to continue calculating the EF by dividing the moles of MgO in the backfill by the total moles of CPR carbon in the waste inventory.

EPA's review of DOE's request to emplace AMWTP waste in the WIPP repository resulted in changes to the Gas Generation conceptual model. These changes were necessary because it was recognized that sulfate reduction (reaction 2) could be the dominant CPR degradation reaction instead of methanogenesis (reaction 3). Two assumptions included in the CCA Gas Generation conceptual model were affected:

- The most important CPR degradation reaction is expected to be C₆H₁₀O₅ (cellulose monomer) + H₂O → 3CH₄ + 3CO₂ (methanogenesis) because of the limited amounts of nitrate and sulfate in the waste; consequently the quantities of N₂ and H₂S produced by microbial degradation of CPR will be negligible.
- CO₂ and H₂S generated by microbial degradation of CPR will not passivate steel because of the small quantities of H₂S produced by CPR degradation and because CO₂ will be consumed by reaction with the MgO backfill.

These assumptions, modified to include the potential availability of large amounts of sulfate for CPR degradation reactions are:

- The most important CPR degradation reaction may be C₆H₁₀O₅ + 6 H⁺ + 3 SO₄²⁻ → 5 H₂O + 6 CO₂ + 3 H₂S because of the sulfate available from the equilibration of brine with Salado minerals. In areas where limited sulfate may be available because of a higher rate of CPR degradation compared to the rate of sulfate transport from the Salado to the waste, the methanogenesis reaction C₆H₁₀O₅ (cellulose monomer) + H₂O → 3 CH₄ + 3 CO₂ (methanogenesis) may be more important. The amount of N₂ produced by microbial

degradation of CPR will be negligible because of limited nitrate in the waste. Substantial quantities of H₂S, CO₂, and CH₄ may be produced by CPR degradation.

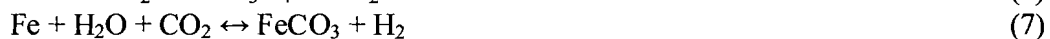
- CO₂ generated by microbial degradation of CPR will not passivate steel because CO₂ will be consumed by reaction with the MgO backfill. H₂S might passivate steel by forming FeS on the steel surfaces if H₂S is produced in sufficient quantities. However, reducing chemical conditions would continue to be maintained by the FeS.

2.2.3 CRA-2004 PA and PABC Gas Generation Conceptual Model

DOE's discussion of the Gas Generation conceptual model in the CRA-2004 introduced additional iron corrosion reactions to the Gas Generation conceptual model. The anoxic corrosion reaction assumed for the CCA PA and PAVT was (DOE 1996 Appendix SOTERM):



However, DOE (2004 Appendix PA Attachment SOTERM) provided a revised summary of iron corrosion reactions based on additional experimental results and cited Telander and Westerman (1997):



These reactions take into account the possible incorporation of water in the iron hydroxide formed during anoxic corrosion (reaction 5), as well as the possible formation of magnetite (Fe₃O₄), siderite (FeCO₃), and iron sulfide (FeS). The formation of magnetite as a corrosion product in the repository could be important because a larger amount of H₂ would be produced per mole of iron (reaction 6) than if Fe(OH)₂·xH₂O formed (reaction 5). However, elsewhere in the CRA-2004 (DOE 2004 Appendix PA), the potential formation of magnetite was discounted because it was only observed at higher temperature, reportedly in tests carried out by Telander and Westerman (1997).

Review of the Telander and Westerman (1997) report indicates that they did not include results of experiments at temperatures greater than 30°C. Wang and Brush (1996) cited a 1995 draft version of Telander and Westerman (1997) that described corrosion experiments in which magnetite was produced only at higher temperatures; consequently, Wang and Brush (1996) assumed that only Fe(OH)₂ would form during anoxic corrosion of iron in the repository. Because Telander and Westerman (1997) did not report magnetite formation at the low-temperature conditions expected in the WIPP repository, magnetite formation should not be included in the Gas Generation conceptual model. The omission of magnetite formation is consistent both with the available experimental data and the current implementation of gas generation in PA.

The presence of significant CO₂ pressures and the formation of significant quantities of siderite are likely to be prevented by the presence of the MgO backfill, which will control CO₂ fugacities

at low levels. Consequently, it has been assumed since the time of the CCA that significant siderite formation would not occur. In addition, any H₂S produced by CPR degradation (reaction 2) will likely result in the replacement of siderite by an iron sulfide phase such as mackinawite (FeS_{1-x}) (Telander and Westerman 1997). Based on the available information, siderite formation is not expected to be a significant process in the repository.

Information developed during the AMWTP review necessitated changes in the Gas Generation conceptual model related to the importance of CPR degradation by sulfate reduction (reaction 2) and the possibility that significant H₂S could be generated by CPR degradation (Section 2.2.2). However, these changes were not incorporated into the CRA-2004 PA conceptual model, because the AMWTP review was in progress while DOE was preparing the CRA-2004.

EPA reviewed the CRA-2004 and required changes to assumptions and parameters for the PABC, because of additional data available from microbial degradation experiments (EPA 2006a, 2006b). Based on new information developed since the CCA PA and PAVT, EPA (2006b) determined that there was a higher probability of microbial degradation of cellulose than had previously been assumed. However, there were no data indicating a higher probability of plastics and rubber degradation. Consequently, for the PABC the probability of significant microbial degradation of cellulose alone was assumed to be 75% and the probability of significant microbial degradation of all CPR material was assumed to be 25% (EPA 2006a).

Microbial degradation rates used in the CCA PA and PAVT were based on the initial rates of gas generation in a series of experiments with cellulose (Wang and Brush 1996). These microbial degradation rates were also applied to plastics and rubber degradation. Continuation of these experiments after the CCA showed that long-term rates were likely to be lower (Gillow and Francis 2003). Although the lower long-term rates were noted by DOE (Wang et al. 2003), the higher microbial degradation rates from the CCA were used in the CRA-2004 PA. Because the lower long-term microbial degradation rates are more likely to be representative of the repository regulatory period, the implementation of microbial gas generation was changed for the PABC. For the PABC, the relatively rapid initial microbial gas generation rate was accounted for by adding additional gas to the repository as an initial condition (Leigh et al. 2005a). The lower long-term rate of microbial degradation was then incorporated in the PABC by sampling from a distribution modified to reflect rates observed in the long-term microbial degradation experiments (Leigh et al. 2005a). DOE also constrained the microbial degradation rate used for humid conditions to be less than the inundated microbial degradation rate and added an additional uncertainty factor to the calculation of the microbial gas generation rates to account for differences in conditions between the experiments and the WIPP underground (Leigh et al. 2005a). EPA (2006a) reviewed both of these changes. Although constraining humid degradation rates to be less than inundated rates appeared to be unsupported by the experimental data, EPA found that this constraint was unlikely to have significantly changed the results of the PABC. EPA (2006a) noted that the additional uncertainty factor applied to the microbial gas generation rates might be reasonable, although this factor was not well supported by the evidence.

The effects on PA of higher microbial degradation probability for cellulosic materials and lower overall microbial gas generation rates were evaluated at the time of the PABC (Leigh et al. 2005a, EPA 2006a). One measure of the effects of the different assumptions can be obtained by

comparing predicted gas pressures and brine saturations for the CRA-2004 PA and the PABC. In the undisturbed scenario (S1), the assumptions led to slower increases in gas pressure and faster increases in brine saturation after closure. Cumulative brine outflow for the undisturbed scenario tended to be slightly higher for the PABC calculations than for the CRA PA calculations (Leigh et al. 2005a). Another scenario considered was for the disturbed repository with a drilling intrusion into a pressurized Castile brine pocket at 350 years (scenario S2). For this scenario, the minimum pressure was higher for the PABC microbial degradation assumptions than for the CRA PA assumptions, but little difference in maximum or average pressure was observed. The maximum saturation was not affected by these assumptions, because the repository was predicted to be fully saturated in both cases. However, for the PABC assumptions, average and minimum brine saturations for the S2 scenario were higher than for the CRA PA microbial gas generation assumptions. The results of these calculations indicate that the total gas pressures can be significantly influenced by the assumed rates of microbial gas generation.

Because new information has become available since the CCA, the following Gas Generation conceptual model assumptions have been revised:

- Anoxic corrosion of steel in the waste and waste containers produces hydrogen (H₂); the chemical reaction that represents the stoichiometry of anoxic corrosion of steel is $\text{Fe} + 2 \text{H}_2\text{O} \rightarrow \text{Fe}(\text{OH})_2 + \text{H}_2$.
- The rate of anoxic corrosion of steel is the principal control on the total quantity of gas generated in the repository.
- The probability that significant microbial degradation of CPR will not occur is 50%, there is a 25% probability that only cellulosic materials will be significantly degraded by microbes, and there is a 25% probability that cellulose, plastics, and rubber will be significantly degraded by microbes.

The revised assumptions, based on additional information are:

- Anoxic corrosion of steel in the waste and waste containers produces hydrogen (H₂); the chemical reactions that represent the stoichiometry of anoxic corrosion of steel are:

$$\text{Fe} + (x+2) \text{H}_2\text{O} \rightarrow \text{Fe}(\text{OH})_2 \cdot x\text{H}_2\text{O} + \text{H}_2$$

$$\text{Fe} + \text{H}_2\text{S} \rightarrow \text{FeS} + \text{H}_2$$
- Both anoxic corrosion of steel and microbial degradation of CPR can affect the total quantity of gas generated in the repository.
- The probability that significant microbial degradation of cellulose will occur without plastics and rubber degradation is 75%, and there is a 25% probability that cellulose, plastics, and rubber will be significantly degraded by microbes.

2.3 CHEMICAL CONDITIONS CONCEPTUAL MODEL

The Chemical Conditions Conceptual model includes assumptions related to the mineralogy of the Salado Formation, the compositions of the Salado and Castile brines that may enter the repository and contact waste, organic ligand concentrations, and the reactions that may control important chemical parameters such as pH, redox, and CO₂ fugacities. The Chemical Conditions conceptual model also includes assumptions regarding the redox states of actinides and metals in solution. The expected chemical conditions in the repository have an important effect on actinide solubilities in brine; these effects are addressed in the Dissolved Actinide Source Term conceptual model (Section 2.4). Thermodynamic and kinetic information was used to develop the assumptions regarding equilibrium and disequilibrium between various components in the Chemical Conditions conceptual model. Other information used to develop the Chemical Conditions conceptual model included experimental data, numerical simulations, waste inventory data, and information derived from literature reviews (Wilson et al. 1996a).

The Chemical Conditions conceptual model includes assumptions about the reactions that will control pH in repository brines. The most common definition of pH, which is an indicator of the relative acidity or alkalinity of a solution, is $\text{pH} = -\log_{10}(\text{hydrogen ion activity})$; this definition is sometimes referred to as the NBS pH scale. Alternatively, relative acidity or alkalinity can be defined using the hydrogen ion concentration as $\text{pmH} = -\log_{10}(\text{hydrogen ion molality})$, which is sometimes referred to as the Mesmer pH scale. For dilute solutions, the hydrogen ion concentration is approximately equal to its activity, so the pH and pmH are nearly equal. However, for more concentrated solutions, the activity of the hydrogen ion can differ significantly from its concentration. For WIPP brines, calculations of pH and pmH indicate that pmH is approximately 1 log unit higher than pH. In some instances, the documentation related to WIPP pH values has not been clear regarding whether pH or pmH is being discussed. In the following discussion, pH refers to the activity-based definition, and pmH is used to describe the concentration-based definition.

2.3.1 CCA and PAVT Chemical Conditions Conceptual Model

The Chemical Conditions conceptual model developed for the CCA and reviewed by the Conceptual Models Peer Review Panel included the following assumptions (DOE 1996 Appendix SOTERM; Wilson et al. 1996a, 1996b, 1997a, and 1997b):

- The Salado Formation is predominantly halite, with accessory anhydrite, gypsum, polyhalite, and magnesite [MgCO₃]. Small quantities of intergranular and intragranular brines are associated with the salt at the repository horizon. These brines are highly concentrated (ionic strengths up to 8 molar), with a composition of mostly sodium, magnesium, potassium, chloride, and sulfate, with smaller amounts of calcium, carbonate, and borate.
- The underlying Castile Formation is composed of thick beds of interlaminated anhydrite and carbonate layered with halite. The Castile Formation contains localized brine reservoirs under sufficient pressure to force brine upward to the land surface if penetrated by a borehole. Castile brines are concentrated solutions containing predominantly sodium chloride with calcium and sulfate, and smaller concentrations of other elements.

- Brine that dissolves actinides under any intrusion scenario will have a composition equal to that of Salado brine, Castile brine, or a mixture of Salado and Castile brines. Culebra groundwater that could enter the repository would quickly dissolve halite and develop a composition similar to Salado brine. Because the Salado and Castile brines bracket the possible brine compositions, experiments and modeling performed only with end-member brine compositions are adequate for describing the repository geochemistry. The Brine A formulation is used to simulate Salado brine and ERDA-6 brine is used to simulate Castile brine.
- Equilibrium is assumed between repository brine, waste, and the Salado minerals halite, anhydrite, brucite, and magnesite.
- Thermodynamic equilibrium is assumed for dissolution and precipitation of actinide-bearing solid phases, but not for redox reactions among the actinides.
- Brine in the repository will be well mixed with waste, and chemical homogeneity and solubility equilibrium will be maintained. Consequently, chemical microenvironments and supersaturated conditions are not believed to persist in the repository for long time periods. Brine composition in the repository will be constant with time after initial, rapid equilibration with the MgO backfill materials.
- CPR degradation may generate CO₂, as described in the Gas Generation conceptual model (Section 2.2). A relatively large excess of MgO will be emplaced with the waste, with 1.95 moles of MgO per mole of CPR carbon. The identity of the dominant CPR degradation reaction and the resulting proportions of CO₂ or CH₄ produced (i.e., sulfate reduction or methanogenesis) will not affect chemical conditions in the repository because of the large excess of MgO.
- In the absence of MgO backfill, low pmH ($-\log_{10}$ of the hydrogen ion molality) and high CO₂ fugacity could be achieved in the repository brine, increasing the solubilities of actinides relative to neutral or slightly basic pmH and low CO₂ fugacity conditions. However, conditions that might lead to high actinide solubilities will not occur in the repository, because excess MgO emplaced as an engineered barrier will buffer the pmH and CO₂ fugacity of the brine so that actinide solubilities are minimized. The pH ($-\log_{10}$ of the hydrogen ion activity) will be buffered between 9 and 10, depending on the brine composition.
- Periclase [MgO] in the backfill will hydrate to form brucite [Mg(OH)₂], which will in turn react with CO₂ to form magnesite. Cementitious material in the repository will contain Ca(OH)₂ that could also react with CO₂ to form calcite [CaCO₃]. This latter reaction could buffer pmH at relatively high values. However, the effect of Ca(OH)₂ is expected to be minimal because of calcite precipitation and reaction of the Ca(OH)₂ with MgCl₂ in the brine to form CaCl₂.
- Carbon dioxide fugacities that will prevail in the repository can be modeled using the brucite-magnesite buffer.
- Microbial degradation of CPR and/or steel corrosion will result in a reducing environment within 100 years of repository closure.

- Oxidation-reduction equilibrium with waste materials (including iron metal and CPR) is not assumed. Steel corrosion and CPR degradation are represented by reaction rates instead of equilibrium. In most cases, significant amounts of uncorroded steel will be present in the repository throughout the 10,000-year regulatory period.
- Steel corrosion in the repository will reduce the oxidation states of some actinides, affecting their solubilities and binding constants.
- The expected oxidation states of the actinides are determined based on experimental data. Americium is assumed to occur in the +III oxidation state, thorium in the +IV oxidation state, plutonium in the +III or +IV oxidation state, neptunium in the +IV or +V oxidation state, and uranium in the +IV or +VI oxidation state.
- Actinide and organic ligand inventories are fixed. Although it is possible that microbial consumption of organic ligands in the waste could occur, because of uncertainty about the presence or viability of these types of microbes, it is assumed that organic ligand concentrations will not be reduced by microbial degradation.
- High pressure in the repository is not expected to significantly affect actinide solubilities, so its effect is not considered in the geochemical calculations. Temperature in the repository is not expected to vary significantly from ambient, so temperature effects on solubility also are not considered important.
- Brine radiolysis could produce reactive species, such as hydrogen peroxide (H_2O_2). Any oxidized species such as hydrogen peroxide are expected to react quickly with iron metal and dissolved iron(II) species in solution. Consequently, radiolysis is not expected to affect the oxidation-reduction conditions in the repository.

The Conceptual Models Peer Review Panel initially found that the Chemical Conditions conceptual model was inadequate, because of unresolved questions about the ability of the MgO engineered barrier to react with CO_2 produced by CPR degradation. In particular, the panel was concerned about the possible formation of impermeable reaction rims on individual MgO pellets or the formation of impermeable reaction rinds on masses of MgO in the repository (Wilson et al. 1996a, 1996b, 1997a). However, after evaluating additional data provided by DOE (Bynum 1997, SNL 1997), the panel found that the Chemical Conditions conceptual model was adequate (Wilson et al. 1997b).

EPA reviewed the Chemical Conditions conceptual model and found that hydromagnesite [$Mg_5(CO_3)_4(OH)_2 \cdot 4H_2O$], a metastable precursor of magnesite, could be a long-term, metastable magnesium-carbonate phase (EPA 1998b, 1998c). Persistence of hydromagnesite would control CO_2 fugacities at higher levels than would be expected in the presence of magnesite; these higher CO_2 fugacities, in turn, resulted in higher predicted actinide solubilities (EPA 1998b). Consequently, EPA (1998c) required the assumption for the PAVT that hydromagnesite could form and persist in place of magnesite during the repository regulatory period. As a result, the following assumptions were modified, with the changes indicated in italics:

- Periclase [MgO] in the backfill will hydrate to form brucite [$Mg(OH)_2$], which will in turn react with CO_2 to form *hydromagnesite, which may convert to magnesite over a long time period*. Cementitious material in the repository will contain $Ca(OH)_2$ that could also

react with CO₂ to form calcite. This latter reaction could buffer pH at relatively high values. However, the effect of Ca(OH)₂ is expected to be minimal because of calcite precipitation and reaction of the Ca(OH)₂ with MgCl₂ in the brine to form CaCl₂.

- Carbon dioxide fugacities that will prevail in the repository can be modeled using the brucite-*hydromagnesite* buffer.
- Equilibrium is assumed between repository brine, waste, and the Salado minerals halite, anhydrite, brucite, and *either* magnesite *or* *hydromagnesite*.

These changes were the only required modifications to DOE's CCA Chemical Conditions conceptual model.

2.3.2 Effects of AMWTP Waste Review on Chemical Conditions Conceptual Model

Review of the effects of AMWTP waste emplacement in WIPP resulted in a change to the Gas Generation conceptual model, as described above in Section 2.2.2. Information derived from the review of the dominant CPR degradation reactions in the repository is also relevant to the Chemical Conditions conceptual model.

The dominant CPR degradation reaction, which affects the proportion of CO₂ produced per mole of CPR carbon degraded, will depend on the quantities of nitrate and sulfate in the system. WIPP waste is the only significant source of nitrate in the WIPP repository system. DOE has stated that sulfate in the waste is the only significant source of sulfate (DOE 1996 Appendix SOTERM; Hansen et al. 2003a, 2003b). However, this assertion is inconsistent with the Chemical Conditions conceptual model which states that WIPP brines remain in equilibrium with anhydrite. In addition, both Salado and Castile brines contain dissolved sulfate (DOE 2004 Appendix PA Attachment SOTERM). Consequently, WIPP waste, brines, and Salado sulfate minerals are potential sources of sulfate for sulfate reduction (reaction 2).

In response to questions from EPA regarding the availability of Salado mineral sulfate, DOE performed an analysis of the transport of sulfate from the Salado minerals to the repository (Kanney et al. 2004). In this analysis, the time scale for complete degradation of CPR was assumed to be 2,000 years. This time scale was based on CPR degradation rates determined from experimental data at the time of the CCA and used in the AMWTP PA; examination of output files from the AMWTP PA indicated that the majority of CPR degradation occurred within 2,000 years for an undisturbed scenario and an E1 intrusion scenario (with brine inflow from a Castile brine pocket). The analysis included three potential sources of sulfate: (1) sulfate in the waste, (2) advection of sulfate in the maximum cumulative volume of brine predicted to flow into the repository in the E1 intrusion simulation of the AMWTP PA, and (3) diffusion into the repository of sulfate produced by dissolution of Salado sulfate minerals. Kanney et al. (2004) also considered additional sulfate transport through possible repository-induced fracture pathways in the DRZ and anhydrite interbeds. These pathways were evaluated for repository gas pressures less than and greater than lithostatic. However, Kanney et al. (2004) did not find these fracture pathways to be significant because of relatively rapid creep closure, relatively quick healing of the fractures in the DRZ, and prevention of brine inflow from the anhydrite interbeds because of high gas pressures.

For the diffusion calculations, Kanney et al. (2004) assumed a constant effective diffusion coefficient of $4.48 \times 10^{-12} \text{ m}^2/\text{sec}$, based on the free liquid diffusion coefficient for sulfate and a maximum porosity in the DRZ of 0.05. This diffusion coefficient was used to calculate a diffusion length of 1.06 m over the 2,000-year time period. All sulfate in the DRZ within the calculated diffusion length was assumed to be available for the sulfate reduction reaction, and the sulfate content of the rock was calculated using the Salado mineral content estimates of Brush (1990). All sulfate in the maximum Castile brine inflow after 2,000 years ($7.74 \times 10^4 \text{ m}^3$) was also included in the available sulfate. Based on these calculations, Kanney et al. (2004) estimated that the percentage of CPR carbon that could degrade by sulfate reduction ranged from 32 to 71%, depending on the waste emplacement scenario.

TEA (2004) performed a technical review of these calculations and questioned some of the assumptions made by Kanney et al. (2004). TEA (2004) questioned the assumed rate of room closure, which did not appear to be consistent with the conceptual model implemented in the CCA PA and PAVT: the CCA PA and PAVT incorporated a DRZ that endures for 10,000 years with permeabilities that are orders of magnitude higher than for intact halite. TEA (2004) also noted that the lateral DRZ would provide advective access to the Anhydrite *b* layer and will endure longer than the vertical DRZ.

TEA (2004) observed that structural disruptions during room closure could bring sulfate-bearing minerals such as anhydrite into direct contact with waste room brines. For example, roof collapse could introduce additional sulfate from Anhydrites *a* and *b*, and from the anhydrite-rich halite between these interbeds. TEA questioned the assumption that CPR degradation would be essentially complete within 2,000 years, because this assumption is not consistent with the length of time over which degradation occurs in waste panels with the increased iron surface areas that would be present with supercompacted AMWTP waste. TEA (2004) noted that CPR degradation continues for over 10,000 years in a number of vectors, because of decreased brine saturation as the iron surface area increases. In addition, microbial degradation rates used in the CCA PA, PAVT, and AMWTP PA are consistent with the higher initial reaction rates observed in microbial degradation experiments. TEA (2004) stated that the use of lower, long-term rates would be more conservative for the purpose of determining the length of time available for sulfate diffusion.

TEA (2004) concluded that not all potential sources for natural sulfate in the Salado Formation that could enter the repository were considered in the analysis by Kanney et al. (2004), and consequently, that an acceptable bounding analysis had not been performed. Because it was deemed possible that sufficient sulfate will be present in the Salado Formation to prevent or significantly limit methanogenesis, EPA (2004) required DOE to continue calculating the EF by assuming that all CPR carbon could be transformed into CO_2 . EPA (2004) also directed DOE to ensure that an MgO EF of 1.67 was maintained during emplacement of the AMWTP waste to ensure a large excess of MgO was present to control chemical conditions in the repository.

The conclusions of the AMWTP review are consistent with the Chemical Conditions conceptual model developed for the CCA. The assumption that the brines are in equilibrium with Salado minerals such as anhydrite is included in the conceptual model. It is also still assumed that brine in the repository will be well mixed with waste, and chemical homogeneity and solubility equilibrium are maintained. The assumptions of limited sulfate mineral availability and

significant sulfate concentration gradients in the repository, as postulated by Kanney et al. (2004), are inconsistent with the existing Chemical Conditions conceptual model.

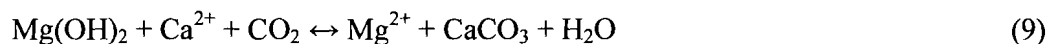
Changes to the MgO EF occurred because MgO minisacks are no longer emplaced with the waste (EPA 2001); consequently, there was a minor change to one assumption in the Chemical Conditions conceptual model:

- CPR degradation may generate CO₂, as described in the Gas Generation conceptual model (Section 2.2). A relatively large excess of MgO will be emplaced with the waste, with 1.67 moles of MgO per mole of CPR carbon. Consequently, the identity of the dominant CPR degradation reaction and the resulting proportions of CO₂ or CH₄ produced (i.e., sulfate reduction or methanogenesis) will not affect chemical conditions in the repository because of the large excess of MgO.

2.3.3 CRA-2004 and PABC Chemical Conditions Conceptual Model

For the CRA-2004, DOE changed the Salado brine formulation used in FMT calculations of actinide solubility from Brine A to GWB (DOE 2004 Appendix PA Attachment SOTERM). The GWB formulation was reported to more closely match the composition of Salado intergranular brines than Brine A. EPA (2006b) reviewed this change in the Chemical Conditions conceptual model and found that it was appropriate and would be likely to have little effect on PA.

Another change made by DOE to the Chemical Conditions conceptual model for the CRA-2004 PA was the assumption that CO₂ fugacity would be controlled by the reaction of calcite and brucite in the absence of significant microbial activity (DOE 2004 Appendix BARRIERS and Appendix PA Attachment SOTERM):



However, EPA (2006b) found this change to be inadequately supported. This issue became irrelevant for the PABC, because a 100% probability of significant microbial degradation of cellulosic materials was assumed (Section 2.2.3). Consequently, it was assumed that the brucite-hydromagnesite reaction would control CO₂ fugacity for the PABC, which is consistent with the Chemical Conditions conceptual model developed for the PAVT.

Only one minor change made to the Chemical Conditions conceptual model for the CRA-2004 and the PABC was accepted by EPA. This change was the use of the GWB brine formulation, instead of the Brine A formulation for Salado brines:

- Brine that dissolves actinides under any intrusion scenario will have a composition equal to that of Salado brine, Castile brine, or a mixture of Salado and Castile brines. Culebra groundwater that could enter the repository would quickly dissolve halite and develop a composition similar to Salado brine. Because the Salado and Castile brines bracket the possible brine compositions, experiments and modeling performed only with end-member brine compositions are adequate for describing the repository geochemistry. The GWB formulation is used to simulate Salado brine and ERDA-6 brine is used to simulate Castile brine.

2.3.4 Recent Chemical Conditions Conceptual Model Revisions

Since the CRA-2004 recertification of WIPP, minor adjustments to the Chemical Conditions conceptual model have been made as a result of further evaluation of the WIPP repository chemistry.

2.3.4.1 *Change in MgO Excess Factor*

In 2006, DOE requested approval from EPA to reduce the relative moles of MgO to CPR carbon emplaced in the repository from 1.67 to 1.20 (Moody 2006). EPA approved this request (Reyes 2008). Consequently, one assumption in the Chemical Conditions conceptual model was revised:

- CPR degradation may generate CO₂, as described in the Gas Generation conceptual model. A relatively large excess of MgO will be emplaced with the waste, with 1.20 moles of MgO per mole of CPR carbon. The identity of the dominant CPR degradation reaction, i.e., sulfate reduction or methanogenesis, and the resulting proportions of CO₂ or CH₄ produced will not affect chemical conditions in the repository because of the continued large excess of MgO.

2.3.4.2 *Assumed pH Range*

The Chemical Conditions conceptual model includes the assumption that excess MgO will buffer brine pH between 9 and 10, depending on the brine composition (Section 2.3.1). However, review of information from the CCA PA, PAVT, CRA-2004 PA, and PABC indicates that a slightly broader pH range has been found to be acceptable. EPA (2006b) provided a comparison of the WIPP brine pH values calculated for the CCA PA, PAVT, and CRA-2004 PA in equilibrium with Salado minerals, hydromagnesite or magnesite, and MgO; these pH values ranged from 8.69 to 9.24, with slightly higher pH values calculated for Castile brine (ERDA-6) than for Salado Brine (Brine A and GWB). The pH range calculated for the PABC was 8.69 to 9.02, depending on the initial brine composition (Brush 2005).

The pH value of 8.69 calculated for the Salado brine is slightly lower than the pH 9 to 10 range stated in the Chemical Conditions conceptual model. However, this slightly lower pH is consistent with the purpose of the pH constraints, because relatively low actinide solubilities were calculated for brines at these pH values. Consequently, the assumption regarding pH in the Chemical Conditions conceptual model should be revised to accommodate these lower pH values:

- In the absence of MgO backfill, low pmH ($-\log_{10}$ of the hydrogen ion molality) and high CO₂ fugacity could be achieved in the repository brine, increasing the solubilities of actinides relative to neutral or slightly basic pmH and low CO₂ fugacity conditions. However, conditions that might lead to high actinide solubilities will not occur in the repository, because excess MgO emplaced as an engineered barrier will buffer the pmH and CO₂ fugacity of the brine so that actinide solubilities are minimized. The pH ($-\log_{10}$

of the hydrogen ion activity) will be buffered between 8 and 10, depending on the brine composition.

2.4 DISSOLVED ACTINIDE SOURCE TERM CONCEPTUAL MODEL

The Dissolved Actinide Source Term conceptual model consists of information and assumptions related to the solubilities in WIPP brines of americium, curium, neptunium, plutonium, thorium, and uranium, which are the radionuclides that may significantly affect WIPP performance. Other radionuclides in WIPP waste, such as strontium and cesium, are not included in the conceptual model because of their relatively short half-lives or limited waste inventory (DOE 1996 Appendix SOTERM). Actinide solubilities are determined using assumptions about the oxidation states of the radionuclides, along with thermodynamic modeling of actinide solubilities under the assumed repository chemical conditions. Information used to develop the Dissolved Actinide Source Term conceptual model included thermodynamic theory and data, research published in peer-reviewed journal articles, and experimental programs conducted by DOE (Wilson et al. 1996a).

2.4.1 CCA and PAVT Dissolved Actinide Source Term Conceptual Model

The following assumptions were incorporated into the Dissolved Actinide Source Term conceptual model for the CCA PA and were reviewed by the Conceptual Models Peer Review Panel (DOE 1996 Appendix SOTERM, Wilson et al. 1996a):

- Equilibrium is maintained between dissolved actinides and actinide solid phases. However, redox reactions among actinides are not assumed to be in equilibrium.
- Brine homogeneity will be maintained due to long-term mixing.
- Anoxic conditions will dominate in the repository.
- Americium and curium will be present only in the +III oxidation state, and thorium will be present only in the +IV oxidation state.
- In the repository brines and equilibrium solid phases, neptunium may be present in the +IV or +V oxidation state, plutonium may be present in the +III or +IV oxidation state, and uranium may be present in the +IV or +VI oxidation state. There is a 50% probability that these actinides will be present in their more reduced states [neptunium(IV), plutonium(III) and uranium(IV)], and a 50% probability that they will be present in their more oxidized states [neptunium(V), plutonium(IV), and uranium(VI)].
- Dissolved actinide concentrations will be controlled by equilibrium with anhydrite, halite, the MgO backfill, actinide-bearing solid phases, and the appropriate brine.
- Because the Salado and Castile brines bracket the possible brine compositions, experiments and modeling performed with end-member brine compositions are adequate for describing actinide solubilities.

- The important ions in WIPP brines are H^+ , Na^+ , K^+ , Mg^{2+} , OH^- , Cl^- , CO_3^{2-} , SO_4^{2-} , and Ca^{2+} . Other ions such as PO_4^{3-} , F^- , Al^{3+} , Fe^{2+} , and Fe^{3+} may be important, but their effects are included only in a qualitative understanding of the chemical environment.
- The water-soluble ligands present in the brine are acetate, citrate, ethylenediaminetetraacetic acid (EDTA) and oxalate. The concentrations of these ligands are based on their total WIPP inventory, and these ligand concentrations remain constant.
- Transition metals (iron, manganese, nickel and chromium) will dissolve from the waste drums and magnesium will dissolve from MgO backfill; the metals and magnesium will compete with actinides for binding sites on the organic ligands, and organic ligands consequently will not significantly increase actinide solubilities.
- Actinide solubilities are modeled using the Pitzer activity coefficient model, which describes the thermodynamics of highly concentrated electrolyte solutions. Brine compositions are assumed to be constant throughout the 10,000-year regulatory period after rapid equilibration with MgO backfill materials.
- Actinides will not be sorbed on immobile substrates in the repository.
- All actinides in the same oxidation state will form the same aqueous species and isostructural compounds; this assumption has been referred to as the “oxidation-state analogy.”
- The solubilities of americium, curium, and plutonium in the +III oxidation state are modeled using the solubility model for americium(III). This model is based on experimental data for americium(III), curium(III), plutonium(III) and the lanthanide analogue neodymium(III).
- The solubilities of thorium, neptunium, plutonium, and uranium in the +IV oxidation state are modeled using the solubility of thorium(IV). The solubility of neptunium(V) is based on experimental data for the neptunium(V).
- A thermodynamic model is not used for uranium(VI); instead, an estimated solubility of 8.8×10^{-5} molal was cited by DOE (1996 Appendix SOTERM) based on an analysis by Hobart and Moore (1996). However, Table SOTERM-2 gives uranium(VI) solubilities of 8.7×10^{-6} molal (Salado brine) and 8.8×10^{-6} molal (Castile brine). The reason for the order-of-magnitude reduction in the uranium(VI) solubility is not given.
- Metastable phases observed in laboratory experiments will become more stable with time, and solubilities observed in these experiments provide an upper concentration limit. The effects of radiolysis will not cause actinide solids to become more soluble over time.
- The pH and CO_2 fugacity of the system is buffered by the solubility of brucite and the brucite-magnesite reaction, respectively.

- Point estimates are used for the actinide solubilities, with estimated uncertainties around these point estimates. A single uncertainty range is used for all actinide oxidation states, and is based on a comparison of measured solubilities and solubilities calculated for the experimental conditions. The actinide solubilities are assumed to be constant over the entire repository regulatory period.

EPA (1997a, 1997b, 1998a, 1998b) reviewed the Dissolved Actinide Source Term conceptual model and determined that metastable hydromagnesite [$Mg_5(CO_3)_4(OH)_2 \cdot 4H_2O$] could form and persist instead of the stable magnesite phase during the 10,000-year repository regulatory period. Because hydromagnesite buffers CO_2 fugacity at higher values than magnesite, the assumption that hydromagnesite might not convert to magnesite during the repository regulatory period results in higher predicted actinide solubilities. This assumption was incorporated into the PAVT. The remaining assumptions in the Dissolved Actinide Source Term conceptual model were reviewed and accepted by EPA (1997a, 1997b, 1998a, 1998b). Therefore, the assumption incorporated into the Dissolved Actinide Source Term conceptual model is:

- The pH and CO_2 fugacity of the system is buffered by the solubility of brucite and the brucite-hydromagnesite reaction, respectively.

2.4.2 Effects of AMWTP Waste Review on Dissolved Actinide Source Term Conceptual Model

The review of the potential effects of AMWTP waste emplacement on PA did not result in any changes to the Dissolved Actinide Source Term conceptual model. EPA (2004) required DOE to maintain sufficient amounts of MgO in the repository to maintain chemical conditions consistent with the Dissolved Actinide Source Term conceptual model. Consequently, no significant actinide solubilities changes would be expected as a result of the emplacement of AMWTP waste.

2.4.3 CRA-2004 and PABC Dissolved Actinide Source Term Conceptual Model

Several changes were made to the Dissolved Actinide Source Term conceptual model for the CRA-2004 PA (DOE 2004 Appendix PA Attachment SOTERM). Two changes that also affected the Chemical Conditions conceptual model were addressed in Section 2.3.3. The first change, which was use of the GWB brine formulation instead of Brine A for modeling the solubility of actinides in Salado brine was found to be appropriate during EPA's review of the CRA-2004 (EPA 2006b); this change was also included in the PABC. However, the assumption that CO_2 fugacity would be controlled by reaction of brucite and calcite (reaction 9) in the absence of significant CPR degradation was not incorporated in the PABC because of the assumption that cellulose degradation was likely to occur in all PA realizations.

For the actinide solubility calculations for the CRA-2004, DOE no longer assumed that transition metals would prevent complexation of actinides by organic ligands (DOE 2004 Appendix PA Attachment SOTERM). Instead, DOE directly included the effects of organic ligands in the actinide solubility calculations. These calculations made use of thermodynamic stability constants for actinide complexes with the ligands, and estimated the effects of competition for ligand binding sites by including the effects of formation of magnesium and calcium complexes

with organic ligands. In these calculations, the stability constants for the complexes formed by the organic ligands and calcium ions (Ca^{2+}) were assigned the same values as the stability complexes formed by these ligands and magnesium ions (Mg^{2+}). These calculations did not include competition from dissolved metals, such as iron, that could be present in the brine. Consequently, these calculations may conservatively overestimate the effects of organic ligands on actinide solubilities. Comparison of actinide solubilities with and without organic ligands indicated that the solubilities of the +III actinides (americium, curium, and plutonium) may be increased by EDTA complexation, and the solubility of neptunium(V) may be increased by oxalate complexation (EPA 2006b).

For the CRA-2004, the same uranium(VI) solubility was assumed as for the CCA, because DOE has not developed an actinide solubility model for the +VI actinide oxidation state (DOE 2004 Appendix PA Attachment SOTERM). EPA (2006b) reviewed this assumption along with additional information from the scientific literature. The results of this review indicated that the fixed 8.8×10^{-6} molar uranium(VI) concentration estimate that was used in the CCA should be revised. Consequently, DOE used an upper limit uranium(VI) concentration of 1×10^{-3} molar in the PABC that was determined by EPA (2006b); because this was a conservative upper-limit value, an uncertainty distribution was not sampled for this parameter (Leigh et al. 2005a).

DOE (2004 Appendix PA Attachment SOTERM) used the uncertainty distribution for the actinide solubilities that was originally developed for the CCA. Because the available solubility data and the FMT thermodynamic database had changed since the CCA PA and PAVT, EPA requested that DOE re-evaluate the uncertainties associated with the actinide solubilities using the currently available actinide solubility and thermodynamic data (EPA 2006b). DOE developed uncertainty ranges for the +III and +IV actinides that are greater than the single range used in the CCA PA and PAVT, are based on larger data sets than were previously used, and only data relevant to the specific oxidation state were used to generate the distributions (Xiong et al. 2004, 2005). EPA found the new uncertainty ranges to be adequate, and these uncertainty ranges were used in the PABC. DOE also developed a new uncertainty range for the solubility of the +V actinides. However, DOE did not use this uncertainty distribution in the PABC, because neptunium is the only actinide expected to be present in the +V oxidation state in the equilibrium repository, and the inventory of neptunium is insufficient to affect the long-term performance of the repository, regardless of its solubility (Brush et al. 2005).

Because of new information, the following assumptions in the Dissolved Actinide Source Term conceptual model have been revised:

- Transition metals (iron, manganese, nickel, and chromium) will dissolve from the waste drums and magnesium will dissolve from MgO backfill; the metals and magnesium will compete with actinides for binding sites on the organic ligands, and organic ligands consequently will not significantly increase actinide solubilities.
- A thermodynamic model is not used for uranium(VI); instead, an estimated solubility of 8.8×10^{-5} molal was cited by DOE (1996 Appendix SOTERM) based on an analysis by Hobart and Moore (1996). However, Table SOTERM-2 gives uranium(VI) solubilities of 8.7×10^{-6} molal (Salado brine) and 8.8×10^{-6} molal (Castile brine). The reason for the order-of-magnitude reduction in the uranium(VI) solubility is not given.

- Point estimates are used for the actinide solubilities, with estimated uncertainties around these point estimates. A single uncertainty range is used for all actinide oxidation states, and is based on a comparison of measured solubilities and solubilities calculated for the experimental conditions. The actinide solubilities are assumed to be constant over the entire repository regulatory period.

The revised assumptions are:

- The effects of organic ligands (acetate, citrate, EDTA, and oxalate) are included in actinide solubility calculations using experimentally derived complexation constants. The effects of competition by calcium and magnesium ions are included using the complexation constants for magnesium. The effects of competition by transition metals such as iron are considered only qualitatively.
- A thermodynamic model is not used for uranium(VI); instead, an upper-limit solubility of 1×10^{-3} M is assumed. Because this is an upper-limit solubility estimate, an uncertainty distribution is not sampled for this parameter.
- Point estimates are used for the +III, +IV and +V actinide solubilities, with estimated uncertainties around these point estimates. A separate uncertainty range is used for each actinide oxidation state that is based on a comparison of measured solubilities and solubilities calculated for the experimental conditions. An upper-limit point estimate is used for uranium(VI) without an uncertainty range. The actinide solubilities are assumed to be constant over the entire repository regulatory period.

3.0 MGO PLANNED CHANGE REQUEST

In April 2006, DOE requested approval from EPA to reduce the MgO EF from 1.67 to 1.20 (Moody 2006). In their reply, EPA requested additional information (Gitlin 2006). EPA noted the importance of MgO as WIPP's only engineered barrier. EPA also discussed the function of the MgO engineered barrier to maintain chemical conditions in the repository, and pointed out that relatively high excess amounts of MgO have been required to counter uncertainties regarding the reactivity of the MgO. Consequently, EPA requested additional information regarding the uncertainties related to MgO effectiveness, the size of the uncertainties, and the potential impact of these uncertainties on long-term performance.

DOE responded with an evaluation of the uncertainties related to the effectiveness of the MgO backfill in WIPP. These uncertainties can be generally described as uncertainties in the amount of CPR that would degrade, in the amounts of CO₂ that would be produced by microbial degradation of CPR, in the amounts of MgO that would be available to react with CO₂, in the amounts of CO₂ consumed per mole of available MgO, and in the amounts of CO₂ that could be consumed by reaction with other materials (Vugrin et al. 2006, 2007). The analyses by Vugrin et al. (2006, 2007) that dealt with each of these uncertainties were reviewed by EPA (SCA 2008).

As part of their analysis, Vugrin et al. (2006) evaluated the potential effects of anhydrite dissolution brought about by sulfate reduction in the repository brine. As sulfate is reduced, anhydrite or other sulfate minerals in the Salado (e.g., gypsum and polyhalite) would be expected to dissolve and release calcium ions:



As calcium concentrations in the brine increase, calcite is expected to precipitate:



As bicarbonate ion is removed by calcite precipitation, gaseous or aqueous CO₂ consumption is expected to occur:



In this manner, calcite precipitation could consume significant amounts of CO₂. Consumption of CO₂ by calcite precipitation would occur in addition to CO₂ consumption by reaction of MgO to form hydromagnesite or magnesite, which could reduce the amount of MgO needed in the repository to control chemical conditions.

In previous evaluations of the chemistry-related conceptual models, calcite precipitation was addressed only with respect to its ability to control pH, either at relatively high values if large amounts of Ca(OH)₂ are present in the repository (Section 2.3.1), or at more moderate values by reaction with brucite (reaction 9) if significant CPR degradation did not occur (Section 2.3.3). The possibility that calcite precipitation could consume significant amounts of CO₂ and supplement the ability of the MgO to control CO₂ fugacities was not previously included in the conceptual models.

3.1 SANDIA NATIONAL LABORATORIES EQ3/6 MODELING OF CALCITE PRECIPITATION EFFECTS

Brush et al. (2006) carried out a series of reaction-path calculations to determine the amount of CO₂ likely to be consumed by calcite precipitation during CPR degradation. Reaction-path calculations were performed using the EQ3/6 (version 7.2c) geochemical software package (Daveler and Wolery 1992, Wolery 1992a, Wolery 1992b, Wolery and Daveler 1992). The EQ3NR portion of the software package is an equilibrium modeling code, similar to FMT, used to calculate aqueous speciation and mineral solubilities in a batch system. The EQ6 portion of the software package can be used to calculate the changes in aqueous speciation and mineral solubilities as a function of reaction progress; such calculations are frequently referred to as “reaction-path” calculations. The EQ6 code is not used independently, but uses the output from initial EQ3NR modeling runs. Brush et al. (2006) first equilibrated the starting brine composition using EQ3NR; the EQ6 code was then used in a two-step process to first model reaction of the brine with Salado minerals and MgO in the repository, and to then model CPR degradation through sulfate reduction. These calculations included other reactions that occur because of the changes in the brine composition as the CPR degradation reaction proceeds, such as hydromagnesite and calcite precipitation and anhydrite dissolution.

The thermodynamic database used by Brush et al. (2006) for their EQ3/6 calculations was developed from the HMW database supplied with the EQ3/6 package. The HMW database uses the Pitzer ion-interaction parameters developed by Harvie et al. (1984); this database was modified to include the solid phases hydromagnesite [Mg₅(CO₃)₄(OH)₂•4H₂O], hydromagnesite [Mg₄(CO₃)₃(OH)₂•3H₂O],¹ MgSO₄, MgCl₂, MgO, and CaO; this revised database was called the HMP database (Xiong 2004). Xiong (2006a) modified the HMP database by adding the necessary thermodynamic data and Pitzer parameters for dissolved citrate and oxalate species and citrate- and oxalate-bearing solids, creating the HMY database. Xiong (2006b) then added thermodynamic data for CaCO₃(am)² to the HMY database to establish the HML database. This database does not include some of the species included in the sulfate reduction reaction (2), such as cellulose monomer and H₂S. This database also does not include thermodynamic data for other species of potential importance in the WIPP repository brines, such as bisulfide (HS⁻) or ferrous iron (Fe²⁺), because Pitzer ion-interaction parameters were unavailable for these species.

The EQ3/6 simulations were performed with the GWB and ERDA-6 WIPP brines. Two brine volumes were modeled for GWB brine: 1,045 m³ and 7,763 m³, which respectively represent the minimum volume predicted for brine release from a panel in the results of the CRA-2004 PA and the maximum volume of GWB that was present in a seven-room panel in the results of the PABC (Brush et al. 2006). Three brine volumes were modeled for ERDA-6 brine; in addition to the volumes assumed for GWB brine, a third volume of 13,267 m³ was assumed that represented the largest volume of ERDA-6 calculated for the PABC in a seven-room panel. Brush et al. (2006) performed a number of different simulations to determine the effects on the quantities of

¹ Two formulas have been reported for hydromagnesite. The Mg₅(CO₃)₄(OH)₂•4H₂O formula is consistent with the hydromagnesite precipitated in WIPP MgO carbonation experiments and corresponds to the hydromagnesite formula accepted by the International Mineralogical Association (IMA 2007). Further reference to hydromagnesite in the present report is to material with a formula of Mg₅(CO₃)₄(OH)₂•4H₂O.

² (am) indicates an amorphous solid phase.

calcite precipitated of: (1) hydromagnesite formation instead of magnesite, (2) the presence of organic ligands, and (3) precipitation of $\text{CaCO}_3(\text{am})$ instead of calcite, which may occur if significant calcite inhibitors are present in the system. Brush et al. (2006) also stated that simulations were performed to test the effects of different proportions of minerals in the Salado Formation. However, the results of these simulations were not discussed in their report and these input and output files were not submitted to EPA.

For each simulation, the proportions and total amounts of the minerals added to the system were calculated based on the 1 kg of water in the brine used in the EQ3/6 simulations, the expected Salado mineralogy (Brush 1990), the volume of the DRZ, the CPR inventory, the amount of MgO assuming a 1.20 EF, the assumed brine volume, and the densities of the two brines. These calculations were documented in the file calcite.xls that was provided to EPA. Brush et al. (2006) set up the EQ6 reaction-path calculations as a two-step titration process. In the first step, the minerals brucite, halite, anhydrite, gypsum, magnesite (or hydromagnesite), and polyhalite were titrated into the brine. Brucite was used instead of periclase to prevent consumption of water in the brine by periclase hydration. Halite, anhydrite, gypsum, magnesite, and polyhalite were used to represent the Salado minerals in the DRZ. In simulations that assumed production of hydromagnesite instead of magnesite, hydromagnesite was used in the first EQ6 step to prevent conversion of the magnesite to hydromagnesite and consumption of water. The amounts of the DRZ minerals added to the brine were set equal to the amounts necessary to provide sufficient sulfate for complete degradation of the CPR by sulfate reduction (reaction 2).

The second step of the EQ6 calculations was designed to simulate CPR degradation, sulfate reduction, and CO_2 generation (reaction 2). Because Pitzer ion-interaction parameters were not available for H_2S and HS^- , the titration was performed by subtracting 2H^+ and SO_4^{2-} from the brine and adding 2CO_2 . This step was designed to simulate CPR degradation by sulfate reduction by subtracting the reactants and adding the products of the reaction. However, this step did not include subtraction of cellulose monomer or addition of H_2S , because these species were not included in the database. Brush et al. (2006) reasoned that H_2S would be consumed by reaction with iron as quickly as it was produced and omitting H_2S would have no effect on the modeling results. The production of water was not included in the simulations, because Brush et al. (2006) speculated that cellulose hydrolysis prior to its microbial degradation would consume as much water as was produced by reaction (2).

The EQ3/6 input information and calculation results are summarized in Tables 3-1 and 3-2. All simulations were set up to prevent the precipitation of dolomite [$\text{CaMg}(\text{CO}_3)_2$] and glauberite [$\text{Na}_2\text{Ca}(\text{SO}_4)_2$]. Dolomite formation was prevented because this phase does not commonly precipitate directly from solution in low-temperature environments. Brush et al. (2006) did not explain why glauberite formation was prevented, and this phase might form at low temperature under some circumstances. However, the suppression of glauberite is unlikely to have had any effects on the results of the calculations, because this phase was not oversaturated in the final solutions. Magnesite formation was suppressed in simulations carried out to evaluate the potential effects of the metastable persistence of hydromagnesite. Calcite and aragonite formation were suppressed in simulations performed to evaluate the possible effects of $\text{CaCO}_3(\text{am})$ formation in the presence of significant calcite inhibitors.

Table 3-1. EQ3/6 Modeling Calculations Using GWB Brine, Brush et al. (2006)

Brine	GWB	GWB	GWB	GWB	GWB
Brine Volume (m³)	1,045	1,045	1,045	7,763	7,763
Organic Ligands	None	Oxalate and citrate	Oxalate and citrate	None	None
EQ6 Output File	06gmin02.6o	06gmin04.6o	06gmin06.6o	06gmid02.6o	06gmid04.6o
Suppressed Minerals	Dolomite, glauberite	Dolomite, glauberite	Dolomite, glauberite, aragonite, calcite	Dolomite, glauberite	Dolomite, glauberite, magnesite
Salado Minerals (% DRZ)	44%	44%	44%	44%	44%
Final pH	11.3	11.3	10.3	8.53	8.32
Final log f_{CO2}	-6.928	-6.928	-6.927	-6.927	-5.479
Final Total Carbonate (m)	0.257	0.259	3.49E-03	2.16E-05	4.28E-04
Final Solid Phases	Brucite, calcite, halite, magnesite, pirssonite, sylvite	Brucite, calcite, halite, magnesite, pirssonite, sylvite	Brucite, CaCO ₃ (am), halite, magnesite, pirssonite, sylvite, whewellite	Anhydrite, brucite, calcite, halite, magnesite	Brucite, calcite, halite, hydromagnesite, oxychloride-Mg, syngenite
Notes				Used as example by Lichtner (2007)	

Table 3-2. EQ3/6 Modeling Calculations Using ERDA-6 Brine, Brush et al. (2006)

Brine	ERDA-6	ERDA-6	ERDA-6	ERDA-6	ERDA-6	ERDA-6
Brine Volume (m³)	1,045	1,045	1,045	7,763	7,763	13,267
Organic Ligands	None	Oxalate and citrate	Oxalate and citrate	None	None	None
EQ6 Output File	06emin02.6o	06emin04.6o	06emin06.6o	06emid02.6o	06emid04.6o	06emax02.6o
Suppressed Minerals	Dolomite, glauberite	Dolomite, glauberite	Dolomite, glauberite, calcite, aragonite	Dolomite, glauberite	Dolomite, glauberite, magnesite	Dolomite, glauberite
Salado Minerals (% DRZ)	45%	45%	45%	45%	45%	45%
Final pH	11.3	11.3	10.3	11.3	10.6	11.3
Final log f_{CO2}	-6.928	-6.928	-6.928	-6.92	-5.479	-6.916
Final Total Carbonate (m)	0.256	0.258	3.49E-03	0.259	0.265	0.2615
Final Solid Phases	Brucite, calcite, halite, magnesite, pirssonite, sylvite	Brucite, calcite, halite, magnesite, pirssonite, sylvite	Brucite, calcite, halite, magnesite, pirssonite, sylvite, whewellite	Brucite, calcite, halite, magnesite, pirssonite	Brucite, calcite, halite, hydromagnesite, pirssonite	Brucite, calcite, halite, hydromagnesite, pirssonite
Notes				Used as example by Lichtner (2007)		

Brush et al. (2006) added only enough DRZ minerals (anhydrite, gypsum, magnesite or hydromagnesite, and polyhalite) to provide sufficient sulfate for degradation of all CPR by sulfate reduction, after the amounts of CPR degraded via denitrification were assessed. This resulted in the addition of only a fraction of the Salado minerals present in the DRZ, based on revised calculations performed for the current report (Section 4.0). These calculations indicate that only about 44% to 45% of the mineral quantities present in the DRZ were included in the EQ3/6 simulations carried out by Brush et al. (2006).

Results of the EQ3/6 simulations with GWB brine indicated that in two cases (Table 3-1), predicted pH values were in the range of 8.32 to 8.53. These pH values are slightly less than the pH range of 9 to 10 assumed in the original Chemical Conditions conceptual model (Wilson et al. 1996a). However, these pH values are similar to those used in the PABC actinide solubility calculations, which ranged from 8.69 to 9.02 and to the revised assumption in the Chemical Conditions conceptual model (Section 2.3.4.2).

Three simulations had final predicted pH values of 10.3 to 10.6 (Tables 3-1 and 3-2). These pH values are only slightly higher than the pH range of 8 to 10 assumed in the Chemical Conditions conceptual model. However, they are more than one pH unit higher than the pH values used to calculate actinide solubilities for the PABC (Brush 2005). These higher pH values could lead to higher predicted actinide solubilities, because the brucite-hydromagnesite or brucite-magnesite reactions would control total carbonate concentrations at higher values in these higher-pH brines. For example, the total carbonate concentration at pH 8.53 in GWB was 2.162×10^{-5} m, whereas at pH 10.3, the total carbonate concentration in GWB was 3.494×10^{-3} m, an increase of two orders of magnitude. Higher total carbonate concentrations might significantly increase actinide solubilities through carbonate complexation.

Six of the EQ3/6 simulations predicted pH values of 11.3 (Tables 3-1 and 3-2). These pH values are significantly greater than those assumed in the Chemical Conditions conceptual model and used in the PABC actinide solubility calculations for the PABC. The high total carbonate concentrations of approximately 0.26 m might have significant effects on actinide solubilities. These high pH values indicate that brucite dissolution does not control pH, which is inconsistent with the Chemical Conditions conceptual model.

SCA (2006) provided preliminary comments on the EQ3/6 modeling results. SCA (2006) noted that Brush et al. (2006) implemented the degradation of CPR via sulfate reduction by subtracting H_2SO_4 , which is a strong acid. Subtracting a strong acid is chemically equivalent to adding a strong base to the system. SCA (2006) questioned whether the omission of H_2S in the reaction simulation could have resulted in the high pH values predicted in most of the calculations, because H_2S would dissociate to HS^- plus H^+ at higher pH. SCA (2006) questioned whether the interaction of H_2S and iron could moderate the pH increase predicted in the EQ3/6 simulations of Brush et al. (2006). SCA (2006) noted that the CPR carbon inventory used by Brush et al. (2006) did not include the emplacement cellulose and plastics used in the repository. Consequently, the inventory value of 1.1×10^9 moles used by Brush et al. (2006) should have been 1.2×10^9 moles. SCA (2006) also noted that the EQ3/6 calculations did not include the potential effects of acetate and EDTA. SCA (2006) stated that although the effects of including acetate and EDTA on the results of the calculations were likely to be small, the thermodynamic data were available and these constituents should be included in the calculations.

The most notable difference between the Brush et al. (2006) modeling results at lower pH and the higher-pH results was the presence of a calcium-bearing sulfate mineral in the final reaction products in the lower-pH calculations (Table 3-1). One set of reaction products contained residual anhydrite, whereas the other contained syngenite [K₂Ca(SO₄)₂•H₂O]. Consequently, the high pH values appear to be the result of limiting the amount of sulfate minerals in the system. The EQ3/6 calculations that predicted high pH values are inconsistent with the Chemical Conditions conceptual model that includes the assumption that the brines will be in equilibrium with anhydrite.

EPA and DOE discussed the results of the EQ3/6 modeling calculations during a Technical Exchange Meeting held in Dallas, Texas, on May 23, 2007. EPA expressed concern that DOE was not providing consistent information on the high pH issue. EPA was informed that the high pH values were the result of inadequate sulfate ions being included in the modeling, but was told later that the results of the Brush et al. (2006) calculations are correct. Consequently, EPA requested that DOE provide additional information clarifying the issues related to the predicted high pH values.

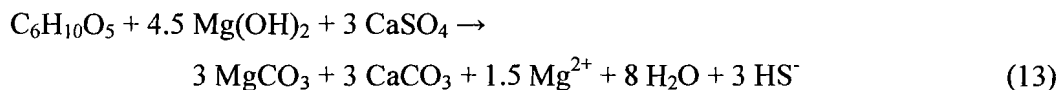
Two additional investigations of the modeling results were conducted by DOE and Sandia National Laboratories. Wolery and Sassani (2007) describe additional EQ3/6 modeling carried out to evaluate the results of the Brush et al. (2006) report; this investigation was performed at the request of Sandia National Laboratories. Lichtner (2007) describes modeling calculations carried out to further investigate the reaction processes in WIPP using the FLOTRAN reactive transport computer code; this investigation was carried out at the request of DOE.

3.2 WOLERY AND SASSANI (2007)

Wolery and Sassani (2007) reviewed the Brush et al. (2006) report and provided additional EQ6 geochemical calculations. These calculations were revised in late October and early November of 2007, before the input and output files were transmitted to EPA. Changes made to these calculations after preparation of the Wolery and Sassani (2007) report were mainly to improve the documentation within the files, but there may have been small differences in the database used for the different sets of calculations (Wolery 2008). The later calculations are referred to in the present report as the Wolery EQ6 calculations to differentiate them from the original calculations used in the Wolery and Sassani (2007) report. The original calculations are summarized in Appendix B.

3.2.1 CPR Degradation Without Iron

Wolery and Sassani (2007) rewrote reaction (2) in terms of the dominant aqueous species in the WIPP brine and also included the effects of anhydrite dissolution and magnesite precipitation:



Based on this reaction, Wolery and Sassani (2007) observed that the combined processes of CPR degradation, brucite and anhydrite dissolution, magnesite and calcite precipitation and sulfate

reduction would not be expected to significantly affect pH, because it neither consumes nor produces hydrogen ion (H^+).

Wolery and Sassani (2007) evaluated the effects of including sulfides (H_2S and HS^-) in the reaction-path calculations by adding these species to the EQ3/6 database without including Pitzer ion-interaction parameters; they then repeated two unpublished titration calculations similar to those reported by Brush et al. (2006), that had produced high pH brines when sulfide species were not included. In these calculations, the reaction was modified to include the production of sulfide species, as shown in reaction (13). Because the Pitzer parameters were unavailable, Wolery and Sassani (2007) stated that the calculations were not quantitatively significant, but were appropriate for qualitatively evaluating the potential formation of high pH brines.

The results of the Wolery EQ6 calculations are presented in the first two columns of Table 3-3. In these calculations, only 49% or 25% of the Salado minerals present in the DRZ were included in the system. The Wolery EQ6 simulations predicted moderate pH values of 6.79 and 7.32, when sulfide species were included in the simulations (Table 3-3), consistent with reaction (13). The brines evolved from an initial sodium-chloride composition to a dominantly magnesium-bisulfide composition at the end of the simulations.

One result of the Wolery EQ6 calculation that included sulfide species and 25% DRZ minerals was a predicted CH_4 fugacity of $10^{13.8}$ (Table 3-3). This fugacity, if it is assumed equal to the CH_4 partial pressure (ideal gas behavior), is many orders of magnitude greater than the 146 atm lithostatic pressure in the WIPP repository (DOE 2004, Appendix PA Attachment SCR). In this simulation, the CH_4 fugacity increased rapidly during the final two steps of the calculations after anhydrite was completely dissolved. Consequently, the final steps of this simulation do not correspond to reaction (13) but instead include methanogenesis, possibly through cellulose reduction by H_2 :



This reaction would not be expected to affect pH. The amount of CH_4 predicted in the simulation that included 25% of the DRZ minerals would not remain in the repository, because the anhydrite interbeds are expected to fracture at gas pressures slightly below lithostatic, allowing gas flow out of the repository (DOE 2004 Appendix PA).

Wolery and Sassani (2007) qualitatively evaluated the potential effects of dissolution of polyhalite on pH. They predicted that the pH of the brine would be likely to increase, as modeled by Brush et al. (2006), if alkaline-earth sulfates (anhydrite, gypsum, and syngenite) were depleted and polyhalite dissolution occurred as sulfate reduction progressed.

Table 3-3. Wolery EQ6 Calculations Using GWB Brine to Assess Effects of Including Sulfide and Iron^a

Brine	GWB	GWB	GWB	GWB	GWB	GWB
Brine Volume (m ³)	1,045	1,045	1,045	1,045	1,045	1,045
Organic Ligands	None	None	None	None	None	None
EQ6 Output File	1GWB-2hs.6o	1GWB-4hs.6o	1GWB-2m1.6o	1GWB-4m1.6o	1GWB-2w1a.6o	1GWB-4w1a.6o
Suppressed Minerals	Dolomite, glauberite, polyhalite	Dolomite, glauberite, polyhalite	Dolomite, glauberite, polyhalite, pyrite	Dolomite, glauberite, polyhalite	Dolomite, glauberite, polyhalite, pyrite	Dolomite, glauberite, polyhalite
Salado Minerals (% DRZ)	49%	25%	49%	25%	49%	25%
Final pH	6.79	7.32	8.59	11.3	8.64	11.3
Final log f _{CO2}	-6.90	-6.91	-6.96	-6.93	-6.95	-6.93
Final log f _{CH4}	-5.89	13.8	-2.50	4.97	13.2	4.62
Final log f _{H2S}	-1.11	-1.08	-1.09	-7.26	-1.21	-7.29
Final Total Carbonate (m)	8.38 × 10 ⁻⁴	4.59 × 10 ⁻⁴	2.59 × 10 ⁻⁵	0.255	2.46 × 10 ⁻⁵	0.257
Notes	Included sulfide aqueous species and solid phases in titration calculations	Included sulfide aqueous species and solid phases in titration calculations	Included sulfide and iron aqueous species and solid phases in titration calculations; relative rates of cellulose and iron reaction set at 1:3	Included sulfide and iron aqueous species and solid phases in titration calculations; relative rates of cellulose and iron reactions set at 1:3	Included iron and sulfide aqueous species and solid phases; cellulose degradation set up as an irreversible reaction; relative rates of cellulose and iron reactions set at 1:3	Included iron and sulfide aqueous species and solid phases; cellulose degradation set up as an irreversible reaction; relative rates of cellulose and iron reaction set at 1:3
Final Solid Phases	Anhydrite, brucite, calcite, halite, magnesite, sylvite	Brucite, calcite, halite, magnesite, oxychloride-Mg, sylvite	Brucite, calcite, halite, magnesite, sylvite, troilite	Brucite, calcite, halite, magnesite, magnetite, pirssonite, pyrite, sylvite, troilite	Brucite, calcite, halite, magnesite, sylvite, troilite	Brucite, calcite, halite, magnesite, magnetite, pirssonite, pyrite, sylvite, troilite

a - EPA received a set of EQ6 input and output files from Dr. Wolery in November (2007). These files were slightly modified from the earlier versions used in the preparation of the Wolery and Sassani (2007) report, but these modifications did not appear to have affected the conclusions of that report. The data in this table were obtained from the November 2007 files. Because Pitzer parameters for the sulfide and iron species are not available, the modeling results should be viewed as only qualitative indicators of the system chemistry and are not appropriate for use in PA (T.J. Wolery, personal communication).

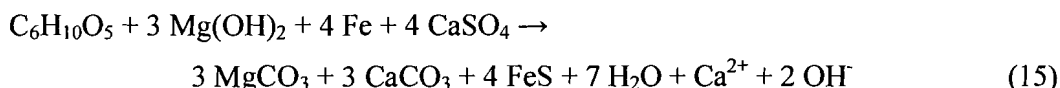
Table 3-4. Wolery EQ6 Calculations Using GWB Brine to Evaluate the Effects of Different Cellulose and Iron Reaction Rates^a

Brine	GWB	GWB	GWB	GWB	GWB	GWB
Brine Volume (m ³)	1,045	1,045	1,045	1,045	1,045	1,045
Organic Ligands	None	None	None	None	None	None
EQ6 Input File 2	1GWB2w1d.6o	1GWB4w1d.6o	1GWB2w1h.6o	1GWB4w1h.6o	1GWB2w1x.6o	1GWB4w1x.6o
Suppressed Minerals	Dolomite, glauberite, polyhalite, pyrite	Dolomite, glauberite, polyhalite	Dolomite, glauberite, polyhalite, pyrite	Dolomite, glauberite, polyhalite	Dolomite, glauberite, polyhalite, pyrite	Dolomite, glauberite, polyhalite
Salado Minerals (% DRZ)	49%	25%	49%	25%	49%	25%
Final pH	11.3	11.3	8.14	8.55	13.2	13.3
Final log f _{CO2}	-6.93	-6.93	-6.97	-6.95	-13.2	-13.2
Final log f _{CH4}	21.1	4.97	-3.06	20.4	13.6	14.5
Final log f _{H2S}	-8.60	-7.26	-0.927	-1.21	-8.54	-8.60
Final Total Carbonate (m)	0.256	0.255	3.55×10^{-5}	2.317×10^{-5}	7.40×10^{-4}	8.17×10^{-4}
Notes	Included sulfide and iron aqueous species and solid phases; cellulose degradation set up as an irreversible reaction; relative rates of cellulose and iron reaction set at 1:6	Included sulfide and iron aqueous species and solid phases; cellulose degradation set up as an irreversible reaction; relative rates of cellulose and iron reaction set at 1:6	Included sulfide and iron aqueous species and solid phases; cellulose degradation set up as an irreversible reaction; relative rates of cellulose and iron reaction set at 2:3	Included sulfide and iron aqueous species and solid phases; cellulose degradation set up as an irreversible reaction; relative rates of cellulose and iron reaction set at 2:3	Included sulfide and iron aqueous species and solid phases; cellulose degradation set equal to zero	Included sulfide and iron aqueous species and solid phases; cellulose degradation set equal to zero
Final Solid Phases	Brucite, calcite, halite, magnesite, magnetite, pirssonite, sylvite, troilite	Brucite, calcite, halite, magnesite, magnetite, pirssonite, pyrite, sylvite, troilite	Brucite, calcite, halite, magnesite, sylvite, troilite	Brucite, calcite, halite, magnesite, pyrite, sylvite	Brucite, calcite, halite, magnetite, portlandite, sylvite, troilite	Brucite, calcite, halite, magnetite, portlandite, sylvite, troilite

a - EPA received a set of EQ6 input and output files from Dr. Wolery in November 2007. These files were slightly modified from the earlier versions used in the preparation of the Wolery and Sassani (2007) report, but these modifications did not appear to have affected the conclusions of that report. The data in this table were obtained from the November 2007 files. Because Pitzer parameters for the sulfide and iron species are not available, the modeling results should be viewed as only qualitative indicators of the system chemistry and are not appropriate for use in PA (T.J. Wolery, personal communication).

3.2.2 CPR Degradation with Iron Corrosion

Wolery and Sassani (2007) also considered the potential effects of iron corrosion. The CPR degradation reaction was modified to include iron oxidation and FeS precipitation:



This reaction could occur and increase the brine pH until the brine reached saturation with respect to portlandite [$\text{Ca}(\text{OH})_2$], where the brine pH would be buffered at a relatively high value. Wolery and Sassani (2007) added iron species to the EQ3/6 database without including Pitzer parameters, because these parameters were unavailable. However, Wolery and Sassani (2007) reasoned that omitting these Pitzer parameters might have relatively small effects on the modeling results because of the low solubility of iron species under these conditions.

Wolery and Sassani (2007) performed EQ6 simulations that correspond to reaction (15). In these calculations, the relative reaction rates of $\text{C}_6\text{H}_{10}\text{O}_5$ and Fe were set equal to 1:3 to be consistent with the Brush et al. (2006) reaction formulation. To be consistent with reaction (15), the relative rates should be 1:4 (Wolery and Sassani 2007). Wolery and Sassani (2007) stated that this difference in rates would not significantly affect the results of the calculations, except to delay potential increases in pH to later in the reaction progress, and might possibly result in slightly lower pH values. The results of two sets of simulations were provided, one set with the reaction carried out as a titration and the other with the reaction set up as an irreversible reaction with cellulose included as a special reactant. Similar results were obtained using the two approaches. However, Wolery and Sassani (2007) recommended using the irreversible reaction approach instead of setting up the reaction as a titration, because in some cases such a titration approach may not provide a complete and accurate representation of an overall process. In particular, the titration approach does not correctly address the production of water by the CPR degradation reactions.

The results of the Wolery EQ6 calculations that included iron are summarized in the final four columns of Table 3-3. The pH values cited by Wolery and Sassani (2007) for both the titration and irreversible reaction calculations (11.6) were higher than the final pH values in the EQ6 files provided in November 2007. The results of the simulations with iron and sulfide included in the reaction differed significantly, depending on the DRZ mineral quantities included; simulations with 49% of the DRZ produced pH values of approximately 8.6, whereas simulations with 25% of the DRZ produced pH values of 11.3. The principal cause of the different pH values was the different amounts of calcium-sulfate minerals (anhydrite and gypsum) included in the calculations. In the calculation with only 25% DRZ minerals, the calcium-sulfate minerals were depleted more rapidly, the pH began to rise earlier in the course of the cellulose degradation process, and the pH rose to higher levels. Another difference that is probably less significant was the suppression of pyrite in the simulations with 49% DRZ minerals; in the calculations with 25% DRZ minerals, pyrite was not suppressed and was included in the final solid phases.

The final calculated CO_2 fugacities were similar for all four calculations (Table 3-3). However, because of the higher pH values in the calculations with 25% of the DRZ, the total carbonate

concentration was much higher than in the 49% DRZ calculations. In addition, three out of the four calculations had high CH₄ fugacities at the end of the simulations. These results indicate that methanogenesis occurred during the simulations, in addition to the sulfate reduction described by reaction (15). The results of the simulations indicate that methanogenesis begins after the sulfate produced by dissolution of anhydrite, gypsum, and polyhalite has been consumed by sulfate reduction. If methanogenesis occurs according to the following reaction, the pH would be expected to increase as a function of reaction progress:

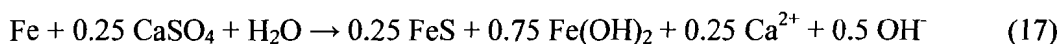


Extremely high pH values were not predicted by the simulations with 49% of the DRZ that included iron (Table 3-3), because only the final one or two steps of the simulations occurred after anhydrite and syngenite were completely dissolved and sulfate ion was consumed.

In the simulations with 25% of the DRZ minerals included in the system, the final predicted pH values were 11.3. The pH remained at or below 9.0 as long as anhydrite was present in the solid phase assemblage. However, when anhydrite was replaced by syngenite as the simulations progressed, the brine pH increased to approximately 9.50. Replacement of syngenite with apthitalite [NaK₃(SO₄)₂] coincided with an increase in brine pH to 11.3 when methanogenesis had not yet begun. In these simulations, methanogenesis did not appear to have caused the increased pH, but instead occurred at high pH as the sulfate present in anhydrite, syngenite, and then apthitalite was reduced to sulfide. The high CH₄ fugacities predicted at the end of three out of the four simulations will not be observed if methanogenesis occurs in the WIPP repository. As previously noted, the anhydrite interbeds are expected to fracture at pressures slightly below lithostatic (146 atm), allowing gas to flow out of the repository.

By defining cellulose as a special reactant and including its degradation as an irreversible reaction, Wolery and Sassani (2007) were able to calculate a mass balance for water. The amount of water in the system increased by factors of 2.7 to 5.1 during the reaction path calculations (files 1GWB-2w1a.6o and 1-GWB-4w1a.6o). This increase occurred because of the water produced by cellulose degradation, which is consistent with reaction (15).

Wolery and Sassani (2007) also tested the effects of different relative rates of cellulose degradation and iron oxidation on the reaction path calculation results (Table 3-4). In these calculations, the previously assumed relative rate of iron corrosion (files 1GWB2w1a.6o and 1GWB4w1a.6o, Table 3-3) was first doubled relative to the cellulose degradation rate (files 1GWB2w1d.6o and 1GWB4w1d.6o, Table 3-4). Although methanogenesis occurred at the end of both simulations after sulfate was depleted, the pH increase to 11.3 occurred before methanogenesis began. Simulations were then performed with the iron corrosion rate halved relative to the cellulose degradation rate (files 1GWB2w1h.6o and 1GWB4w1h.6o, Table 3-4). Moderate final pH values were calculated in both simulations, even though significant methanogenesis occurred in the calculation with 25% of the DRZ minerals included in the system. Finally, the potential effects of iron corrosion and sulfate reduction in the absence of CPR degradation were assessed by performing the EQ6 reaction-path calculations with the cellulose degradation rate set to zero (files 1GWB2w1x.6o and 1GWB4w1x.6o, Table 3-4). Without CPR degradation, sulfate reduction could occur by reaction with iron metal:



Extremely high pH values were observed as a result of the iron corrosion and sulfate reduction reaction. In these simulations, pH values in excess of 11 were observed even when anhydrite remained in the system.

The results of these simulations indicate that two factors could be important for controlling brine pH as CPR degrades and iron corrodes in the repository: (1) the amounts of alkaline earth sulfates (anhydrite and gypsum) available for dissolution during sulfate reduction and (2) the relative rates of CPR degradation and iron corrosion. If the amounts of anhydrite and gypsum are relatively limited, the pH may be significantly increased during the sulfate reduction reaction. In addition, if iron corrosion and iron sulfide solid phase formation are rapid relative to the CPR degradation rate, the modeling results indicate that high pH may occur in WIPP brines.

3.3 LICHTNER (2007)

Lichtner (2007) carried out reaction-path calculations to evaluate the approach taken in the Brush et al. (2006) EQ3/6 calculations. Lichtner (2007) used the FLOTRAN reactive-transport computer code (Lichtner 2001) to consider two aspects of the Brush et al. (2006) modeling approach: (1) whether the conceptual model was appropriate, and (2) whether the reaction-path simulations carried out by Brush et al. (2006) were reasonable.

Lichtner (2007) carried out FLOTRAN calculations that reproduced two EQ6 titration calculations performed by Brush et al. (2006); the original simulations are indicated in Tables 3-1 and 3-2. These simulations were performed with either GWB or ERDA-6 brine, and with limited quantities of Salado minerals, which equaled 44 to 45% of the minerals predicted to be present in the DRZ. In the Brush et al. (2006) calculations, a relatively moderate pH of 8.53 was predicted using GWB brine, whereas a relatively high pH of 11.3 was predicted using ERDA-6 brine.

Lichtner (2007) reviewed the EQ6 results of Brush et al. (2006) for the two selected simulations. Lichtner (2007) noted abrupt pH increases in the simulation with ERDA-6 brine upon the disappearance of eugsterite [$\text{Na}_4\text{Ca}(\text{SO}_4)_3 \cdot 2\text{H}_2\text{O}$], anhydrite, and finally syngenite. In the simulation with GWB brine, sulfate concentrations remain relatively constant as sulfate titrated out of the system is replaced by anhydrite dissolution. In comparison, sulfate concentrations in the simulation with ERDA-6 brine declined as the pH increased above approximately 9.5.

The two selected EQ6 simulations of Brush et al. (2006) were repeated using the FLOTRAN code and substantially the same results were obtained. However, Lichtner (2007) noted that removing oxychloride-Mg from the starting mineral assemblage for the GWB brine simulations resulted in high pH. Additional FLOTRAN simulations were carried out with the inclusion of organic matter and iron metal in the system. These results were qualified by noting that Pitzer parameters for sulfide and iron species were not included in the calculations, and the possible passivation of iron by sulfide was not considered (Lichtner 2007). High pH values were predicted after anhydrite and syngenite disappeared from the mineral assemblage, when complete degradation of organic matter had occurred. Hydrogen gas partial pressures at the end

of the simulations were 600 atm, which is significantly in excess of lithostatic pressure at the repository depth.

Based on the results of these calculations, Lichtner (2007) provided a number of observations and recommendations:

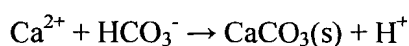
- High pH needs to be considered as a possible outcome from interaction of WIPP brine with waste materials and Salado formation minerals
- Modeling results appear to be sensitive to the choice of primary minerals
- The titration model used in WIPP simulations appears to be too limited in scope, because it forces a pre-selected overall reaction on the system, time was not explicitly considered, and the potential effects of volume changes in the minerals during reaction were not included
- A more realistic model of the system should be developed that includes organic matter, iron and sulfide, with the appropriate Pitzer data and that explicitly takes into account mineral reaction kinetics
- Perform column and batch type experiments as feasible to determine reaction products and kinetics for degradation of organic matter, sulfate reduction, and interaction with host rock minerals
- Develop a self-consistent thermodynamic database for minerals, gases, and aqueous species relevant to WIPP
- Consider the role of lead used in shielding on geochemical reactions
- A more rigorous approach would take into account the spatial distribution of the waste and host rock, explicitly accounting for mass transfer by advection/dispersion and diffusion combined with chemical reactions
- The effects of microenvironments which persist over long time spans through diffusion-limited mass transfer to primary flow domains should be considered

3.4 OCTOBER 2007 EPA/DOE TECHNICAL EXCHANGE MEETING

EPA and DOE staff and their contractors participated in a technical exchange meeting in Las Vegas, Nevada, on October 3, 2007. The purpose of this meeting was to discuss the Brush et al. (2006) geochemical modeling results, particularly the high predicted pH values and the possible implications of these results for the chemistry-related conceptual models. Details of this meeting are provided in SCA (2007). The meeting was attended by Peter Lichtner, David Sassani, and Thomas Wolery, who provided summaries of their reviews of the EQ3/6 modeling performed by Brush et al. (2006).

The potential effects of excess calcium-sulfate minerals on the reaction-path calculations were addressed. Brush et al. (2006) assumed for the EQ3/6 calculations that the amount of Salado minerals present in the system was the quantity needed to provide the moles of sulfate for CPR degradation by sulfate reduction. Limiting the amount of calcium-sulfate minerals in the calculations ensured that these minerals would be completely consumed, which may have caused the high pH values. Wolery and Sassani (2007) observed that this effect was related to the titration approach used by Brush et al. (2006), and recommend incorporating the CPR degradation reaction directly into EQ3/6.

During the discussion, it was agreed that the presence of additional calcium-sulfate minerals in the system might prevent high pH values, because excess calcium ion could result in the release of hydrogen ion via the calcite precipitation reaction:



This reaction could buffer pH, preventing pH values significantly greater than 9 or 10. The presence of excess anhydrite is assumed in the Chemical Conditions conceptual model, so the assumption that all calcium-sulfate minerals could be consumed by reaction would constitute a significant change to the model.

Anoxic corrosion of iron and the precipitation of FeS(s) apparently caused the high pH in the geochemical calculations carried out by Lichtner (2007) and by Wolery and Sassani (2007). The available WIPP data on the CPR degradation rates, anoxic corrosion of iron, and iron sulfide formation rates were not communicated to the authors prior to preparation of their reports. The assumed rates of these reactions could have significantly affected the results of their calculations. For example, high H₂S gas pressures in iron corrosion tests in WIPP brines have resulted in low long-term FeS(s) formation rates (Telander and Westerman 1997), which could prevent high pH values. The participants agreed that additional geochemical calculations were necessary before conclusions could be reached about the probability of high pH values in the repository brines and the important geochemical processes in the WIPP system. It is possible that including the effects of excess calcium-sulfate minerals and slow FeS(s) formation in WIPP could prevent significantly elevated brine pH values.

The following conclusions were developed based on information presented at the meeting:

- Updating the geochemical modeling calculations of Brush et al. (2006) to include iron and sulfide aqueous species and solids, as well as CPR, could have significant effects on the predicted pH values. If high pH values (greater than 10) are expected to be sustained in WIPP brines, then pH-buffering reactions influenced by silica aqueous species and solids may also be important.
- The limited amounts of calcium-sulfate minerals used in the EQ3/6 calculations may have resulted in the high calculated pH values by Brush et al. (2006), as well as the calculations performed by the technical reviewers.
- Water produced by CPR degradation could affect brine quantities and ionic strength.
- Reaction rates could have an impact on transient geochemical conditions and could result in actinide solubilities that are not bounded by the assumption of equilibrium.

- The potential evolution toward a high-pH, magnesium-sulfide brine could affect predicted actinide solubilities.
- $H_2(g)$ and $CH_4(g)$ generation and transport within the system could affect the geochemical modeling results.
- The potential effects of changes in mineral volumes and porosity as a result of the geochemical reactions should be considered.
- Because of the availability of additional WIPP-relevant geochemistry data, it is appropriate to consider whether significant improvements can be made to the WIPP geochemistry conceptual model. It may be possible to incorporate the effects of some processes (such as anoxic iron corrosion) that were previously included in PA through simplifying assumptions.

4.0 EPA EQ3/6 MODELING CALCULATIONS

The geochemical modeling calculations performed by Brush et al. (2006), Wolery and Sassani (2007), and Lichtner (2007) were not completely consistent with the chemistry-related conceptual models (Section 2.0). Geochemical modeling calculations must adequately incorporate important assumptions in the conceptual models to ensure that the system being modeled corresponds to the expected features and behavior of the WIPP system. Additional EQ3/6 geochemical reaction-path modeling calculations that more closely correspond to the conceptual model assumptions were therefore performed as part of the present investigation.

4.1 CONCEPTUAL MODEL CONSIDERATIONS

Based on the results of the Brush et al. (2006) modeling calculations, it appears that the amounts of Salado minerals included in the calculations can significantly affect predicted brine chemistry. The results of modeling calculations performed by Wolery and Sassani (2007) and by Lichtner (2007) showed that the reaction of iron and sulfide in the system may have important effects. Finally, results obtained by Wolery and Sassani (2007) indicated that the relative rates of iron corrosion and CPR degradation may also affect brine chemistry. These potential issues were considered in formulating the input files for the EQ3/6 verification calculations.

Stein (1985) investigated the Salado Formation mineralogy by examining core materials obtained 50 feet above and 50 feet below a test room at WIPP. Stein (1985) identified six different lithologies in the cores based on visual appearance: (1) "clean" halite, (2) polyhalitic halite, (3) argillaceous halite, (4) mixed argillaceous-polyhalitic halite, (5) anhydrite layers, and (6) clay seams. Core samples were selected for testing from approximately every other foot of the cores, and included all of the dominant lithologies. However, it was not clear that the amounts of each lithology in the selected core samples were representative of their relative abundance.

Crushed core samples were tested to determine the weight fraction that was soluble in water, and this fraction was assumed to consist of halite. Samples of the water-insoluble residues were removed for qualitative mineralogical identification by x-ray diffraction (XRD). The remaining water-insoluble fraction was subjected to boiling in an EDTA solution, which was assumed to remove divalent carbonates and sulfates, such as calcite and anhydrite. The final residue that was insoluble in both water and EDTA was assumed to be composed of silicate minerals, such as quartz and clays.

Stein (1985) stated that the average water-soluble (halite) fraction of the tested core samples was 94.44 wt%. However, Brush (1990) used the data reported in Table 1 of Stein (1985) to calculate that 93.2 wt% of the core material was halite. The average value reported by Brush (1990) was checked as part of the present investigation and found to be correct. Based on the XRD data, Stein (1985) identified quartz, magnesite, anhydrite, gypsum, halite, polyhalite, bassanite [$\text{CaSO}_4 \cdot 0.5\text{H}_2\text{O}$], alkali feldspar [$(\text{Na,K})\text{AlSi}_3\text{O}_8$], and clay minerals in the water-insoluble fraction of the cores. Because this XRD evaluation of the mineralogical composition was only semiquantitative, Brush (1990) assumed that the non-halite fraction of the Salado Formation was equal parts magnesite, anhydrite, gypsum, and polyhalite (1.7 wt% each). The resulting mineral percentages of halite, magnesite, anhydrite, gypsum, and polyhalite summed to

100%. Brush (1990) did not include clay minerals, feldspar, and quartz in the assumed mineralogy because of the lack of Pitzer data for aqueous silica species; bassanite was not included in the assumed mineralogy, because it was observed in only one sample.

The relative amount of polyhalite in the Salado Formation could impact the geochemical modeling results if the available calcium-bearing sulfate minerals are limited. Accordingly, the XRD data from the water-insoluble residues from the core samples were re-examined (Table 4-1). Of the 44 samples evaluated, only four of the samples had reported polyhalite in the XRD data. In three of these four samples, polyhalite appeared to be less abundant than other minerals in the sample. Only one sample (FH-210) had results indicating that polyhalite was the most abundant non-halite mineral.

The difficulty of determining the mineralogical composition of the Salado core samples by visual examination can be illustrated by comparing the XRD data from many of the samples with their lithological descriptions that indicate the presence of polyhalite. For example, the lithological description of sample FH-202 from within MB 139 is "polyhalitic halite." However, XRD of the water-insoluble residue did not identify polyhalite in this sample. In fact, within the estimated extent of the DRZ above and below the rooms, as currently excavated up to the Anhydrite *a* layer, polyhalite was identified by XRD only in sample FH-224 (Table 4-1). Consequently, it is probable that the percentage of polyhalite in the Salado Formation near the repository horizon will be significantly less than the other non-halite minerals, such as anhydrite, magnesite, and quartz.

The assumption that repository brines will be in equilibrium only with Salado Formation minerals within the DRZ is not part of the Chemical Conditions conceptual model. The assumption that the brines will only equilibrate with minerals from within the DRZ originated in the analysis by Kanney et al. (2004), and could conflict with the Chemical Conditions conceptual model assumption that repository brines will be in equilibrium with halite, anhydrite, brucite, and magnesite. Modeling calculations carried out by Brush et al. (2006), Wolery and Sassani (2007), and Lichtner (2007) have demonstrated that assuming that limited amounts of Salado minerals are available to equilibrate with the brines may have a significant effect on predicted repository chemical conditions. To ensure that sufficient quantities of Salado minerals were available to brine during the reaction-path calculations described in this section, it was assumed for most calculations that mineral quantities equal to 100% of the estimated DRZ volume were present in the system. At the end of the simulations, the results were checked to confirm that excess anhydrite remained in equilibrium with the brine, which is consistent with the currently accepted Chemical Conditions conceptual model. To confirm the sensitivity of the reaction-path modeling results to limited availability of anhydrite and gypsum, a few calculations were also performed with smaller proportions of Salado minerals.

The thermodynamic database used in most of the calculations was the HMX database provided by Wolery and Sassani (2007). Wolery and Sassani (2007) developed this database by adding iron and sulfide species without Pitzer parameters to the HMO database of Brush et al. (2006). This database also contained thermodynamic data for the organic ligands assumed to be present in the waste inventory: acetate, citrate, EDTA, and oxalate.

Table 4-1. Stein (1985) Salado Core Sample Data

Sample Number	Sample (m)	Water-Insoluble Residue (wt %)	EDTA-Insoluble Residue (wt %)	Water-Insoluble Mineralogy ^a	Comments	Sample Description (Stein 1985, Appendix B)
FH-201	0.61-0.76	0.36	0.21	Q>M>H	Downward core, in DRZ	Clear with trace polyhalite
FH-202	1.22-1.43	34.35	0.17	A>H>M?	Downward core, Marker Bed 139, in DRZ	Polyhalitic halite
FH-203	2.53-2.74	2.02	0.65	Q>A>M	Downward core	8.3 to 8.5 ft mixed clay/polyhalite; 8.5 to 9 ft clear
FH-204	3.29-3.44	0.93	0.48	M≥Q≥H (traces)	Downward core	Clear, trace polyhalite (5 pieces)
FH-205	3.96-4.13	0.05		Q	Downward core	Polyhalitic (4 pieces)
FH-206	4.74-4.83	3.89	2.05	Q>A>M=H	Downward core	Mixed clay/polyhalite
FH-207	5.15-5.32	0.20	0.10	M>Q>P≥A	Downward core	Clear, coarsely crystalline, trace polyhalite
FH-208	5.61-5.82	0.40		G>H>A>Q>M	Downward core	Polyhalitic (3 pieces)
FH-209	5.99-6.11	0.17	0.06	M>Q	Downward core	Polyhalitic (3 pieces)
FH-210	6.55-6.71	1.87	0.28	P>G>M>Q	Downward core	Clear mottled with polyhalite
FH-211	7.01-7.16	0.51	0.25	Q>M>H>A	Downward core	Clear mottled with polyhalite
FH-212	7.65-7.83	0.81	0.425	M>Q>G	Downward core	Clear to mod. Reddish-orange, trace polyhalite
FH-213	7.92-8.08	0.65	0.34	M≥Q	Downward core	Clear to mod. Reddish-orange, trace polyhalite
FH-214	8.61-8.79	0.205	0.0125	G>>P	Downward core	Clear to mod. Reddish-orange, trace polyhalite, with some horizontal fractures
FH-215	9.30-9.46	0.07		insufficient sample	Downward core	Clear, coarsely crystalline, very little polyhalite
FH-216	9.45-11.58	1.47	0.89	M>Q	Downward core	Clear, trace gray clay, polyhalite
FH-217	11.96-12.15	2.51	0.94	M>Q≥G	Downward core	Grayish-brown mixed clay/polyhalite
FH-218	12.50-12.65	1.77	0.86	M>Q≥H	Downward core	Mixed clay/polyhalite, coarsely crystalline, very little polyhalite
FH-219	12.95-13.11	3.12	1.77	M≥Q	Downward core	Mixed clay/polyhalite, medium crystalline, very little polyhalite
FH-220	13.41-13.56	1.245	0.81	M>Q	Downward core	Mixed clay/polyhalite, coarsely crystalline
FH-221	13.81-13.98	0.54	0.35	M>Q	Downward core	Clear, coarsely crystalline
FH-222	14.33-14.48	0.79	0.45	M>Q	Downward core	Clear, trace gray clay
FH-223	14.95-15.10	0.30	0.13	M≥Q	Downward core	Clear, Trace gray clay/polyhalite
FH-224	1.22-1.37	61.14	0.92	A>G>P	Downward core, in DRZ	Medium reddish-orange polyhalite/anhydrite

a - Q = quartz, M = magnesite, H = halite, A = anhydrite, G = gypsum, P = polyhalite, B = bassanite; indicated abundances are approximate

Table 4-1. Stein (1985) Salado Core Sample Data (continued)

Sample Number	Sample (m)	Water-Insoluble Residue (wt %)	EDTA-Insoluble Residue (wt %)	Water-Insoluble Mineralogy ^a	Comments	Sample Description (Stein 1985, Appendix B)
FH-228	0.12–0.27	0.14	0.05	Q, M	Upward core, now excavated	Halite, clear to medium reddish-brown to light gray, coarsely, some fine to medium crystalline. Trace polyhalite and clay
FH-229	0.70–0.85	0.08	0.025	Q, A, trace M, trace H	Upward core, now excavated	Halite, clear to medium reddish-brown to light gray, coarsely, some fine to medium crystalline. Trace polyhalite and clay
FH-230	1.45–2.06	0.24	0.11	Q, M	Upward core, now excavated	Halite, clear to medium reddish-brown to light gray, coarsely, some fine to medium crystalline. Trace polyhalite and clay
FH-231	2.16–2.23	28.32	0.03	A	Upward core, Anhydrite <i>b</i> , now excavated	Anhydrite <i>b</i> with halite 7.2 to 7.3 ft
FH-232	2.36–2.48	0.36	0.025	A	Upward core, in DRZ	Halite, clear to medium reddish-orange, medium to coarsely crystalline, white anhydrite stringers
FH-233	2.48–2.77	0.05	0.01	A	Upward core, in DRZ	Halite, clear to medium reddish-orange, medium to coarsely crystalline, white anhydrite stringers
FH-234	3.20–3.32	1.35	0.002	A	Upward core, in DRZ	Halite, clear to medium reddish-orange, medium to coarsely crystalline, white anhydrite stringers
FH-235	3.70–3.84	0.29	0.001	Q, M, A	Upward core, in DRZ	Halite, clear to medium reddish-orange, medium to coarsely crystalline, white anhydrite stringers, with trace gray clay
FH-236	4.27–4.40	87.08	0.20	A	Upward core, Anhydrite <i>a</i> , in DRZ	Anhydrite <i>a</i>
FH-237	4.91–5.06	1.86	0.10	A, G, B, trace H	Upward core, in DRZ	Polyhalite halite
FH-238	8.84–8.99	6.31	2.81	Q, M	Upward core, in DRZ	Halite with brown clay, coarsely crystalline

a - Q = quartz, M = magnesite, H = halite, A = anhydrite, G = gypsum, P = polyhalite, B = bassanite

Table 4-1. Stein (1985) Salado Core Sample Data (continued)

Sample Number	Sample (m)	Water-Insoluble Residue (wt %)	EDTA-Insoluble Residue (wt %)	Water-Insoluble Mineralogy ^a	Comments	Sample Description (Stein 1985, Appendix B)
FH-239	10.38–10.52	3.10	1.36	Q, M	Upward core, in DRZ	Argillaceous halite
FH-240	11.25–11.46	26.30	0.60	Q, A, trace M, trace G	Upward core, in DRZ	Anhydrite with some halite
FH-241	11.64–11.80	0.30	0.002	A	Upward core, in DRZ	Halite with trace polyhalite, magnesite stringers
FH-242	13.12 - 13.27	1.62	1.10	Q, trace M, trace A	Upward core, in DRZ	Argillaceous halite
FH-243	14.39–14.54	0.75	0.215	Q, A, trace M, trace G	Upward core, in DRZ	Halite, trace polyhalite and clay
FH-244	15.13–15.24	9.68	5.68	Q, trace M, trace A	Upward core, in DRZ	Argillaceous halite
FH-245	15.64–15.88	9.30	2.22	Q, M, trace A	Upward core, in DRZ	Argillaceous halite, break at 52.1 ft
FH-246	6.11–6.23	0.80	0.29	Q,M, trace A	Upward core, in DRZ	Halite, trace of clay and polyhalite
FH-247	7.15–7.30	13.53	0.36	trace Q, trace M, A	Upward core, in DRZ	Halite with gray anhydrite, trace clay
FH-248	7.77–7.92	0.05	0.0125	Q, A, trace M	Upward core, in DRZ	Halite- clear, coarsely crystalline
FH-249	13.72–13.91	0.55	0.25		Upward core, in DRZ	Halite, trace brown clay, coarsely crystalline

a - Q = quartz, M = magnesite, H = halite, A = anhydrite, G = gypsum, P = polyhalite, B= bassanite

The amounts of Salado minerals included in the EQ3/6 calculations (Table 4-2) were based on their expected proportions to brine volumes in the repository. These proportions must be scaled to 1 kg of water in the brine for input into the EQ3/6 calculations. The moles of halite, anhydrite, gypsum, magnesite, and polyhalite in the DRZ were calculated for GWB brine and for ERDA-6 brine, with the same assumptions about brine volumes as those made by Brush et al. (2006). The moles of iron and CPR carbon were calculated based on inventory data for the PABC (Leigh et al. 2005b), and the moles of MgO were calculated by multiplying the moles of CPR carbon by the Excess Factor of 1.20. However, the results of these calculations differed slightly from those of Brush et al. (2006) because in that investigation, the amount of CPR carbon from emplacement cellulosics and plastics in the inventory was not included.

A number of iron sulfide phases may form in the repository. In the presence of H₂S, the expected sequence of iron sulfide phases that would form over time would be in the order: mackinawite [FeS_{1-x}] → troilite [FeS] → pyrrhotite [Fe_{1-x}S] → pyrite [FeS₂] (Telander and Westerman 1993). Telander and Westerman (1997) only identified mackinawite in their experiments with iron corrosion in an H₂S atmosphere. This phase was not included in the EQ3/6 database, so troilite was assumed to be the stable iron-sulfide phase in the reaction-path calculations.

The relative rates of CPR degradation and iron corrosion may affect the final results of the EQ3/6 calculations. If reaction (15) takes place as written, the moles of iron corroded and the moles of sulfate reduced will be exactly equal, and all Fe²⁺ and sulfide will precipitate as FeS. The rates of CPR degradation and iron corrosion used in the PABC were based on the results of long-term degradation experiments with cellulose, as well as long-term anoxic iron corrosion experiments in brine. Comparison of the average rates used in the PABC indicated that approximately 9 moles of iron would corrode per mole of cellulose degraded. There is some evidence that H₂S will reduce the anoxic corrosion rate of iron (Telander and Westerman 1997), although the available evidence does not demonstrate that it will be completely inhibited by H₂S partial pressures of 1 atm or less (Telander and Westerman 1993, 1997). Consequently, the maximum ratio of iron corroded to cellulose degraded in the EQ3/6 calculations was set equal to 9:1.

Table 4-2. Amounts of Salado Minerals Calculated for EQ3/6 Input Files, Equivalent to 100% of the DRZ; Scaled to 1 kg Water in Brine

Brine	GWB	GWB	ERDA-6	ERDA-6	ERDA-6
Brine Volume (m ³)	1,045	7,763	1,045	7,763	13,267
Carbon (moles) ^a	133	17.9	125	16.8	9.85
Brucite (moles)	161	21.7	152	20.4	11.9
Halite (moles)	6,430	866	6,050	814	476
Anhydrite (moles)	50.4	6.78	47.3	6.37	3.73
Gypsum (moles)	39.8	5.36	37.4	5.04	2.95
Magnesite (moles)	88.7	11.9	83.4	11.2	6.57
Hydromagnesite (moles)	17.7	2.39	16.7	2.24	1.31
Polyhalite (moles)	11.4	1.53	10.7	1.44	0.842
Iron (moles)	108	14.5	101	13.6	7.98

a - Moles of CPR carbon remaining after degradation by microbial reactions utilizing waste sulfate and nitrate

4.2 GWB CALCULATIONS

The first step in the modeling calculations was to reproduce results obtained by Wolery and Sassani (2007). This ensured that the EQ3/6 software was properly installed and that the input files were correct. This calculation was performed with the reaction formulated as a titration. The CPR degradation reaction (2) was simulated by adding 2 CO₂ to the solutions and subtracting 2 H⁺ + SO₄²⁻. The amounts of Salado minerals included in the calculations were equal to 49% of the mineral quantities expected to be present in the DRZ with 1,045 m³ of GWB brine assumed to be present in the repository (Table 4-2). For this calculation, the HMO database was used, which is the database used by Wolery and Sassani (2007) for the equivalent calculations. The EQ3/6 modeling calculations reproduced the previous results, with the final pH predicted to be 11.3 (Table 4-3, Figure 4-1). Figure 4-1 shows that the pH was less than 9 until anhydrite dissolved. The pH then increased to approximately 9.5 until the mineral syngenite dissolved and the pH increased to 11.3. Another EQ3/6 modeling calculation performed by Wolery and Sassani (2007) was repeated as part of the current investigation. In this calculation, set up as a titration, the amounts of Salado minerals present at the start of the simulation were reduced to quantities consistent with 25% of the DRZ (Table 4-3). The results were similar to those obtained with 49% of the DRZ, except the sulfate minerals were depleted and the brine pH increased earlier during the course of the reaction progress. These results reproduced those of Wolery and Sassani (2007), demonstrating that the software was properly installed and functioning as expected.

In formulating the input files for these two simulations, it was assumed that the percentages of Salado minerals in the DRZ available to the brine were 49% or less, and the brine did not remain in equilibrium with anhydrite. Consequently, these calculations are not consistent with the existing Chemical Conditions conceptual model (Section 2.3). Wolery and Sassani (2007) had previously demonstrated that addition of iron and sulfide species to the titration calculations resulted in relatively high pH values when the quantities of sulfate-bearing minerals were limited (Section 3.2.2, Table 3-3). To evaluate the effect of an excess amount of anhydrite on the pH of the titration calculations with iron and sulfide species included in the system, another EQ3/6 calculation was performed. This calculation was the same as the Wolery and Sassani (2007) calculation (output file 1GWB-2m1.6o), except the quantities of Salado minerals included at the

beginning of the simulation equaled the amounts predicted to be present if 100% of the DRZ is available for reaction, and hydromagnesite was assumed to be the magnesium-carbonate product phase. The results of this calculation indicated a final pH of 7.89, and anhydrite was present in the final mineral assemblage (Table 4-3, Figure 4-2). This pH is reasonably consistent with the moderately alkaline pH values (pH 8 to 10) in the Chemical Conditions conceptual model.

As an alternative to performing the reaction-path calculations as a titration, Wolery and Sassani (2007) recommended carrying out the EQ3/6 calculations by including cellulose as a special reactant. Wolery and Sassani (2007) recommended using cellulose as a reactant in the modeling calculations to ensure that the reactions were set up correctly in the input file and to account for the possible production or consumption of water by the overall reaction. The titration reaction with 100% of the DRZ and with hydromagnesite assumed to be present instead of magnesite was repeated with cellulose included as a special reactant in modeling calculations for the present investigation (Table 4-3, Figure 4-3). The results of this calculation were similar to the results obtained using the titration approach, except oxychloride-Mg was not present in the final reaction products and the pH was slightly higher than in the titration calculations (Figure 4-2). Because the use of cellulose as a special reactant more directly represents expected repository reactions, the majority of the calculations in the current investigation were performed using this approach.

The effects of limited availability of sulfate minerals for the CPR degradation reaction were tested by repeating the calculations with 49% and 25% of the DRZ minerals available to react (Table 4-3). These calculations were similar to those of Wolery and Sassani (2007), except for slight differences in the amounts of Salado minerals (Table 4-2), and the assumption that hydromagnesite would not transform into magnesite. The results were similar to the results obtained by Wolery and Sassani (2007) (Table 3-3), except for slightly higher pH values. The results of the calculations with 49% of the DRZ minerals available for reaction are illustrated in Figure 4-4. The pH of the solution remained relatively stable between approximately 8.1 and 8.3, until sulfate reduction occurred to the point at which anhydrite was no longer stable. After sulfate reduction progressed further and syngenite was no longer stable, the pH rose rapidly as a function of reaction progress. As observed in the results reported by Wolery and Sassani (2007), the predicted methane fugacity values for both the 49% and 25% DRZ calculations were higher than could realistically occur in the repository (Table 4-3). In calculations with 25% of the DRZ minerals available to react (Figure 4-5), iron metal was predicted to become stable at conditions with an extremely high methane fugacity (approximately 10^{36} or higher). These conditions will not exist in the repository, because the methane pressure corresponding to this fugacity would certainly exceed the lithostatic pressure. As a result of these high gas pressures, it is expected that the gas would fracture the anhydrite interbeds and escape from the repository. It is also uncertain whether iron metal would be thermodynamically stable in the presence of water: the Gas Generation conceptual model assumes that iron corrosion would occur in the presence of water to form $\text{Fe}(\text{OH})_2 \cdot x\text{H}_2\text{O}$. However, iron was predicted to stably persist only at high methane fugacities, probably as a consequence of the unrealistically reducing conditions. The lack of Pitzer parameters for iron species also could have affected the results of these calculations.

Table 4-3. Results of EQ3/6 Modeling Calculations with 1,045 m³ GWB Brine Performed for the Present Investigation

Brine	GWB	GWB	GWB	GWB	GWB	GWB
Brine Volume (m ³)	1,045	1,045	1,045	1,045	1,045	1,045
Organic Ligands	None	None	None	None	None	None
EQ6 Output File	g25tm1sn.6o	g22tm1sn.6o	g21th1.6o	g21chlfe.6o	g25chlfe.6o	g22chl.6o
Suppressed Minerals	Dolomite, glauberite	Dolomite, glauberite	Dolomite, glauberite, polyhalite, magnesite, magnetite, pyrite	Dolomite, glauberite, polyhalite, magnesite, magnetite, pyrite	Dolomite, glauberite, polyhalite, magnesite, magnetite, pyrite	Dolomite, glauberite, polyhalite, magnesite, magnetite, pyrite
Salado Minerals (% DRZ)	49	25	100	100	49	25
Relative rates cellulose:Fe	n.a.	n.a.	1:3 *	1:3	1:3	1:3
Final pH	11.3	11.3	7.89	8.14	10.9	12.0
Final log f _{CO2}	-6.93	-6.93	-5.48	-5.48	-5.48	-5.48
Final log f _{CH4}	n.a.	n.a.	-5.70	-5.76	36.2	44.1
Final log f _{H2S}	n.a.	n.a.	-0.874	-0.937	-5.22	-6.34
Final Total Carbonate (m)	0.250	0.249	8.50 × 10 ⁻⁴	5.21 × 10 ⁻⁴	6.11 × 10 ⁻⁴	1.71
Final Solid Phases	Brucite, calcite, halite, magnesite, pirssonite, sylvite	Brucite, calcite, halite, magnesite, pirssonite, sylvite	Anhydrite, brucite, calcite, halite, hydromagnesite, oxychloride-Mg, syngenite, troilite	Anhydrite, brucite, calcite, halite, hydromagnesite, syngenite, troilite	Brucite, calcite, halite, hydromagnesite, pirssonite, sylvite, troilite	Brucite, calcite, halite, hydromagnesite, iron, sylvite, troilite
Reaction Progress	66	66	66	66.5	66.5	63.9 **
Database	HMO	HMO	HMX	HMX	HMX	HMX
Notes	Reproduced the titration results of Wolery and Sassani (2007)	Reproduced the titration results of Wolery and Sassani (2007)	Modified the titration results of Wolery and Sassani (2007) by including 100% of the DRZ minerals and suppressing magnesite formation	Cellulose included as a special reactant; modified results of Wolery and Sassani (2007) by including 100% of the DRZ minerals and suppressing magnesite formation	Cellulose included as a special reactant; modified results of Wolery and Sassani (2007) by suppressing magnesite formation	Cellulose included as a special reactant; modified results of Wolery and Sassani (2007) by including 25% of the DRZ minerals and suppressing magnesite formation

n.a. = Not Applicable.

* Input of iron equaled sulfide generation.

** Calculation ended when maximum number of steps was reached. Additional reaction would be expected to slightly increase pH.

The effects of magnesite formation instead of hydromagnesite on the results of the simulations were evaluated by repeating the calculations with a GWB brine volume of 1,045 m³, 100% of the DRZ minerals available for reaction, and allowing magnesite to form (Table 4-4). The formation of magnesite instead of hydromagnesite resulted in a slight increase in pH, but no other significant differences. Organic ligands (acetate, citrate, EDTA, and oxalate) at concentrations consistent with those expected in the repository did not affect the EQ3/6 simulation results (Table 4-4). The potential effects of the inhibition of calcite formation were examined by suppressing both calcite and aragonite precipitation in a separate EQ3/6 calculation; the result was a slightly higher pH of 9.00, instead of 8.14 (Tables 4-3 and 4-4). In the simulations with 100% of the DRZ assumed to be available for reaction, the brines remained saturated with respect to anhydrite and the pH remained between 8 and 10, consistent with the Chemical Conditions conceptual model.

The maximum predicted GWB brine volume of 7,763 m³ was used in another set of EQ3/6 calculations, assuming either 100% of the DRZ minerals or 25% of the DRZ minerals were available to react. The results of the calculations with 7,763 m³ of GWB brine and 100% of the DRZ minerals (Table 4-4, Figure 4-6) were very similar to the results previously obtained with 1,045 m³ of GWB brine and 100% of the DRZ minerals (Table 4-3, Figure 4-3). However, the predicted pH values obtained with 7,763 m³ of GWB brine and only 25% of the DRZ minerals available (Table 4-4, Figure 4-7) are not consistent with the results obtained with the smaller GWB brine volume (Table 4-3, Figure 4-5). In both sets of calculations with 25% of the DRZ minerals and GWB brine, the pH was predicted to remain at slightly alkaline levels during the early stages of reaction progress as anhydrite and syngenite dissolved (Figures 4-5 and 4-7). However, as the reaction proceeded and sulfate was consumed, only a slight pH increase occurred in the simulation with 7,763 m³ of GWB brine, compared to the dramatic increase observed in the simulation with 1,045 m³. In both simulations, metallic iron was predicted to become stable in the presence of brine and extremely high methane fugacities were predicted (Figures 4-5 and 4-7, Tables 4-3 and 4-4). These conditions are unlikely to exist in the repository because of the limitations on gas pressure and because the Gas Generation conceptual model includes the assumption that metallic iron will not be stable in the presence of brine. The brines in these simulations do not remain in equilibrium with anhydrite, which is an assumption included in the Chemical Conditions conceptual model, and such an extreme limitation on the amount of sulfate available appears inconsistent with the Salado mineralogy. Consequently, these simulations with 25% of the DRZ minerals available are unlikely to accurately represent repository conditions. The predicted stability of metallic iron in the presence of water is likely to be a consequence of the unrealistically high methane fugacity; the lack of Pitzer parameters for iron may also have had an effect on the results of these calculations.

Table 4-4. Results of EQ3/6 Modeling Calculations with GWB Brine: Effects of Magnesite Formation, Organic Ligands, Calcite Suppression, and Increased GWB Brine Volume

Brine	GWB	GWB	GWB	GWB	GWB
Brine Volume (m³)	1,045	1,045	1,045	7,763	7,763
Organic Ligands	None	Acetate, citrate, EDTA, oxalate	None	None	None
EQ6 Output File	g21cm1fe.6o	g21chl0r.6o	g21chlnc.6o	g21ch7.6o	g22ch7.6o
Suppressed Minerals	Dolomite, glauberite, polyhalite, magnetite, pyrite	Dolomite, glauberite, polyhalite, magnesite, magnetite, pyrite	Dolomite, glauberite, polyhalite, magnesite, magnetite, pyrite, calcite, aragonite	Dolomite, glauberite, polyhalite, magnesite, magnetite, pyrite	Dolomite, glauberite, polyhalite, magnesite, magnetite, pyrite
Salado Minerals (% DRZ)	100	100	100	100	25
Relative rates cellulose: Fe	1:3	1:3	1:3	1:3	1:3
Final pH	8.75	8.14	9.00	8.22	8.43
Final log f_{CO2}	-6.95	-5.48	-5.48	-5.48	-5.48
Final log f_{CH4}	-6.14	-5.76	-4.31	-5.98	35.9
Final log f_{H2S}	-1.32	-5.87	-1.49	-1.17	-7.40
Final Total Carbonate (m)	2.66×10^{-5}	5.22×10^{-4}	1.50×10^{-3}	4.55×10^{-4}	6.05×10^{-4}
Final Solid Phases	Anhydrite, brucite, calcite, halite, magnesite, sylvite, syngenite, troilite	Anhydrite, brucite, calcite, halite, hydromagnesite, sylvite, syngenite, troilite	Anhydrite, brucite, CaCO ₃ (am), halite, hydromagnesite, sylvite, syngenite, troilite	Anhydrite, brucite, calcite, halite, hydromagnesite, oxychloride-Mg, syngenite, troilite	Brucite, calcite, halite, hydromagnesite, iron, troilite
Reaction Progress	66.5	66.5	66.5	8.95	8.95
Database	HMX	HMX	HMX	HMX	HMX
Notes	Cellulose included as a special reactant; magnesite allowed to precipitate	Cellulose included as a special reactant; organic ligands included	Cellulose included as a special reactant, formation of calcite and aragonite suppressed	Cellulose included as a special reactant, larger GWB brine volume assumed	Cellulose included as a special reactant, larger GWB brine volume assumed

Examination of the Salado mineralogy data indicates that the proportions of polyhalite may have been overestimated, and Brush et al. (2006) found that polyhalite dissolution may account for high predicted pH values in simulations with limited sulfate availability. To test the effects of smaller amounts of polyhalite on predicted pH values, simulations were repeated with 1,045 m³ of GWB brine, and 49% of the DRZ minerals for available for reaction, with the amount of polyhalite included equal to either half the amount previously used or with no polyhalite included (Table 4-5). The results with half of the predicted polyhalite yield a slightly increased final pH value (11.1 compared to a pH of 10.9 with all of the predicted polyhalite). However, with no polyhalite included in the Salado mineral assemblage, the predicted pH of 9.00 was significantly lower. In both calculations with reduced amounts of polyhalite, extremely high methane fugacities and the stable persistence of iron were predicted. These conditions resulted from limitations on the amount of sulfate available in the system and are not consistent with the Chemical Conditions conceptual model. As previously noted, such conditions of high methane fugacity will not occur in the repository.

The relative rates of CPR degradation and iron corrosion used in the majority of the calculations were the same as those used by Wolery and Sassani (2007), with one mole of cellulose degraded per three moles of iron corroded. The effects of the relative rates of iron corrosion to CPR degradation were determined by first repeating the simulation with the iron corrosion rate equal to half of the previous rate (2 moles of cellulose per three moles of iron). This simulation with 1,045 m³ of GWB brine and 100% of the DRZ minerals available for reaction resulted in similar results, although the lower iron corrosion rate resulted in a slightly lower predicted pH of 7.69. Increasing the iron corrosion rate by a factor of three (1 mole of cellulose per 9 moles of iron) approximately corresponds to the average CPR degradation rate and iron corrosion rate used in the PABC. The higher corrosion rate used in a simulation with 1,045 m³ of GWB brine and 100% of the DRZ minerals available to react resulted in a slight increase in the predicted pH, from 8.14 (Table 4-3) to 8.48 (Table 4-5). Wolery and Sassani (2007) predicted that high brine pH values could develop in the absence of cellulose degradation if iron corrosion occurred with only 49% or 25% of the DRZ minerals available to react (Section 3.2.2). These simulations were repeated with the cellulose degradation rate set to zero, but with 100% of the DRZ minerals available to react. In this case, the brine pH did not increase significantly (Table 4-5).

In the calculations with the higher relative iron corrosion rates (Table 4-5), the iron reaction products included both iron sulfide (troilite) and iron oxide (hematite). These calculations are therefore not entirely consistent with the Gas Generation conceptual model, which assumes that Fe(OH)₂·xH₂O will form as a product of anoxic corrosion of iron. Repetition of these calculations with hematite formation suppressed would likely result in the predicted formation of Fe(OH)₂, which is the iron hydroxide phase in the database most similar to Fe(OH)₂·xH₂O. Replacement of hematite by Fe(OH)₂·xH₂O in the reaction products is unlikely to result in significant changes in the predicted brine chemistry.

Table 4-5. Results of EQ3/6 Modeling Calculations with GWB Brine: Effects of Polyhalite, Iron Corrosion Rates, and CPR Degradation Rate

Brine	GWB	GWB	GWB	GWB	GWB
Brine Volume (m ³)	1,045	1,045	1,045	1,045	1,045
Organic Ligands	None	None	None	None	None
EQ6 Output File	g25ch1p5.6o	g25ch1np.6o	g21ch1i5.6o	g21ch13x.6o	g21ch104.6o
Suppressed Minerals	Dolomite, glauberite, polyhalite, magnesite, magnetite, pyrite	Dolomite, glauberite, polyhalite, magnesite, magnetite, pyrite	Dolomite, glauberite, polyhalite, magnesite, magnetite, pyrite	Dolomite, glauberite, polyhalite, magnesite, magnetite, pyrite	Dolomite, glauberite, polyhalite, magnesite, magnetite, pyrite
Salado Minerals (% DRZ)	49% with half the predicted polyhalite	49% with no polyhalite	100	100	100
Relative rates cellulose:Fe	1:3	1:3	2:3	1:9	0:4
Final pH	11.1	9.00	7.69	8.48	8.42
Final log f _{CO2}	-5.48	-5.48	-5.48	-5.48	-5.48
Final log f _{CH4}	37.8	39.7	-5.74	-10.4	-10.4
Final log f _{H2S}	-7.06	-6.76	-0.924	-5.60	-5.60
Final Total Carbonate (m)	0.929	2.34×10^{-3}	1.82×10^{-3}	4.59×10^{-4}	4.44×10^{-4}
Final Solid Phases	Brucite, calcite, halite, hydromagnesite, sylvite, iron, troilite	Brucite, calcite, halite, hydromagnesite, iron, troilite	Anhydrite, brucite, calcite, halite, hydromagnesite, oxychloride-Mg, syngenite, troilite	Anhydrite, brucite, calcite, halite, hydromagnesite, syngenite, hematite, troilite	Anhydrite, brucite, calcite, halite, hydromagnesite, syngenite, hematite, troilite
Reaction Progress	66.5	66.5	66.5	66.5	27
Database	HMX	HMX	HMX	HMX	HMX
Notes	Cellulose included as a special reactant, half of the predicted DRZ polyhalite included in starting mineral assemblage	Cellulose included as a special reactant, no polyhalite included in starting mineral assemblage	Cellulose included as a special reactant, relative rate of iron corrosion reaction halved	Cellulose included as a special reactant, relative rate of iron corrosion reaction tripled	Relative rate of iron corrosion four times the anhydrite dissolution rate and no cellulose degradation

4.3 ERDA-6 CALCULATIONS

EQ3/6 calculations were also performed with ERDA-6 brine to evaluate the effects of brine composition on the modeling results. Two titration simulations were carried out to reproduce unpublished results used by Wolery and Sassani (2007). The first simulation did not include iron and sulfide species, whereas the second simulation did include these species (Table 4-6). The results of these calculations were similar to the unpublished results and indicated that, if 100% of the DRZ minerals are available to react, the brine would remain in equilibrium with anhydrite and pH values are likely to remain moderately alkaline. These results are consistent with the Chemical Conditions conceptual model.

The EQ3/6 calculation with ERDA-6 brine and with iron and sulfide included was repeated with cellulose defined as a special reactant and assuming that hydromagnesite would persist in the repository. This simulation was used as the “base case” for comparison with additional simulations. This simulation with 100% of the DRZ minerals assumed to be available for reaction resulted in a final predicted pH of 8.20. Comparing the results of this simulation to the equivalent calculation with GWB brine indicates that the initial brine composition had little effect on the predicted final brine pH or mineral assemblage (Tables 4-3 and 4-6).

The calculation with 1,045 m³ of ERDA-6 brine was repeated assuming that only 49% of the DRZ minerals were available to react; the results included a relatively high pH (10.9) and methane fugacity (10³⁶). These results are virtually identical to those obtained with GWB brine under the same conditions (Table 4-3). In both cases, these high methane fugacities are not expected to occur in the repository, because the anhydrite interbeds would be expected to fracture as gas pressures increased above lithostatic, allowing the gas to escape.

The effects of larger ERDA-6 brine volumes on the EQ3/6 simulation results were evaluated by repeating the calculation with 100% of the DRZ minerals available for reaction with 7,763 m³ and 13,267 m³ of ERDA-6 brine. The only difference between the results obtained with the three different ERDA-6 brine volumes was slightly higher pH values predicted for the larger brine volumes (Table 4-6). Comparison of the results with 100% of the DRZ minerals available for 7,763 m³ of GWB and ERDA-6 brine indicated only slight differences in the results, with slightly higher pH values predicted for ERDA-6 brine and the presence of oxychloride-Mg in the final mineral assemblage for GWB brine (Tables 4-4 and 4-6).

Table 4-6. Results of EQ3/6 Modeling Calculations with ERDA-6 Brine

Brine	ERDA-6	ERDA-6	ERDA-6	ERDA-6	ERDA-6	ERDA-6
Brine Volume (m ³)	1,045	1,045	1,045	1,045	7,763	13,267
Organic Ligands	None	None	None	None	None	None
EQ6 Output File	e21tm1.6o	e21tm1fe.6o	e21ch166.6o	e25ch133.6o	e21ch7.6o	e21ch3.6o
Suppressed Minerals	Dolomite, glauberite	Dolomite, glauberite	Dolomite, glauberite, polyhalite, magnesite, magnetite, pyrite	Dolomite, glauberite, polyhalite, magnesite, magnetite, pyrite	Dolomite, glauberite, polyhalite, magnesite, magnetite, pyrite	Dolomite, glauberite, polyhalite, magnesite, magnetite, pyrite
Salado Minerals (% DRZ)	100	100	100	49	100	100
Relative rates cellulose:Fe	1:3 *	1:3	1:3	1:3	1:3	1:3
Final pH	9.24	9.24	8.20	10.88	8.40	8.45
Final log f _{CO2}	-6.92	-6.92	-5.48	-5.48	-5.48	-5.48
Final log f _{CH4}	n.a.	-13.4	-5.79	36.1	-6.11	-6.29
Final log f _{H2S}	n.a.	-8.62	-0.963	-4.96	-1.31	-1.50
Final Total Carbonate (m)	5.69 × 10 ⁻⁵	5.74 × 10 ⁻⁵	5.22 × 10 ⁻⁴	0.587	4.78 × 10 ⁻⁴	4.78 × 10 ⁻⁴
Final Solid Phases	Anhydrite, brucite, calcite, halite, magnesite, syngenite	Anhydrite, brucite, calcite, halite, hematite, magnesite, pyrite, syngenite	Anhydrite, brucite, calcite, halite, hydromagnesite, syngenite, troilite	Brucite, calcite, halite, hydromagnesite, pirssonite, sylvite, troilite	Anhydrite, brucite, calcite, halite, hydromagnesite, syngenite, troilite	Anhydrite, brucite, calcite, halite, hydromagnesite, syngenite, troilite
Reaction Progress	62.5	62.5	62.5	62.5	8.50	4.925
Database	HMO	HMX	HMX	HMX	HMX	HMX
Notes	Repeated unpublished titration results considered by Wolery and Sassani (2007)	Repeated unpublished titration results of considered by Wolery and Sassani (2007)	Cellulose included as a special reactant; included 100% of the DRZ minerals and suppressed magnesite formation	Cellulose included as a special reactant; included 49% of the DRZ minerals and suppressed magnesite	Cellulose included as a special reactant; included 100% of the DRZ minerals and suppressed magnesite formation	Cellulose included as a special reactant; included 100% of the DRZ minerals and suppressed magnesite formation

* Input of iron equaled sulfide generation

4.4 MODELING RESULTS SUMMARY

Examination of the EQ3/6 modeling results (Tables 4-3 through 4-6) indicates that the most important factor controlling predicted pH values is the amount of sulfate available compared to the amount of CPR degraded. If it is assumed that excess Salado sulfate minerals are available for reaction, predicted pH values remain slightly alkaline for both potential end-member brine compositions (GWB or ERDA-6), the entire range of brine volumes, and different relative rates of iron corrosion and CPR degradation. In simulations with 100% of the DRZ minerals available for reaction, brines remained in equilibrium with anhydrite and had moderately alkaline pH values ranging from 7.69 to 9.00. These results are consistent with the existing Chemical Conditions conceptual model, which includes the assumption that the brines will remain in equilibrium with the Salado minerals halite, anhydrite, brucite, and either magnesite or hydromagnesite. The Chemical Conditions conceptual model includes the assumption that the repository brine pH values will be buffered between 8 and 10, depending on the brine composition. The predicted pH range from the EQ3/6 calculations is slightly lower than this assumed range, but these values are reasonably consistent with the pH values of 8.69 to 9.02 used to model actinide solubilities in the GWB and ERDA-6 brines for the PABC (Brush 2005), which resulted in low actinide solubilities consistent with the Dissolved Actinide Source Term conceptual model.

The results of the simulations with limited availability of DRZ sulfate minerals indicated that under some circumstances, CPR degradation and iron corrosion could lead to relatively high pH values and high total carbonate concentrations (Tables 4-3 through 4-6). Such conditions of high pH and high total carbonate concentrations could lead to relatively high actinide solubilities compared to the concentrations predicted for the PABC. Consequently, it is important to determine whether such conditions are likely to occur in the repository.

Kanney et al. (2004) evaluated the potential diffusive transport of sulfate from the DRZ to the WIPP waste. However, a number of questions were raised about this evaluation (TEA 2004). A new analysis of the likely diffusive transport of sulfate during the repository regulatory period was therefore carried out (Appendix C). This evaluation included a more detailed examination of the Salado mineralogy and a more rigorous solution of the diffusion equation. The results of this evaluation indicated that under inundated conditions, sufficient sulfate should be available for microbial degradation of CPR by the sulfate reduction reaction. Relatively high brine saturation would be required for direct brine release, when the pH of the brine would be important because of its effect on actinide solubilities. This analysis found that methanogenesis is likely if CPR degradation occurred under humid conditions, because brine would not be available for diffusive transport of sulfate from the Salado Formation. Under these conditions, the brine pH is relatively unimportant for repository performance, because direct brine release cannot occur.

High pH values would only be predicted to occur under circumstances with relatively high brine saturations, when an extremely large fraction of the CPR degrades at a rate that exceeds the rate of sulfate transport from the Salado Formation. SCA (2006) provided a preliminary review of the available literature regarding microbial and radiolytic processes that may result in CPR degradation in the WIPP environment. One conclusion of that report was that cellulosic materials might be completely degraded within the 10,000-year regulatory time frame.

However, SCA (2006) concluded that complete degradation of plastic and rubber in the repository was less certain. Cellulosic materials in the WIPP waste and emplacement materials account for approximately 32% of the CPR carbon, with an estimated 61% present as plastic waste and emplacement materials and only 7% present as rubber waste (SCA 2006).

Examination of the pH as a function of the extent of reaction in Figures 4-1 to 4-7 indicates that relatively rapid degradation of all cellulosic materials in the WIPP waste and emplacement materials would not be expected to result in high pH values. For example, the results of EQ3/6 calculations with 1,045 m³ of GWB brine, and only 25% of the Salado minerals available for reaction are illustrated in Figure 4-5. Complete degradation of cellulosic materials without significant plastics or rubber degradation would correspond to a reaction progress (X_i) of 21.3.³ At this value of X_i , the pH value predicted by the EQ3/6 simulations was 8.16, a moderately alkaline value consistent with the Chemical Conditions conceptual model. Higher pH values would only be expected in the unlikely event of rapid and extensive microbial degradation of plastics, with all of the carbon converted to CO₂ or methane.

The final compositions for GWB or ERDA-6 brine after complete CPR degradation by sulfate reduction were predicted using EQ3/6; these brine compositions are compared to the results of FMT modeling of equilibrium brine interactions with brucite, anhydrite, halite, and hydromagnesite for the PABC (Table 4-7). The largest differences between the FMT modeling results and the EQ3/6 reaction path calculation results are the ionic strength of the brines and the total sulfide concentrations. However, the parameters most likely to affect predicted actinide solubilities are pH and total carbonate concentration, which do not vary significantly as a function of CPR degradation by sulfate reduction. Consequently, there is no evidence that CPR degradation and production of large quantities of sulfide will significantly affect actinide solubilities, and the existing conceptual models appear to adequately describe the important actinide solubility processes. The potential for high sulfide concentrations and formation of FeS was previously acknowledged, and its effects were included in the Gas Generation conceptual model (Section 2.2).

³ The reaction progress (X_i) indicates the amount of a modeled reaction that has taken place relative to the starting condition.

Table 4-7. Effects of CPR Degradation and Iron Corrosion Reactions on Brine Compositions

Brine	GWB	GWB	GWB	ERDA-6	ERDA-6	ERDA-6
Brine Volume (m ³)	–	1,045	7,763	–	1,045	13,267
Final pH	8.69	8.14	8.22	9.02	8.20	8.45
Final log f _{CO2}	-5.50	-5.48	-5.48	-5.50	-5.48	-5.48
Final log f _{CH4}	–	-5.76	-5.98	–	-6.03	-6.29
Final log f _{H2S}	–	-0.937	-1.17	–	-1.23	-1.50
Ionic Strength	6.72	11.6	9.38	6.72	11.4	8.68
Calcium (m)	0.012	0.028	0.018	0.013	0.025	0.009
Chloride (m)	6.236	4.942	6.004	5.975	4.823	5.701
Potassium (m)	0.560	1.365	1.347	0.109	1.253	0.877
Magnesium (m)	0.635	1.792	1.064	0.121	1.578	0.461
Sodium (m)	4.981	4.373	4.541	6.054	4.875	5.877
Sulfate (m)	0.209	0.336	0.239	0.191	0.402	0.507
Sulfide (m)	–	3.720	1.554	–	3.663	0.963
Iron (m)	–	1.168 × 10 ⁻¹⁰	3.256 × 10 ⁻¹⁰	–	1.133 × 10 ⁻¹⁰	3.987 × 10 ⁻¹⁰
Carbonate (m)	4.019 × 10 ⁻⁴	5.213 × 10 ⁻⁴	4.549 × 10 ⁻⁴	5.353 × 10 ⁻⁴	5.227 × 10 ⁻⁴	4.78 × 10 ⁻⁴
Final Solid Phases	Anhydrite, brucite, halite, hydromagnesite oxychloride-Mg	Anhydrite, brucite, calcite, halite, hydromagnesite, syngenite, troilite	Anhydrite, brucite, calcite, halite, hydromagnesite, oxychloride-Mg, syngenite, troilite	Anhydrite, brucite, halite, hydromagnesite	Anhydrite, brucite, calcite, halite, hydromagnesite, syngenite, troilite	Anhydrite, brucite, calcite, halite, hydromagnesite, syngenite, troilite
FMT/EQ6 Output File	FMT_CRA1BC _GWB_ HMAG_NOOR GS_008.OUT	g21ch1fe.6o	g21ch7.6o	FMT_CRA1BC_ ER6_HMAG_ NOORGS_012. OUT	e21ch166.6o	e21ch3.6o

Calculation to reproduce the results of Wolery and Sassani (2007);
 reaction progress (X_i) of 66 corresponds to complete degradation of CPR carbon

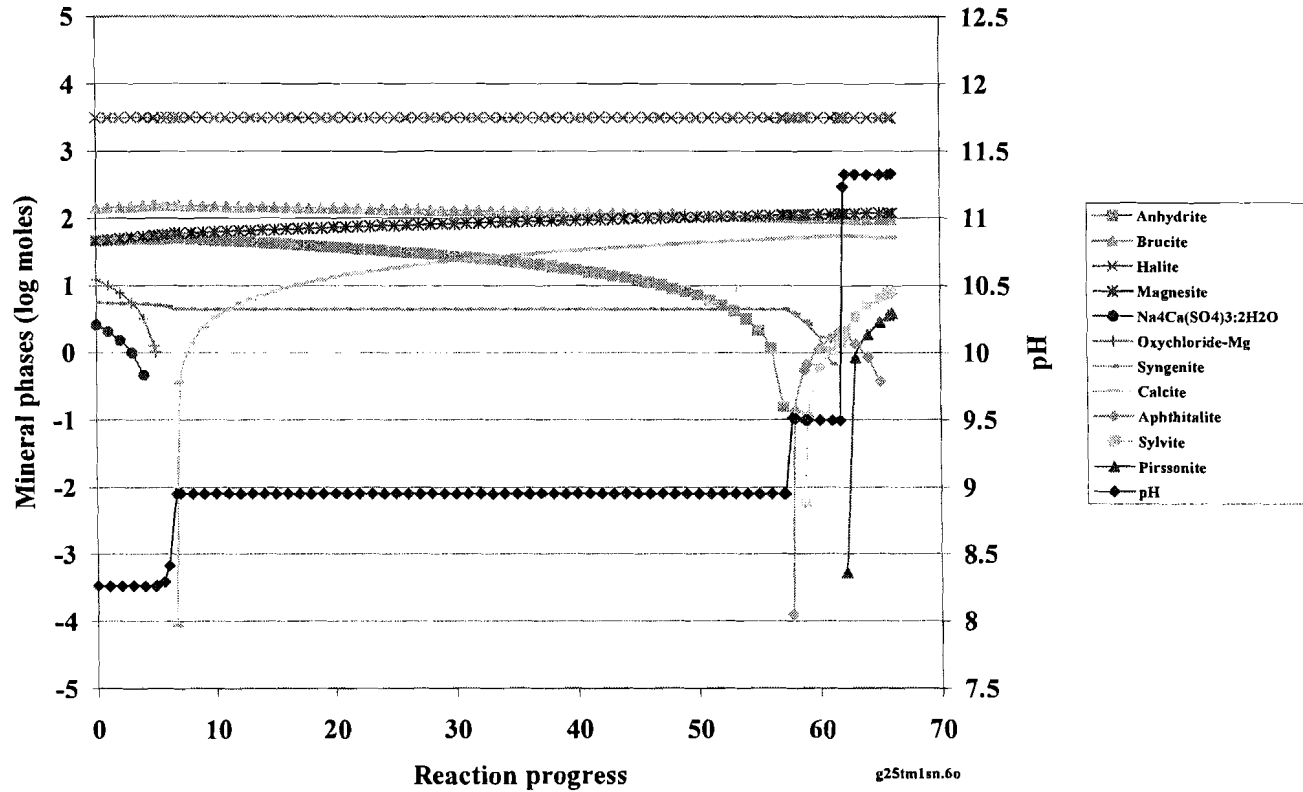


Figure 4-1. Titration Calculation with 1,045 m³ GWB Brine, 49% of the DRZ Salado Minerals, Magnesite Reaction Product

Revised calculation; reaction progress (X_i) of 66.5 corresponds to complete degradation of CPR carbon

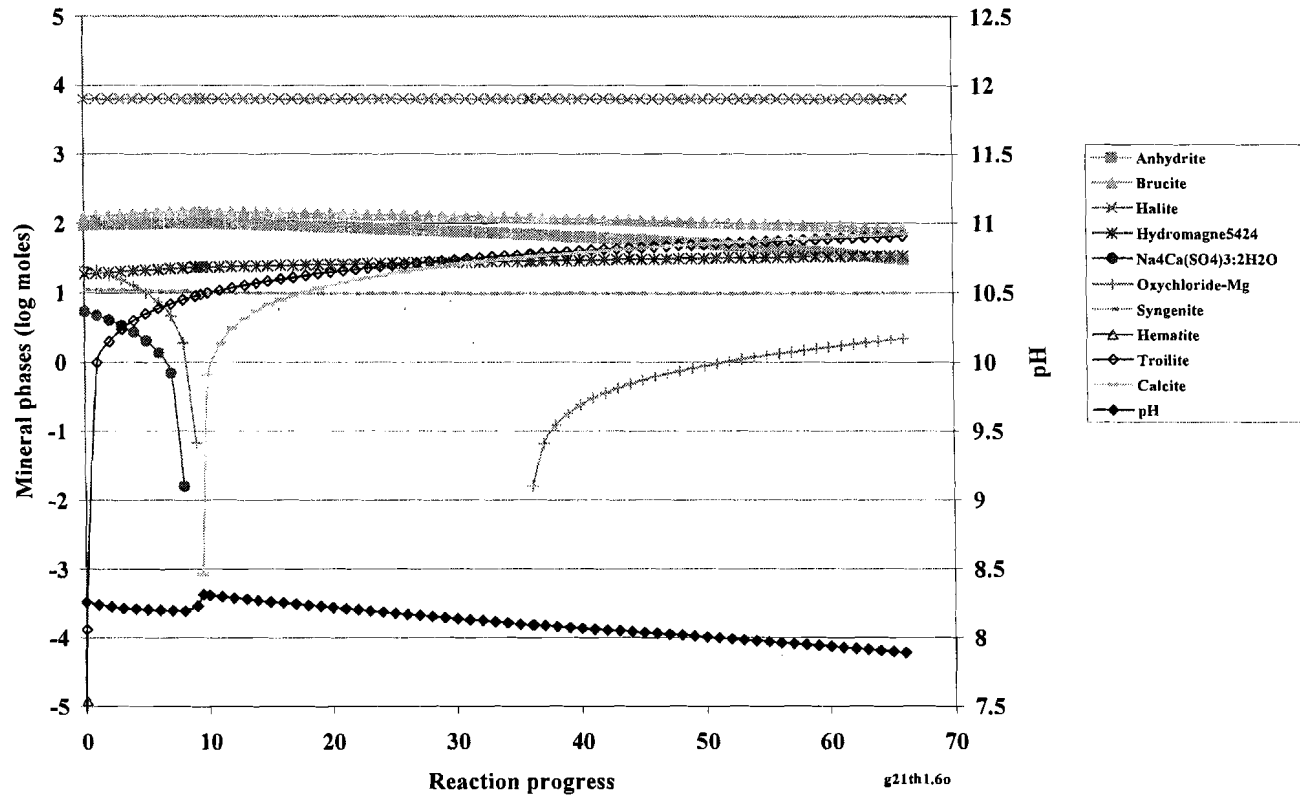


Figure 4-2. Titration Calculation, Iron and Sulfide Species Included, 1,045 m³ GWB brine, 100% of the DRZ Salado Minerals, Hydromagnesite Reaction Product

Revised calculation; reaction progress (Xi) of 66.5 corresponds to complete degradation of CPR carbon

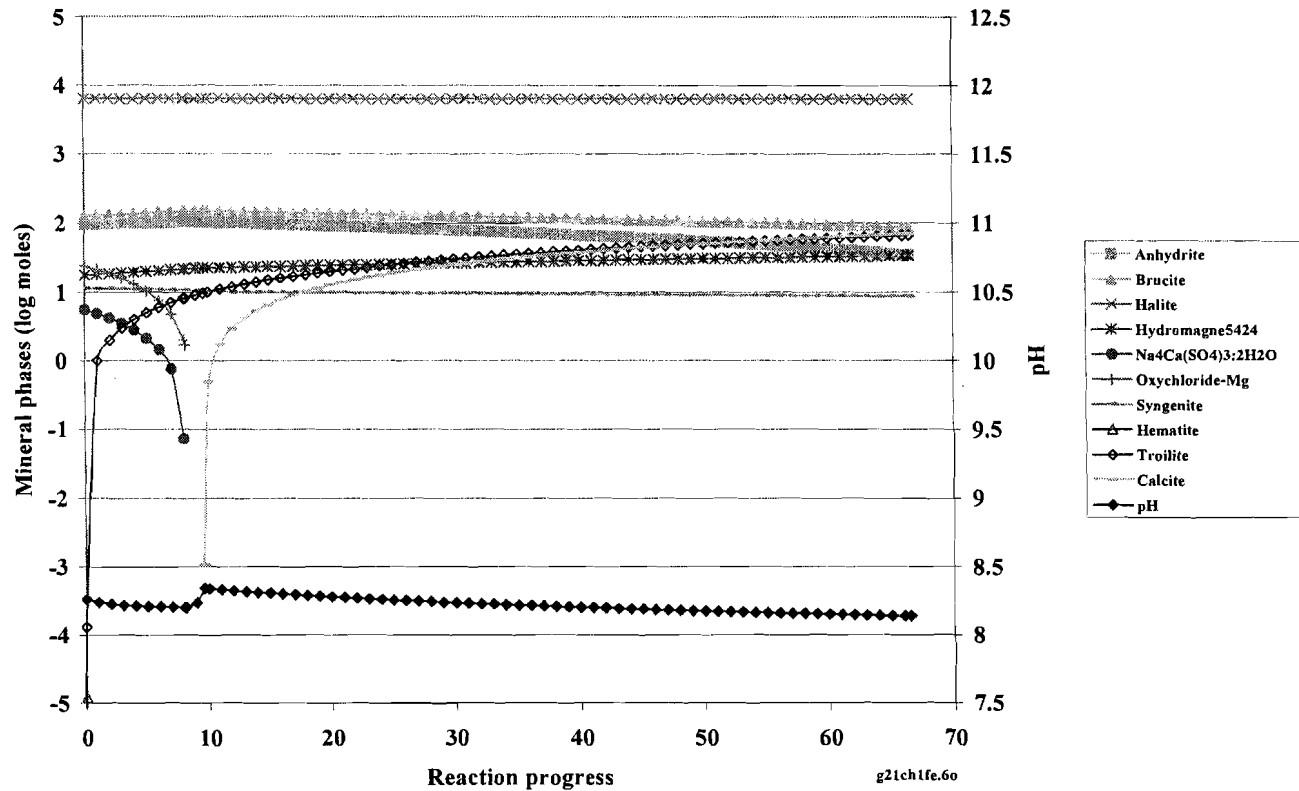


Figure 4-3. Cellulose Calculation, Iron and Sulfide Species Included, 1,045 m³ GWB brine, 100% of the DRZ Salado Minerals, Hydromagnesite Reaction Product

Revised calculation; reaction progress (Xi) of 66.5 corresponds to complete degradation of CPR carbon

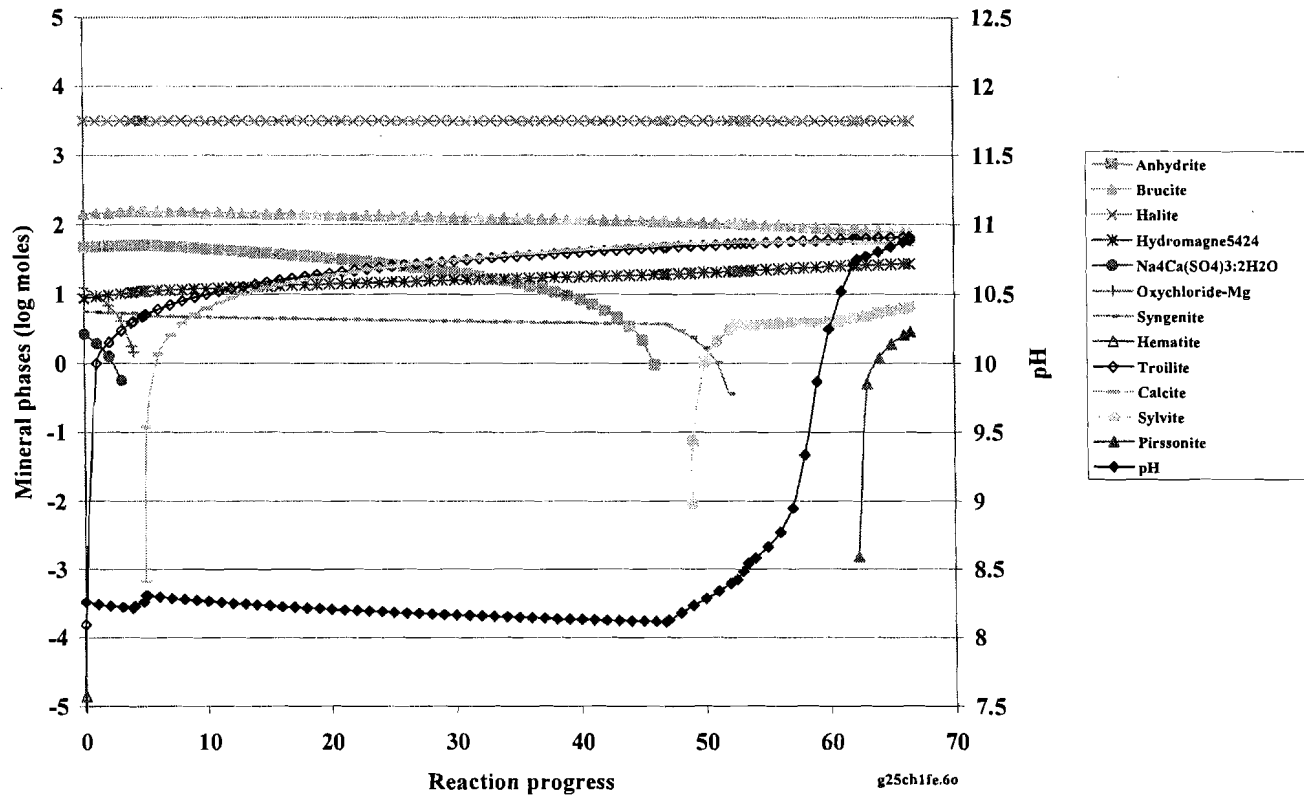


Figure 4-4. Cellulose Calculation, Iron and Sulfide Species Included, 1,045 m³ GWB brine, 49% of the DRZ Salado Minerals, Hydromagnesite Reaction Product

Revised calculation; reaction progress (X_i) of 66.5 corresponds to complete degradation of CPR carbon

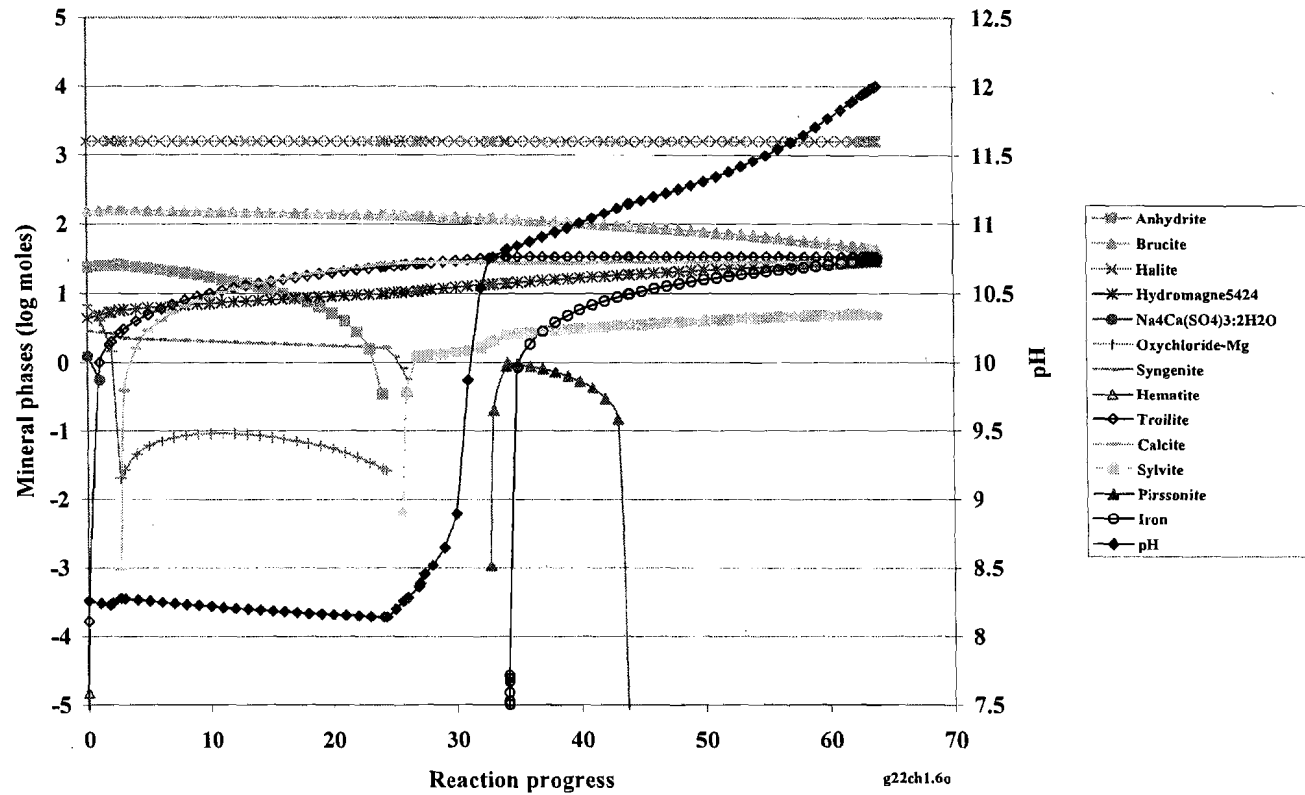


Figure 4-5. Cellulose Calculation, Iron and Sulfide Species Included, 1,045 m³ GWB brine, 25% of the DRZ Salado Minerals, Hydromagnesite Reaction Product

Revised calculation; reaction progress (X_i) of 8.95 corresponds to complete degradation of CPR carbon

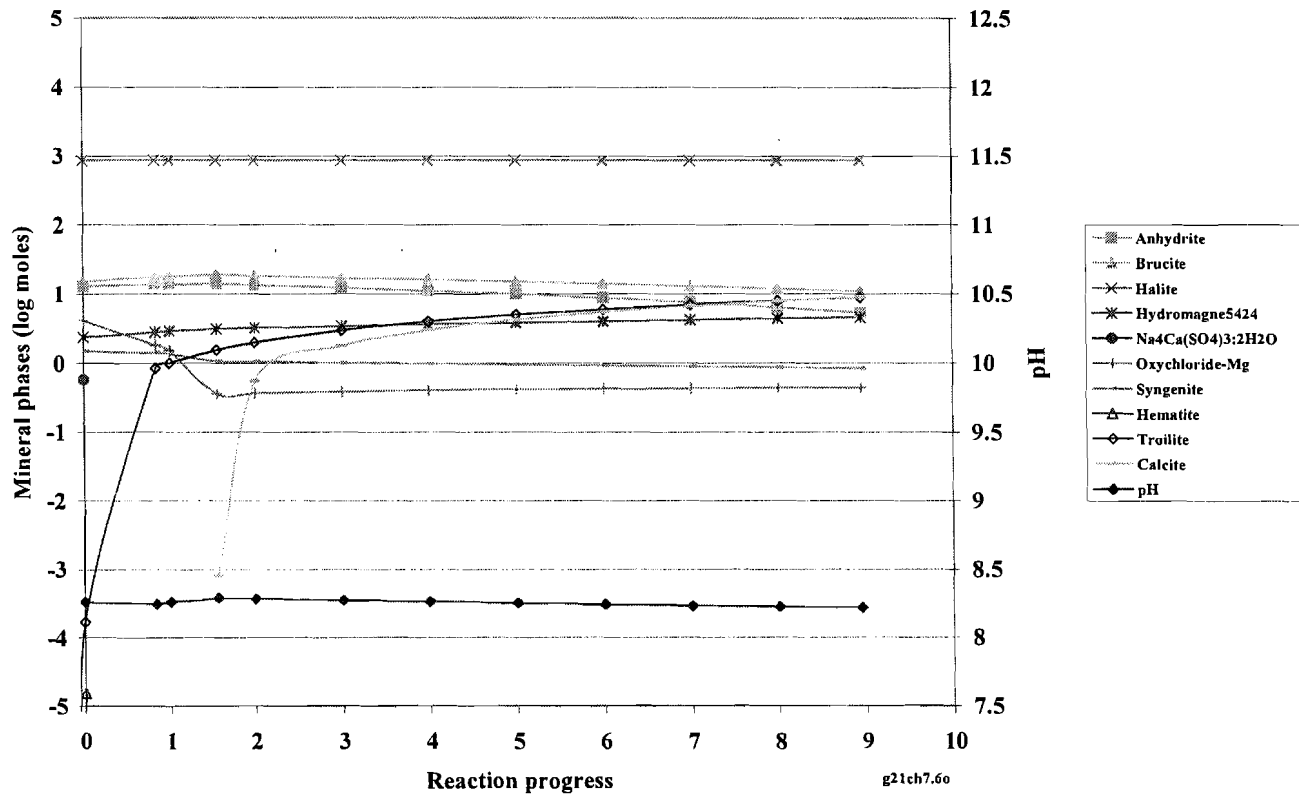


Figure 4-6. Cellulose Calculation, Iron and Sulfide Species Included, 7,763 m³ GWB brine, 100% of the DRZ Salado Minerals, Hydromagnesite Reaction Product

Revised calculation; reaction progress (X_i) of 8.95 corresponds to complete degradation of CPR carbon

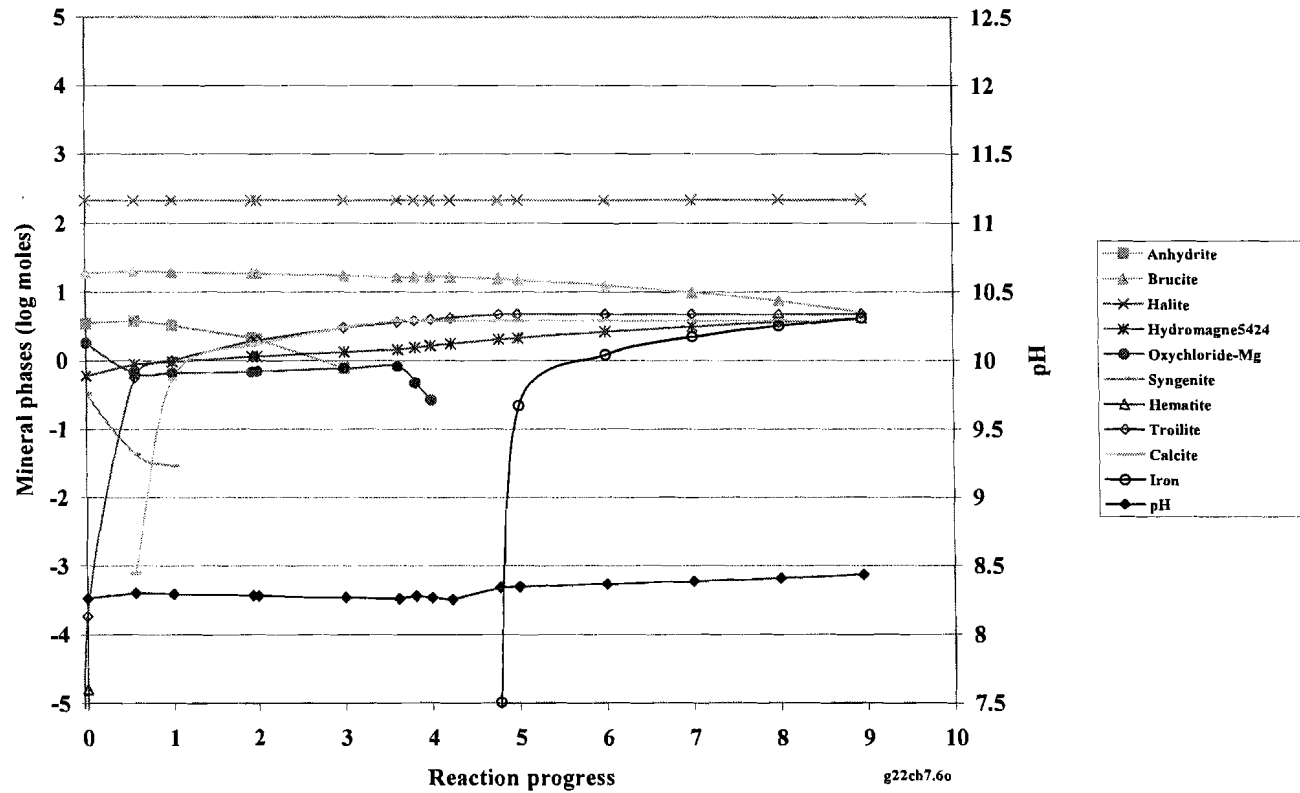


Figure 4-7. Cellulose Calculation, Iron and Sulfide Species Included, 7,763 m3 GWB brine, 25% of the DRZ Salado Minerals, Hydromagnesite Reaction Product

5.0 WATER BALANCE CONSIDERATIONS

Chemical processes may consume or produce water in the repository, changing the amount of brine available to react with iron or to dissolve actinides. Because of regulatory limits, free liquids in the waste are not expected to be a significant source of water in the repository. Significant sources of water include inflow from the Salado Formation in response to changes in the flow field caused by repository excavation and flow up a borehole from pressurized brine pockets in the Castile Formation. Consumption of water by reaction with MgO to form brucite or hydromagnesite has not been included in PA. Similarly, the potential effects of CPR degradation on the amount of water in the repository have not been included in PA because of uncertainties associated with microbial degradation. Anoxic corrosion of iron in the waste and waste containers is expected to consume water, and its effects are included in calculations of brine saturation in PA. However, the effects of formation of FeS instead of $\text{Fe}(\text{OH})_2 \cdot x\text{H}_2\text{O}$ during iron corrosion on the quantity of water consumed have not been included in PA.

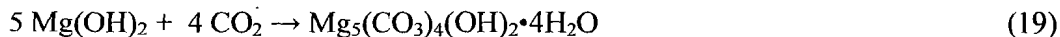
5.1 BRINE CONSUMPTION BY REACTION WITH MGO

Reaction of brine with MgO in the backfill to form brucite could consume significant quantities of brine. For example, if all MgO in the repository reacted with water in the brine to form brucite:

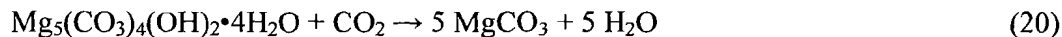


then 1.44×10^9 moles of water would be consumed, assuming the amount of MgO placed in the repository equals the EF (1.20) times the PABC CPR carbon inventory of 1.2×10^9 moles (Leigh et al. 2005b). The water consumed per panel would be 1.50×10^8 moles, based on the fraction of the total repository volume in a seven-room panel, which is equal to 0.1044 (Brush et al. 2006). This amount of water is equivalent to 3,175 m³ of GWB brine, based on the GWB brine composition and density. This volume of brine is potentially significant, when compared to the GWB brine volumes used in the chemistry calculations (Table 5-1).

CPR degradation will produce CO₂ that can react with brucite to form hydromagnesite:



Reaction of brucite to form hydromagnesite neither consumes nor produces water. Over the repository regulatory period of 10,000 years, hydromagnesite may transform to the more stable magnesite. In this case, the water in hydromagnesite would be released back into the brine:

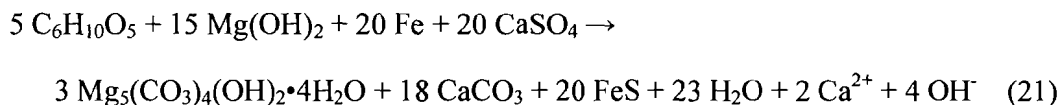


Because the extent to which hydromagnesite will convert to magnesite during the 10,000-year regulatory period is uncertain, a reasonable limiting assumption is that all brine consumed by reaction with MgO that is later carbonated could be released by magnesite formation. However, brucite that persists in the repository would be expected to reduce brine volumes, as would the metastable persistence of hydromagnesite.

5.2 EFFECTS OF CPR DEGRADATION ON WATER BALANCE

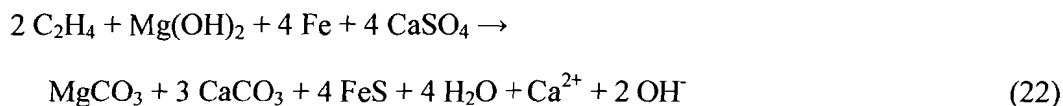
Because of uncertainties related to the amounts of water produced or consumed by CPR degradation, the effects of CPR degradation on the amount of brine present in the repository have not been included in PA. This assumption was reasonable at the time of the CCA PA and PAVT, because of the relatively low probabilities assigned to CPR degradation and the assumption by DOE that methanogenesis, which consumes water, would be the dominant reaction. However, the probability of cellulose degradation assumed for the PABC was higher than for the PAVT. In addition, the relatively large amounts of Salado sulfate available for CPR degradation means that methanogenesis is relatively less likely to occur. Consequently, the assumption that water produced or consumed by CPR degradation can be neglected in PA should be re-examined.

Because of the limited amounts of nitrate in the WIPP waste and the abundant sulfate in the Salado Formation minerals, sulfate reduction may be the most important cellulose degradation reaction. The sulfate reduction reaction should produce water as described by reaction (15) above if magnesite is produced; this reaction will produce 1.167 moles of H₂O per mole of carbon in cellulose that is consumed. Cellulosic materials represent approximately 32% of the CPR carbon in the PABC inventory (SCA 2006). Consequently, if all cellulose in the waste degrade according to reaction (15), 4.5×10^8 moles of water would be produced. This water would be expected to dissolve Salado Formation minerals and attain a composition similar to GWB. This amount of water would be equivalent to 988 m³ of GWB brine per panel. The sulfate reduction reaction (15) can be rewritten in terms of hydromagnesite to account for the possible persistence of this metastable phase:



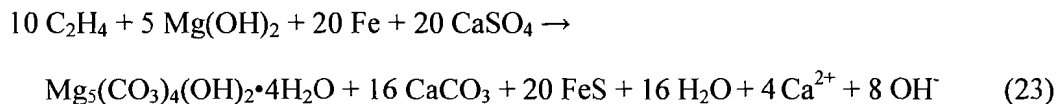
In this case, each mole of carbon in cellulose would produce 0.767 moles of water. Assuming that cellulose in the waste degrade according to reaction (21), the amount of water produced would be equivalent to 649 m³ of GWB brine per panel.

Reactions (15) and (21) do not describe all potential CPR degradation reactions, because these reactions are written in terms of cellulose. Plastics and rubber will be present in the WIPP waste, with plastics assumed to contain approximately 61% of the CPR carbon in the inventory. If these materials degrade, they are likely to produce different quantities of water, depending on their chemical composition. For example, polyethylene is expected to be the most significant plastic present in the WIPP waste and waste emplacement materials. If the sulfate reduction reaction for plastics degradation in the presence of iron is written in terms of polyethylene monomer (C₂H₄):



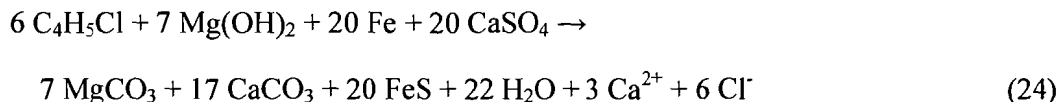
then one mole of water would be produced for each mole of CPR carbon in plastic that degrades. If the entire amount of CPR carbon in plastics degrades according to this reaction, then 7.64×10^7 moles of water could be produced per panel. Interaction of this water with Salado Formation

minerals would result in 1,614 m³ of GWB brine per panel. If hydromagnesite forms and does not convert to magnesite within the regulatory period, the reaction can be rewritten as:

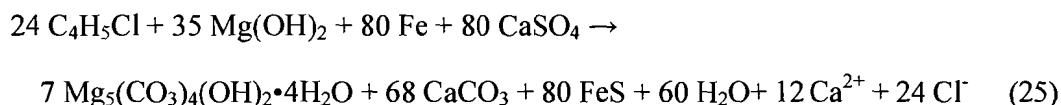


In this case, because of the incorporation of water into the hydromagnesite structure, only 0.8 moles of water would be produced per mole of CPR carbon in plastic that is degraded. If the entire plastic inventory degrades according to reaction (23), then 1,291 m³ of GWB brine could be produced per panel.

The amount of rubber in the PABC inventory is much smaller than the amounts of cellulose or plastics, representing approximately 7% of the carbon present in the CPR. If the composition of rubber can be approximated by neoprene monomer (C₄H₅Cl), the sulfate reduction reaction that produces magnesite can be written as:



Based on this reaction, 0.917 moles of water will be produced for each mole of carbon in rubber that is degraded, which is equivalent to 170 m³ of GWB brine per panel. If the neoprene degrades via sulfate reduction and hydromagnesite persists:



then 0.625 moles of water will be produced per mole of carbon in rubber that is degraded, which is equivalent to 116 m³ of GWB brine per panel. The total volumes of brine that could be produced by CPR degradation can be compared to the different brine volumes assumed for the EQ3/6 geochemical modeling calculations (Table 5-1). The total volumes of brine that could be produced by complete CPR degradation differ, depending on whether it is assumed that hydromagnesite will persist throughout the repository regulatory period or whether the more stable magnesite phase will form. However, for both magnesite and hydromagnesite formation, the volume of water that could be produced may be significant, when compared to other processes that may affect the water balance in a panel (Table 5-1).

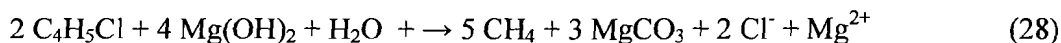
According to the Gas Generation conceptual model, if insufficient amounts of sulfate are available during CPR degradation, then methanogenesis may occur. Cellulose degradation by methanogenesis may occur via reaction (4), which can be rewritten in terms of the species likely to be present in the repository as:



which would produce 0.333 moles of water per mole of carbon in the cellulose. If polyethylene degrades by methanogenesis to form magnesite:

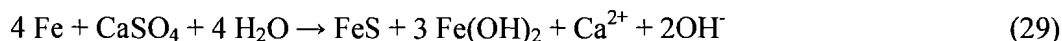


this reaction consumes 0.25 moles of water per mole of CPR carbon in the polyethylene. Similarly, degradation of neoprene by methanogenesis may occur via the reaction:



The cellulose, plastic, and rubber methanogenesis reactions seem likely to produce or consume relatively small amounts of water, if they occur.

Because the amount of brine in the repository can affect the amounts of CPR degradation and anoxic corrosion, addressing the potential effects of CPR degradation on the water balance, at least for degradation of cellulose, may result in more realistic PA calculations. The assumption that water production by cellulose degradation is unlikely to be significant may no longer be adequately supported, given the revised assumption of higher probabilities of cellulose degradation and the recognition of the abundant sulfate minerals present in the Salado Formation. The brine volumes summarized in Table 5-1 indicate that under some circumstances, the brine volumes created by CPR degradation could be significant. In addition, in the absence of CPR degradation, anoxic corrosion of iron may occur by reaction with sulfate in anhydrite to form FeS:



This reaction would consume only one mole of water per mole of iron corroded, in contrast to reaction (4), which consumes two moles of water per mole of iron. Consequently, if reaction (29) occurred in the repository, it could affect the amount of brine consumed by anoxic corrosion by as much as a factor of 2 (Table 5-1). Because the consumption of brine by anoxic corrosion is explicitly accounted for in PA, the potential effects of FeS precipitation should be considered. Examination of the brine volumes in Table 5-1, however, indicates that the water produced by CPR degradation may be at least partially offset by the water consumed by reaction with MgO.

Table 5-1. GWB Brine Volumes Associated with Repository Chemical Processes and Modeled Cumulative Brine Inflow for the Undisturbed PABC Scenario

Process	Brine Volume Per Panel	
	Maximum Brine Consumed by MgO Hydration and Carbonation	Magnesite
	Brucite or hydromagnesite	3,175 m ³
Maximum Brine Produced by Cellulose Degradation	Magnesite	988 m ³
	Hydromagnesite	649 m ³
Maximum Brine Produced by Plastics Degradation	Magnesite	1,614 m ³
	Hydromagnesite	1,291 m ³
Maximum Brine Produced by Rubber Degradation	Magnesite	170 m ³
	Hydromagnesite	116 m ³
Maximum Total Brine Production by CPR Degradation (Cellulose + Plastics + Rubber)	Magnesite	2,772 m ³
	Hydromagnesite	2,056 m ³
Castile Brine (Clayton 2006)	Maximum calculated in PABC	13,267 m ³
Salado Brine (Clayton 2006)	Maximum calculated in PABC	7,763 m ³
Salado or Castile Brine (Clayton 2006)	Minimum necessary for direct brine release	1,045 m ³
Brine Consumed by Anoxic Corrosion	Fe(OH) ₂	4,060 m ³
	0.25 FeS + 0.75 Fe(OH) ₂	2,030 m ³

6.0 EFFECTS OF MINERAL VOLUME CHANGES

Lichtner (2007) noted that the reaction-path calculations carried out by Brush et al. (2006) did not consider the possible effects of mineral volume changes. Significant mineral volume increases during reaction could decrease porosity and permeability, which could affect repository performance. The results of selected reaction-path modeling calculations described in Section 4.0 were used to determine the possible mineral volume changes caused by MgO hydration, CPR degradation, brucite carbonation, and iron corrosion.

The volume changes for complete reaction of the CPR by sulfate reduction and iron reaction to form troilite were determined using the initial and final quantities of the minerals from selected EQ3/6 calculations and their molar volumes (Robie et al. 1978). The molar volume of cellulose was approximated as 135 cm³/mole, based on the density of standard paper (1.201 g/cm³, SIMetric 2008) and the molecular weight of cellulose (162.14 g/mole). The results of these calculations are summarized in Table 6-1. Reaction of MgO, iron, CPR, and Salado minerals resulted in relatively small decreases in mineral volumes. This result seems inconsistent with the relatively large volume increase expected to result from the hydration and carbonate of MgO, because the molar volumes of brucite (24.63 cm³/mole), hydromagnesite (211.10 cm³/mole) and magnesite (28.02 cm³/mole) are significantly larger than the molar volume of periclase (11.25 cm³/mole). However, the increased volume of the hydrated and carbonated magnesium phases appears to be offset by the consumption of CPR and the dissolution of relatively large amounts of sulfate minerals, including polyhalite, gypsum, and anhydrite.

These calculations do not represent a complete consideration of the volume changes that may occur during the interactions of waste, MgO, iron, Salado minerals, and brine. For example, the EQ3/6 calculations overestimate the amount of brine present at the end of the simulations, because brucite was used instead of MgO to prevent excessive consumption of water during the initial steps of the simulations. Consequently, the amounts of minerals present at the end of the simulation are likely to be underestimated, because the amounts dissolved in the final brine are likely to be somewhat overestimated. In addition, the EQ3/6 simulations did not predict anoxic corrosion of iron to form Fe(OH)₂. These calculations also do not take into account the possible reaction and volume changes of other waste materials. Despite these limitations, however, these calculations indicate that large-scale mineral volume changes are unlikely to occur as the result of the CPR degradation, sulfate reduction, and iron corrosion reactions. Because large volume changes appear to be unlikely, large-scale changes in porosity and permeability are also unlikely. This conclusion is consistent with a previous evaluation of possible porosity and permeability changes that could be caused by hydromagnesite formation (EPA 1998a).

Table 6-1. Volume Changes Predicted Using Results of Selected EQ3/6 Reaction Path Simulations; All Simulations Assumed 100% of the DRZ Minerals Were Available for Reaction

Initial Brine Volume and Magnesium-Carbonate Mineral	1,045 m³ GWB, Hydromagnesite	1,045 m³ GWB, Magnesite	7,763 m³ ERDA-6, Hydromagnesite	13,267 m³ ERDA-6, Hydromagnesite
EQ6 Output File	g21ch1fe.6o	g21cm1fe.6o	e21ch7.6o	e21ch3.6o
Initial Volume Per Panel of CPR, Iron, MgO, and DRZ Minerals (m ³)	169,093	169,093	169,093	169,093
Product Mineral Phases	Anhydrite, brucite, calcite, halite, hydromagnesite, syngenite, iron, troilite	Anhydrite, brucite, calcite, halite, magnesite, sylvite, syngenite, iron, troilite	Anhydrite, brucite, calcite, halite, hydromagnesite, syngenite, iron, troilite	Anhydrite, brucite, calcite, halite, hydromagnesite, syngenite, iron, troilite
Final Volume Per Panel (m ³)	168,768	166,158	168,185	167,652
Mineral Volume Change Per Panel (m ³)	-364	-3,293	-908	-1,441

7.0 ADEQUACY OF CHEMISTRY CONCEPTUAL MODELS

The current chemistry-related conceptual models are summarized in Appendix A. Changes to the conceptual models since the approval of the models by the Conceptual Model Peer Review Panel have resulted from evaluations of additional experimental data related to microbial degradation of CPR, actinide solubilities, and organic complexation of actinides.

Revisions have been made to a number of assumptions in the Gas Generation conceptual model, including a higher probability of cellulose degradation, the assumption that the sulfate reduction reaction may be more important than methanogenesis for CPR degradation because of the availability of sulfate from Salado minerals, and the assumption that both microbial degradation of CPR and anoxic corrosion may be significant sources of gas in the repository. In addition, because of the possible importance of sulfate reduction reactions, iron corrosion is assumed to produce both $\text{Fe}(\text{OH})_2 \cdot x\text{H}_2\text{O}$ and FeS , rather than only $\text{Fe}(\text{OH})_2 \cdot x\text{H}_2\text{O}$. These changes were made based on additional experimental data obtained since the CCA PA and PAVT and more detailed evaluation of existing data. These changes do not represent major revisions to the conceptualization of repository processes, but instead are refinements of the original conceptual model. The existing Gas Generation conceptual model, as summarized in Appendix A, is consistent with the currently available information about gas generation processes in WIPP and adequately represents likely repository conditions.

Assumptions related to the Chemical Conditions conceptual model have been revised since the Conceptual Model Peer Review. These revisions include a change in the proportions of MgO to CPR carbon placed in the repository to control CO_2 fugacities, which has changed from its initial value of 1.95 to its current value of 1.20. However, this change was approved only after a technical review established that the pH and CO_2 fugacity in the repository would continue to be controlled by the smaller excess of MgO (Reyes 2008, SCA 2008). The Chemical Conditions conceptual model changes have also included a change in the Salado brine formulation from Brine A to GWB. This change in brine formulation was evaluated during review of the CRA-2004 PA and PABC and found to be a minor change that was unlikely to significantly affect calculations related to repository performance (EPA 2006a, 2006b). Inclusion of the possibility that either the brucite-hydromagnesite or brucite-magnesite reactions may buffer CO_2 fugacities in the repository was an additional change to the original Chemical Conditions conceptual model. This change, made at the time of the PAVT, results in a more conservative evaluation of possible CO_2 fugacities than the assumption of magnesite stability that was reviewed by the Conceptual Models Peer Review Panel. The current Chemical Conditions conceptual model (Appendix A) is substantially the same as the version reviewed by the Conceptual Models Peer Review Panel. This conceptual model is adequately representative of the expected chemical conditions in the repository, and review of the available information has not indicated a need for revisions.

The Dissolved Actinide Source Term conceptual model now includes the assumption that organic ligands may affect the solubilities of the +III and +V actinides. In the original conceptual model, it was assumed that competition by transition metal ions such as iron would prevent significant actinide complexation by organic ligands. This change was made to the Dissolved Actinide Source Term conceptual model because of newly available data on actinide complexation by organic ligands in WIPP brines. This assumption has a conservative effect on

actinide solubility calculations and does not represent a major change to the conceptual model. The other change made to the Dissolved Actinide Source Term conceptual model was an increase in the assumed uranium(VI) solubility used in PA. This change was made in response to the availability of additional literature data on uranium +VI solubility in brines. This change does not represent a significant difference in the expected chemical behavior of the repository and consequently is only a minor revision of the conceptual model. The available information related to actinide solubilities in WIPP brines remains consistent with the current Dissolved Actinide Source Term conceptual model, which is summarized in Appendix A.

8.0 CONCLUSIONS AND RECOMMENDATIONS

The Gas Generation, Chemical Conditions, and Dissolved Actinide Source Term conceptual models have changed since they were reviewed and accepted by the original CCA Conceptual Models Peer Review Panel (Wilson et al. 1996a, 1996b, 1997a, 1997b). These changes have been relatively small adjustments made in response to ongoing investigations of repository processes such as microbial degradation of CPR and actinide solubilities. These changes have not represented significant modifications to the conceptualization of expected repository chemical processes. Consequently, these changes do not necessitate additional peer review of the chemistry-related conceptual models.

Some EQ3/6 geochemical calculations performed for DOE (Brush et al. 2006, Wolery and Sassani 2007, and Lichtner 2007) indicated that high pH brines could be present in the WIPP repository as the result of CPR degradation and iron corrosion. The predicted pH values were in excess of the pH 8 to 10 range assumed in the Chemical Conditions and Dissolved Actinide Source Term conceptual models. Such high pH values could result in higher predicted actinide solubilities than had previously been used in PA; if these high pH values are likely to occur in the repository, it would represent a significant change to these conceptual models. Evaluation of the EQ3/6 geochemical calculations, including additional calculations carried out as part of the present study, indicates that pH values in excess of 10 were only predicted in simulations that did not include equilibrium of the brines with anhydrite, which is an assumption of the Chemical Conditions conceptual model. Evaluation of likely rates of sulfate diffusion from the Salado Formation indicated that sufficient sulfate is likely to be available under conditions of high brine saturation in the repository as CPR degrades. Consequently, these high pH values are unlikely to occur in the repository brines and the current chemistry-related conceptual models continue to adequately represent expected repository conditions. Based on the mineralogy changes predicted in the EQ3/6 calculations, mineral volume changes are unlikely to significantly change as a function of CPR degradation and MgO hydration and carbonation.

Although the current chemistry-related conceptual models appear to remain adequate for WIPP PA, some potential issues related to implementation were identified as part of this review. The current implementation only accounts for water consumed by anoxic corrosion of iron in the repository. However, other processes may affect the water balance in the repository: FeS precipitation in place of Fe(OH)₂, MgO hydration, magnesite formation, and CPR degradation. The potential importance of these other factors on the water balance in the repository should be evaluated.

Another potential implementation issue is the rate of plastics and rubber degradation in the 25% of PA realizations in which this degradation is assumed to occur. Currently, it is assumed that plastics and rubber degradation will occur at the same rate as cellulose degradation, which is likely to overestimate plastic and rubber degradation rates. Additional evaluation of the potential effects of lower plastics and rubber degradation rates and their effects on PA would be required to determine if changes to these rates would be warranted.

9.0 REFERENCES

- Brush, L.H. 1990. *Test Plan for Laboratory and Modeling Studies of Repository and Radionuclide Chemistry for the Waste Isolation Pilot Plant*. SAND90-0266. Sandia National Laboratories, Albuquerque, New Mexico.
- Brush, L.H. 2005. *Results of Calculations of Actinide Solubilities for the WIPP Performance Assessment Baseline Calculations*. Analysis Report, Sandia National Laboratories, Carlsbad, New Mexico, ERMS 539800.
- Brush, L.H., J. Garner, and E. Vugrin 2005. *PA Implementation of Uncertainties Associated with Calculated Actinide Solubilities*. Memorandum to D. Kessel, Sandia National Laboratories, Carlsbad, New Mexico, February 2, 2005.
- Brush, L.H., Y. Xiong, J.W. Garner, A. Ismail, and G.T. Roselle. 2006. *Consumption of Carbon Dioxide by Precipitation of Carbonate Minerals Resulting from Dissolution of Sulfate Minerals in the Salado Formation in Response to Microbial Sulfate Reduction in the WIPP*. Sandia National Laboratories, Carlsbad, New Mexico.
- Bynum, R.V. 1997. *Confirmation of the Ability of a Designed Backfill to Control the Chemical Environment in the WIPP*. Sandia National Laboratories, TP97-01, Revision 1.
- Clayton, D. 2006. *Update of the Minimum Brine Volume for a Direct Brine Release and New Maximum Castile and Salado Brine Volumes in a Waste Panel*. Memorandum to L.H. Brush, Sandia National Laboratories, Carlsbad, New Mexico, October 11, 2006, ERMS 544453.
- Daveler, S.A., and T.J. Wolery. 1992. *EQPT, A Data File Preprocessor for the EQ3/6 Software Package: User's Guide and Related Documentation (Version 7.0)*. UCRL-MA-110662 PT II. Lawrence Livermore National Laboratory, Livermore, California.
- DOE (U.S. Department of Energy) 1996. *Title 40 CFR Part 191 Compliance Certification Application for the Waste Isolation Pilot Plant*. DOE/CAO-1996-2184, October 1996, Carlsbad Field Office, Carlsbad, New Mexico.
- DOE (U.S. Department of Energy) 2004. *Title 40 CFR 191 Parts B and C Compliance Recertification Application*. U.S. Department of Energy Field Office, March 2004. Docket A-98-49 Category II-B2.
- EPA (Environmental Protection Agency) 1997a. *Compliance Application Review Documents for the Criteria for the Certification and Recertification of the Waste Isolation Pilot Plant's Compliance with the 40 CFR Part 191 Disposal Regulations: Final Certification Decision. CARD 23: Models and Computer Codes*. U.S. Environmental Protection Agency Office of Radiation and Indoor Air. Washington, DC. Docket A-93-02 Item V-B-2.
- EPA (Environmental Protection Agency) 1997b. *Compliance Application Review Documents for the Criteria for the Certification and Recertification of the Waste Isolation Pilot Plant's Compliance with the 40 CFR Part 191 Disposal Regulations: Final Certification Decision*.

CARD 24: Waste Characterization. U.S. Environmental Protection Agency Office of Radiation and Indoor Air. Washington, DC. Docket A-93-02 Item V-B-2.

EPA (Environmental Protection Agency) 1997c. *Compliance Application Review Documents for the Criteria for the Certification and Recertification of the Waste Isolation Pilot Plant's Compliance with the 40 CFR Part 191 Disposal Regulations: Final Certification Decision.* *CARD 44: Engineered Barrier.* U.S. Environmental Protection Agency Office of Radiation and Indoor Air. Washington, DC. Docket A-93-02 Item V-B-2.

EPA (U.S. Environmental Protection Agency) 1998a. *Final WIPP Certification Decision Response to Comments, Criteria for the Certification of the Waste Isolation Pilot Plant's Compliance with 40 CFR Part 191 Disposal Regulations: Certification Decision.* Office of Radiation and Indoor Air, Washington DC. Docket No. A-93-02 Item V-C-1.

EPA (Environmental Protection Agency) 1998b. *Technical Support Document for Section 194.24: EPA's Evaluation of DOE's Actinide Source Term.* Environmental Protection Agency Office of Radiation and Indoor Air, Washington, DC. Docket A-93-02 Item V-B-17.

EPA (Environmental Protection Agency) 1998c. *Technical Support Document: Overview of Major Performance Assessment Issues.* Environmental Protection Agency Office of Radiation and Indoor Air, Washington, DC. Docket A-93-02 Item V-B-5.

EPA (Environmental Protection Agency) 2001. *Approval of Elimination of Minisacks.* Environmental Protection Agency Office of Radiation and Indoor Air, Washington, DC., Docket A-98-49 Item II-B-3, Item 15.

EPA (Environmental Protection Agency) 2004. Letter from Frank Marcinowski, U.S. Environmental Protection Agency Office of Radiation and Indoor Air, Washington DC, to R. Paul Detwiler, U.S. Department of Energy Carlsbad Field Office, March 26, 2004.

EPA (Environmental Protection Agency) 2006a. *Technical Support Document for Section 194.23: Review of the 2004 Compliance Recertification Performance Assessment Baseline Calculation.* Office of Radiation and Indoor Air, Docket No. A-98-49, Item II-B1-3, March 2006.

EPA (Environmental Protection Agency) 2006b. *Technical Support Document for Section 194.24: Evaluation of the Compliance Recertification Actinide Source Term and Culebra Dolomite Distribution Coefficient Values.* Office of Radiation and Indoor Air, Docket No. A-98-49, Item II-B1-16, March 2006.

Gillow, J., and A.J. Francis. 2003. *Microbial Gas Generation Under Expected Waste Isolation Pilot Plant Repository Conditions.* Final Report, Revision 0, October 6, 2003, ERMS 532877. Docket A-98-49 Item II-B2-35

Gitlin, B.C. 2006. U.S. Environmental Protection Agency, Office of Air and Radiation, Washington, DC. Letter to D.C. Moody, U.S. Department of Energy, Carlsbad Field Office, Carlsbad, New Mexico. April 28, 2006.

Hansen, C.W., L.H. Brush, M.B. Gross, F.D. Hansen, B. Thompson, J.S. Stein, and B-Y Park. 2003a. *Effects of Supercompacted Waste and Heterogeneous Waste Emplacement on Repository Performance*. Rev. 0. Sandia National Laboratories Carlsbad Programs Group, Carlsbad, New Mexico. October 7, 2003.

Hansen, C.W., L.H. Brush, M.B. Gross, F.D. Hansen, B-Y Park, J.S. Stein, and B. Thompson. 2003b. *Effects of Supercompacted Waste and Heterogeneous Waste Emplacement on Repository Performance*. Rev. 1. Sandia National Laboratories Carlsbad Programs Group, Carlsbad, New Mexico. October 17, 2003.

Harvie, C. E., N. Møller, and J. H. Weare. 1984. The prediction of mineral solubilities in natural waters: the Na-K-Mg-Ca-H-Cl-SO₄-OH-HCO₃-CO₃-H₂O-system to high ionic strengths at 25°C. *Geochimica Cosmochimica Acta* 48:723-752.

Hobart, D.E., and R.C. Moore. 1996. *Analysis of Uranium (VI) Solubility Data for WIPP Performance Assessment*. WBS 1.1.10.1.1. Sandia National Laboratories, May 28, 1996, ERMS 239856.

IMA (International Mineralogical Association) 2007. *IMA/CNMC List of Mineral Names*. Compiled by E.H. Nickel and M.E. Nichols, June 5, 2007. Accessed July 13, 2007 at <http://www.geo.vu.nl/users/ima-cnmmn/MINERALlist.pdf>.

Kanney, J.F., A.C. Snider, T.W. Thompson, and L.H. Brush. 2004. *Effect of Naturally Occurring Sulfate on the MgO Safety Factor in the Presence of Supercompacted Waste and Heterogeneous Waste Emplacement*. Sandia National Laboratories, Carlsbad Programs Group, Carlsbad, New Mexico. March 5, 2004.

Lambert, S.J. 1992. Geochemistry of the Waste Isolation Pilot Plant (WIPP) site, southeastern New Mexico, USA. *Applied Geochemistry* 7:513-531.

Leigh, C., J. Kanney, L. Brush, J. Garner, R. Kirkes, T. Lowry, M. Nemer, J. Stein, E. Vugrin, S. Wagner, and T. Kirchner. 2005a. *2004 Compliance Recertification Application Performance Assessment Baseline Calculation*. Sandia National Laboratories, Carlsbad, New Mexico, ERMS 541521.

Leigh, C., J. Trone, and B. Fox. 2005b. *TRU Waste Inventory for the 2004 Compliance Recertification Application Performance Assessment Baseline Calculation*. Sandia National Laboratories, Carlsbad, New Mexico, ERMS 541118.

Lichtner, P. C. 2001. *FLOTRAN User Manual*. Report No. LA-UR-02-2349, Los Alamos National Laboratory, Los Alamos, New Mexico.

Lichtner, P.C. 2007. *Interim Report on Geochemical Interactions at the WIPP Disposal Site*. Los Alamos National Laboratory LA-UR-07-6165, October 15, 2007.

Moody, D.C. 2006. U.S. Department of Energy, Carlsbad Field Office, Letter to E.A. Cotsworth, U.S. Environmental Protection Agency. April 10, 2006. ERMS 543262.

Reyes, J. 2008. U.S. Environmental Protection Agency, Washington DC, Letter to D.C. Moody, U.S. Department of Energy. February 11, 2008.

Robie, R.A., B.S. Hemingway, and J.R. Fisher. 1978. *Thermodynamic Properties of Minerals and Related Substances at 298.15 K and 1 Bar (10^5 Pascals) Pressure and at Higher Temperatures*. U.S. Geological Survey Bulletin 1452, U.S. Government Printing Office, Washington, DC.

SCA (S. Cohen and Associates) 2006. *Preliminary List of Issues Associated with DOE's Effective Excess Factor Calculations*. Draft Technical Memorandum from J.A. Schramke to C.O. Byrum and R.T. Peake, U.S. Environmental Protection Agency, Office of Radiation and Indoor Air, Washington DC, December 21, 2006.

SCA (S. Cohen and Associates) 2007. *EPA/DOE Technical Exchange Meeting: EQ3/6 Modeling. October 3, 2007, Las Vegas, Nevada*. Prepared for the U.S. Environmental Protection Agency Office of Radiation and Indoor Air, Washington, DC.

SCA (S. Cohen and Associates) 2008. *Review of MgO Uncertainties in the Waste Isolation Pilot Plant*. Prepared for the U.S. Environmental Protection Agency, Office of Radiation and Indoor Air, Washington DC, January 24, 2008.

Simetric (2008). *Density of Materials*. http://www.simetric.co.uk/si_materials.htm, Accessed May 10, 2008.

Snider, A.C. 2003. *Verification of the Definition of Generic Weep Brine and the Development of a Recipe for this Brine*. Unpublished Analysis Report, Sandia National Laboratories, Carlsbad, New Mexico, April 8, 2003, ERMS 527505. Docket A-98-49 Item II-B2-39.

SNL (Sandia National Laboratories) 1997. *Chemical Conditions Model: Results of the MgO Backfill Efficacy Investigation*. Prepared for the U.S. Department of Energy, Carlsbad Area Office, April 23, 2007, Docket No. A-93-02 Item II-A-39.

Stein, C.S. 1985. *Mineralogy in the Waste Isolation Pilot Plant (WIPP) Facility Stratigraphic Horizon*. SAND-85-0321, Sandia National Laboratories, Albuquerque, New Mexico, September 1985.

TEA (Trinity Engineering Associates) 2004. *Review of Effects of Supercompacted Waste and Heterogeneous Waste Emplacement on WIPP Repository Performance. Final Report*. Prepared for U.S. Environmental Protection Agency, Office of Radiation and Indoor Air, Washington, DC, March 17, 2004.

Telander, M.R., and R.E. Westerman. 1993. *Hydrogen Generation by Metal Corrosion in Simulated Waste Isolation Pilot Plant Environments: Progress Report for the Period November 1989 through December 1992*. Sandia National Laboratories Contractor Report, SAND92-7347, Albuquerque, New Mexico.

Telander, M.R., and R.E. Westerman. 1997. *Hydrogen Generation by Metal Corrosion in Simulated Waste Isolation Pilot Plant Environments*. Sandia National Laboratories Contractor Report, SAND96-2538, Albuquerque, New Mexico.

Triay, I. 2002. Letter from Dr. I. Triay, Manager, U.S. Department of Energy Carlsbad Field Office, to F. Marcinowski, Director, U.S. Environmental Protection Agency Radiation Protection Division, dated December 10, 2002. (Docket A-98-49, Item II-B-15).

Vugrin, E.D., M.B. Nemer, and S. Wagner. 2006. *Uncertainties Affecting MgO Effectiveness and Calculation of the MgO Effective Excess Factor*. Revision 0, Sandia National Laboratories, Carlsbad, New Mexico.

Vugrin, E.D., M.B. Nemer, and S. Wagner. 2007. *Uncertainties Affecting MgO Effectiveness and Calculation of the MgO Effective Excess Factor*. Revision 1, Sandia National Laboratories, Carlsbad, New Mexico. ERMS 546377.

Wang, Y. and L.H. Brush. 1996. *Estimates of Gas-Generation Parameters for the Long-Term WIPP Performance Assessment*. Unpublished memorandum to M.S. Tierney, Sandia National Laboratories, Albuquerque, New Mexico, January 26, 1996, WPO 31943. ERMS 231943.

Wang, Y., L.H. Brush, H. Gao, and J.S. Stein. 2003. Re-evaluation of Microbial Gas Generation Rates for Long-Term WIPP Performance Assessment. *Sandia National Laboratories Technical Baseline Reports, WBS 1.3.5.3, Compliance Monitoring; WBS 1.3.5.4, Repository Investigations, Milestone RI 03-210, January 31, 2003*. Sandia National Laboratories, Carlsbad, New Mexico, pp. 3.1-1 to 3.1-12.

Wilson, C., D. Porter, J. Gibbons, E. Oswald, G. Sjoblom, and F. Caporuscio. 1996a. *Conceptual Models Peer Review Report*, Prepared for the U.S. Department of Energy, Carlsbad, New Mexico, July 1996, Docket No. A-93-02 Item II-G-1.

Wilson, C., D. Porter, J. Gibbons, E. Oswald, G. Sjoblom, and F. Caporuscio. 1996b. *Conceptual Models Supplementary Peer Review Report*, Prepared for the U.S. Department of Energy, Carlsbad, New Mexico, December 1996, Docket No. A-93-02 Item II-G-12.

Wilson, C., D. Porter, J. Gibbons, E. Oswald, G. Sjoblom, and F. Caporuscio. 1997a. *Conceptual Models Second Supplementary Peer Review Report*, Prepared for the U.S. Department of Energy, Carlsbad, New Mexico, January 1997, Docket No. A-93-02 Item II-G-21.

Wilson, C., D. Porter, J. Gibbons, E. Oswald, G. Sjoblom, and F. Caporuscio. 1997b. *Conceptual Models Third Supplementary Peer Review Report*, Prepared for the U.S. Department of Energy, Carlsbad, New Mexico, April 1997, Docket No. A-93-02 Item II-G-22.

Wolery, T.J. 1992a. *EQ3/6, A Software Package for Geochemical Modeling of Aqueous Systems: Package Overview and Installation Guide (Version 7.0)*. UCRL-MA-110662 PT I. Lawrence Livermore National Laboratory, Livermore, California.

Wolery, T.J. 1992b. *EQ3NR, A Computer Program for Geochemical Aqueous Speciation-Solubility Calculations: Theoretical Manual, User's Guide, and Related Documentation*

(Version 7.0). UCRL-MA-110662 PT III. Lawrence Livermore National Laboratory, Livermore, California.

Wolery, T.J., and S.A. Daveler. 1992. *EQ6, A Computer Program for Reaction-Path Modeling of Aqueous Geochemical Systems: Theoretical Manual, User's Guide, and Related Documentation (Version 7.0)*. UCRL-MA-110662 PT IV. Lawrence Livermore National Laboratory, Livermore, California.

Wolery, T.J., and D.C. Sassani. 2007. *Analysis of Sulfate Reduction Modeling by Brush et al. (2006)*. Prepared by Lawrence Livermore National Laboratory and Sandia National Laboratories, September 4, 2007.

Wolery, T.J. 2008. E-mail correspondence to J.A. Schramke, S. Cohen & Associates, Vienna, Virginia. February 5, 2008.

Xiong, Y.-L. 2004. *Incorporation of Six Solid Phases Including Hydromagnesite (5424) and Hydromagnesite (4323) into EQ3/6 HMW Database and Its Modified Version HMP*. Memorandum to L.H. Brush, August 4, 2004. Sandia National Laboratories, Carlsbad, New Mexico, ERMS 536321.

Xiong, Y.-L. 2006a. *Incorporation of Calcium Citrate Hydrate, Earlandite; Calcium Oxalate Monohydrate, Whewellite; and Aqueous Species of Citrate and Oxalate into the EQ3/6 HMP Database and Its Modified Version HMY*. Memorandum to L.H. Brush, Sandia National Laboratories, Carlsbad, New Mexico, October 18, 2006. ERMS 544529.

Xiong, Y.-L. 2006b. *Incorporation of Amorphous Calcium Carbonate into the EQ3/6 HMY Database and Its Modified Version HML*. Memorandum to L.H. Brush, Sandia National Laboratories, Carlsbad, New Mexico, October 26, 2006. ERMS 544629.

Xiong, Y.-L., E.J. Nowak, and L.H. Brush. 2004. *Updated Uncertainty Analysis of Actinide Solubilities for the Response to EPA Comment C-23-16*. Sandia National Laboratories, Carlsbad, New Mexico, ERMS 538219. Docket A-98-49 Item II-B2-40.

Xiong, Y., E.J. Nowak, and L.H. Brush. 2005. *Updated Uncertainty Analysis of Actinide Solubilities for the Response to EPA Comment C-23-16*. Rev. 1 (Supersedes ERMS 538219) Sandia National Laboratories, Carlsbad, New Mexico, ERMS 539595.

APPENDIX A: FINAL CHEMISTRY-RELATED CONCEPTUAL MODELS

The chemistry-related conceptual models were originally reviewed and accepted for the CCA PA and PAVT by the Conceptual Model Peer Review Panel (Wilson et al. 1996a, 1996b, 1997a, 1997b) and by the EPA (1997a, 1997b, 1998a, 1998b, 1998c). Additional information relevant to the chemistry-related conceptual models became available during EPA's review of the AMWTP waste emplacement (EPA 2004, TEA 2004) and the CRA (EPA 2006a, 2006b); this information resulted in some changes to the conceptual models. The final features of the conceptual models are summarized in the following sections.

A.1 GAS-GENERATION CONCEPTUAL MODEL ASSUMPTIONS

- A small amount of oxygen will be trapped in the repository immediately after closure. This oxygen is assumed to be quickly consumed by anoxic corrosion or aerobic microbial degradation of CPR and these processes will not generate significant amounts of gas.
- Anoxic corrosion can occur in the repository as soon as the shafts are sealed.
- Anoxic corrosion of steel in the waste and waste containers produces hydrogen (H₂); the chemical reactions that represent the stoichiometry of anoxic corrosion of steel are:
$$\text{Fe} + (x+2) \text{H}_2\text{O} \leftrightarrow \text{Fe}(\text{OH})_2 \cdot x\text{H}_2\text{O} + \text{H}_2$$
$$\text{Fe} + \text{H}_2\text{S} \leftrightarrow \text{FeS} + \text{H}_2$$
- The amounts of aluminum in the waste and steel contained in rockbolts, netting, and equipment that will be left underground after closure are too small to cause significant gas generation.
- Anoxic corrosion cannot occur unless brine is present in the repository and in contact with the steel; anoxic corrosion consumes brine and the corrosion rate is a function of brine saturation.
- Anoxic corrosion is a function of the surface area of steel in the repository and it consumes steel, so the reaction may be limited by the amount of steel in the repository; however, the rate of anoxic corrosion is more likely to be limited by the available amount of brine.
- Microbial degradation of CPR in the waste and waste emplacement materials may produce CO₂, nitrogen (N₂), hydrogen sulfide (H₂S), and methane (CH₄); natural analogue data indicate that CPR degradation processes will occur in the sequence: denitrification → sulfate reduction → methanogenesis.
- CPR degradation is represented by a zero-order reaction rate, so the microbial gas generation rate is independent of the CPR concentration.

- Both anoxic corrosion of steel and microbial degradation of CPR can affect the total quantity of gas generated in the repository.
- CO₂ will be removed from the repository brines and gas phase by reaction with the MgO backfill, so CO₂ generated from CPR degradation will not significantly affect repository gas pressures.
- The most important CPR degradation reactions may be $C_6H_{10}O_5 + 6 H^+ + 3 SO_4^{2-} \rightarrow 5 H_2O + 6 CO_2 + 3 H_2S$ because of the sulfate available from the equilibration of brine with Salado minerals. In areas where limited sulfate may be available because of a higher rate of CPR degradation compared to the rate of sulfate transport from the Salado to the waste, the methanogenesis reaction $C_6H_{10}O_5$ (cellulose monomer) + H₂O → 3 CH₄ + 3 CO₂ (methanogenesis) may be more important. The amount of N₂ produced by microbial degradation of CPR will be negligible because of limited nitrate in the waste. Substantial quantities of H₂S, CO₂, and CH₄ may be produced by CPR degradation.
- CO₂ generated by microbial degradation of CPR will not passivate steel, because CO₂ will be consumed by reaction with the MgO backfill. H₂S might passivate steel by forming FeS on the steel surfaces if H₂S is produced in sufficient quantities. However, reducing chemical conditions would continue to be maintained by the FeS.
- The probability that significant microbial degradation of cellulose will occur without plastics and rubber degradation is 75%, and there is a 25% probability that cellulose, plastics, and rubber will be significantly degraded by microbes.
- The effects of CPR degradation on the amount of brine in the repository are uncertain, so they are not accounted for in PA.
- Gas generation will take place homogeneously throughout the repository because of the assumed homogeneous distribution of waste.
- Radiolysis of water in the waste and brine and radiation of plastics and rubber in the waste will not have significant effects on the amounts of gas generated.

A.2 CHEMICAL CONDITIONS CONCEPTUAL MODEL ASSUMPTIONS

- The Salado Formation is predominantly halite, with accessory anhydrite, gypsum, polyhalite, and magnesite. Small quantities of intergranular and intragranular brines are associated with the salt at the repository horizon. These brines are highly concentrated (ionic strengths up to 8 molar), with a composition of mostly sodium, magnesium, potassium, chloride, and sulfate, with smaller amounts of calcium, carbonate, and borate.
- The underlying Castile Formation is composed of thick beds of interlaminated anhydrite and carbonate layered with halite. The Castile Formation contains localized brine reservoirs under sufficient pressure to force brine upward to the land surface if penetrated by a borehole. Castile brines are concentrated solutions containing predominantly sodium chloride with calcium and sulfate, and smaller concentrations of other elements.

- Brine that dissolves actinides under any intrusion scenario will have a composition equal to that of Salado brine, Castile brine, or a mixture of Salado and Castile brines. Culebra groundwater that could enter the repository would quickly dissolve halite and develop a composition similar to Salado brine. Because the Salado and Castile brines bracket the possible brine compositions, experiments and modeling performed only with end-member brine compositions are adequate for describing the repository geochemistry. The GWB formulation is used to simulate Salado brine and ERDA-6 brine is used to simulate Castile brine.
- Equilibrium is assumed between repository brine, waste, and the Salado minerals halite, anhydrite, brucite, and either magnesite or hydromagnesite.
- Thermodynamic equilibrium is assumed for dissolution and precipitation of actinide-bearing solid phases, but not for redox reactions among the actinides.
- Brine in the repository will be well mixed with waste, and chemical homogeneity and solubility equilibrium will be maintained. Consequently, chemical microenvironments and supersaturated conditions are not believed to persist in the repository for long time periods. Brine composition in the repository will be constant with time after initial, rapid equilibration with the MgO backfill materials.
- CPR degradation may generate CO₂, as described in the Gas Generation conceptual model (Section 2.2). A relatively large excess of MgO will be emplaced with the waste, with 1.20 moles of MgO per mole of CPR carbon. The identity of the dominant CPR degradation reaction and the resulting proportions of CO₂ or CH₄ produced (i.e., sulfate reduction or methanogenesis) will not affect chemical conditions in the repository because of the large excess of MgO.
- In the absence of MgO backfill, low pmH ($-\log_{10}$ of the hydrogen ion molality) and high CO₂ fugacity could be achieved in the repository brine, increasing the solubilities of actinides relative to neutral or slightly basic pmH and low CO₂ fugacity conditions. However, conditions that might lead to high actinide solubilities will not occur in the repository, because excess MgO emplaced as an engineered barrier will buffer the pmH and CO₂ fugacity of the brine so that actinide solubilities are minimized. The pH ($-\log_{10}$ of the hydrogen ion activity) will be buffered between 8 and 10, depending on the brine composition.
- Periclase [MgO] in the backfill will hydrate to form brucite [Mg(OH)₂], which will in turn react with CO₂ to form hydromagnesite, which may convert to magnesite over a long time period. Cementitious material in the repository will contain Ca(OH)₂ that could also react with CO₂ to form calcite. This latter reaction could buffer pmH at relatively high values. However, the effect of Ca(OH)₂ is expected to be minimal because of calcite precipitation and reaction of the Ca(OH)₂ with MgCl₂ in the brine to form CaCl₂.
- Carbon dioxide fugacities that will prevail in the repository can be modeled using the brucite-hydromagnesite buffer.
- Microbial degradation of CPR and/or steel corrosion will result in a reducing environment within 100 years of repository closure.

- Oxidation-reduction equilibrium with waste materials (including iron metal and CPR) is not assumed. Steel corrosion and CPR degradation are represented by reaction rates instead of equilibrium. In most cases, significant amounts of uncorroded steel will be present in the repository throughout the 10,000-year regulatory period.
- Steel corrosion in the repository will reduce the oxidation states of some actinides, affecting their solubilities and binding constants.
- The expected oxidation states of the actinides are determined based on experimental data. Americium is assumed to occur in the +III oxidation state, thorium in the +IV oxidation state, plutonium in the +III or +IV oxidation state, neptunium in the +IV or +V oxidation state, and uranium in the +IV or +VI oxidation state.
- Actinide and ligand inventories are fixed. Although it is possible that microbial consumption of organic ligands in the waste could occur, because of uncertainty about the presence or viability of these types of microbes, it is assumed that organic ligand concentrations will not be reduced by microbial degradation.
- High pressure in the repository is not expected to significantly affect actinide solubilities, so its effect is not considered in the geochemical calculations. Temperature in the repository is not expected to vary significantly from ambient, so temperature effects on solubility also are not considered important.
- Brine radiolysis could produce reactive species, such as hydrogen peroxide (H_2O_2). Any oxidized species such as hydrogen peroxide are expected to react quickly with iron metal and dissolved iron(II) species in solution. Consequently, radiolysis is not expected to affect the oxidation-reduction conditions in the repository.

A.3 DISSOLVED ACTINIDE SOURCE TERM CONCEPTUAL MODEL ASSUMPTIONS

- Equilibrium is maintained between dissolved actinides and actinide solid phases. However, redox reactions among actinides are not assumed to be in equilibrium.
- Brine homogeneity will be maintained due to long-term mixing.
- Anoxic conditions will dominate in the repository.
- Americium and curium will be present only in the +III oxidation state, and thorium will be present only in the +IV oxidation state.
- In the repository brines and equilibrium solid phases, neptunium may be present in the +IV or +V oxidation state, plutonium may be present in the +III or +IV oxidation state, and uranium may be present in the +IV or +VI oxidation state. There is a 50% probability that these actinides will be present in their more reduced states [neptunium(IV), plutonium(III) and uranium(IV)], and a 50% probability that they will be present in their more oxidized states [neptunium(V), plutonium(IV), and uranium(VI)].

- Dissolved actinide concentrations will be controlled by equilibrium with anhydrite, halite, the MgO backfill, actinide-bearing solid phases, and the appropriate brine.
- Because the Salado and Castile brines bracket the possible brine compositions, experiments and modeling performed with end-member brine compositions are adequate for describing actinide solubilities.
- The important ions in WIPP brines are H^+ , Na^+ , K^+ , Mg^{2+} , OH^- , Cl^- , CO_3^{2-} , SO_4^{2-} , and Ca^{2+} . Other ions such as PO_4^{3-} , F^- , Al^{3+} , Fe^{2+} , and Fe^{3+} may be important, but their effects are included only in a qualitative understanding of the chemical environment.
- The water-soluble ligands present in the brine are acetate, citrate, ethylenediaminetetraacetic acid (EDTA) and oxalate. The concentrations of these ligands are based on their total WIPP inventory, and these ligand concentrations remain constant.
- The effects of organic ligands (acetate, citrate, EDTA, and oxalate) are included in actinide solubility calculations using experimentally derived complexation constants. The effects of competition by calcium and magnesium ions are included, using the complexation constants for magnesium. The effects of competition by transition metals such as iron are considered only qualitatively.
- Actinide solubilities are modeled using the Pitzer activity coefficient model, which describes the thermodynamics of highly concentrated electrolyte solutions. Brine compositions are assumed to be constant throughout the 10,000-year regulatory period after rapid equilibration with MgO backfill materials.
- Actinides will not be sorbed on immobile substrates in the repository.
- All actinides in the same oxidation state will form the same aqueous species and isostructural compounds; this assumption has been referred to as the “oxidation-state analogy.”
- The solubilities of americium, curium, and plutonium in the +III oxidation state are modeled using the solubility model for americium(III). This model is based on experimental data for americium(III), curium(III), plutonium(III) and the lanthanide analogue neodymium(III).
- The solubilities of thorium, neptunium, plutonium, and uranium in the +IV oxidations state are modeled using the solubility of thorium(IV). The solubility of neptunium(V) is based on experimental data for the neptunium(V).
- A thermodynamic model is not used for uranium(VI); instead, an upper-limit solubility of 1×10^{-3} M is assumed. Because this is an upper-limit solubility estimate, an uncertainty distribution is not sampled for this parameter.
- Metastable phases observed in laboratory experiments will become more stable with time, and solubilities observed in these experiments provide an upper concentration limit. The effects of radiolysis will not cause actinide solids to become more soluble over time.

- The pH and CO₂ fugacity of the system is buffered by the solubility of brucite and the brucite-hydromagnesite reaction, respectively.
- Point estimates are used for the +III, +IV and +V actinide solubilities, with estimated uncertainties around these point estimates. A separate uncertainty range is used for each actinide oxidation state that is based on a comparison of measured solubilities and solubilities calculated for the experimental conditions. An upper-limit point estimate is used for uranium(VI) without an uncertainty range. The actinide solubilities are assumed to be constant over the entire repository regulatory period.

A.4 REFERENCES

EPA (Environmental Protection Agency) 1997a. *Compliance Application Review Documents for the Criteria for the Certification and Recertification of the Waste Isolation Pilot Plant's Compliance with the 40 CFR Part 191 Disposal Regulations: Final Certification Decision. CARD 23: Models and Computer Codes*. U.S. Environmental Protection Agency Office of Radiation and Indoor Air. Washington, DC. Docket A-93-02 Item V-B-2.

EPA (Environmental Protection Agency) 1997b. *Compliance Application Review Documents for the Criteria for the Certification and Recertification of the Waste Isolation Pilot Plant's Compliance with the 40 CFR Part 191 Disposal Regulations: Final Certification Decision. CARD 44: Engineered Barrier*. U.S. Environmental Protection Agency Office of Radiation and Indoor Air. Washington, DC. Docket A-93-02 Item V-B-2.

EPA (U.S. Environmental Protection Agency) 1998a. *Final WIPP Certification Decision Response to Comments, Criteria for the Certification of the Waste Isolation Pilot Plant's Compliance with 40 CFR Part 191 Disposal Regulations: Certification Decision*. Office of Radiation and Indoor Air, Washington DC. Docket No. A-93-02 Item V-C-1.

EPA (Environmental Protection Agency) 1998b. *Technical Support Document for Section 194.24: EPA's Evaluation of DOE's Actinide Source Term*. Environmental Protection Agency Office of Radiation and Indoor Air, Washington, DC. Docket A-93-02 Item V-B-17.

EPA (Environmental Protection Agency) 1998c. *Technical Support Document: Overview of Major Performance Assessment Issues*. Environmental Protection Agency Office of Radiation and Indoor Air, Washington, DC. Docket A-93-02 Item V-B-5.

EPA (Environmental Protection Agency) 2004. Letter from Frank Marcinowski, U.S. Environmental Protection Agency Office of Radiation and Indoor Air, Washington DC, to R. Paul Detwiler, U.S. Department of Energy Carlsbad Field Office, March 26, 2004.

EPA (Environmental Protection Agency) 2006a. *Technical Support Document for Section 194.23: Review of the 2004 Compliance Recertification Performance Assessment Baseline Calculation*. Office of Radiation and Indoor Air, Docket No. A-98-49, Item II-B1-3, March 2006.

EPA (Environmental Protection Agency) 2006b. *Technical Support Document for Section 194.24: Evaluation of the Compliance Recertification Actinide Source Term and Culebra*

Dolomite Distribution Coefficient Values. Office of Radiation and Indoor Air, Docket No. A-98-49, Item II-B1-16, March 2006.

TEA (Trinity Engineering Associates) 2004. *Review of Effects of Supercompacted Waste and Heterogeneous Waste Emplacement on WIPP Repository Performance, Final Report.* Prepared for U.S. Environmental Protection Agency, Office of Radiation and Indoor Air, Washington, DC, March 17, 2004.

Wilson, C., D. Porter, J. Gibbons, E. Oswald, G. Sjoblom, and F. Caporuscio. 1996a. *Conceptual Models Peer Review Report.* Prepared for the U.S. Department of Energy, Carlsbad, New Mexico, July 1996, Docket No. A-93-02 Item II-G-1.

Wilson, C., D. Porter, J. Gibbons, E. Oswald, G. Sjoblom, and F. Caporuscio. 1996b. *Conceptual Models Supplementary Peer Review Report.* Prepared for the U.S. Department of Energy, Carlsbad, New Mexico, December 1996, Docket No. A-93-02 Item II-G-12.

Wilson, C., D. Porter, J. Gibbons, E. Oswald, G. Sjoblom, and F. Caporuscio. 1997a. *Conceptual Models Second Supplementary Peer Review Report.* Prepared for the U.S. Department of Energy, Carlsbad, New Mexico, January 1997, Docket No. A-93-02 Item II-G-21.

Wilson, C., D. Porter, J. Gibbons, E. Oswald, G. Sjoblom, and F. Caporuscio. 1997b. *Conceptual Models Third Supplementary Peer Review Report.* Prepared for the U.S. Department of Energy, Carlsbad, New Mexico, April 1997, Docket No. A-93-02 Item II-G-22.

APPENDIX B: WOLERY AND SASSANI (2007) EQ3/6 MODELING RESULTS

Table B.1 Wolery and Sassani (2007) Modeling Results

Brine	GWB	GWB	GWB	GWB	GWB	GWB
Brine Volume (m ³)	1,045	1,045	1,045	1,045	1,045	1,045
Organic Ligands	None	None	None	None	None	None
EQ6 Output File	1-gwb-02.6o	1-gwb-2x.6o	hstest.6o	test.6o	testk.6o	testm.6o
Suppressed Minerals	Dolomite, glauberite	Dolomite, glauberite, polyhalite	Dolomite, glauberite, polyhalite, pyrite	Dolomite, glauberite, polyhalite, pyrite	Dolomite, glauberite, polyhalite, pyrite	Dolomite, glauberite, polyhalite, pyrite
Salado Minerals (% DRZ)	49%	49%	49%	49%	49%	49%
Final pH	11.3	6.88	7.46	11.6	11.6	12.2
X _i (moles)	66	63	66	66	66	66
Final log f _{CO2}	n.r.	n.r.	n.r.	-7.062	-7.063	-13.21
Final Total Carbonate (m)	0.250	5.470 × 10 ⁻⁴	2.049 × 10 ⁻⁴	0.445	0.451	1.251 × 10 ⁻⁵
Notes	Reran unpublished titration calculation without iron or sulfides	Titration calculation that included sulfide aqueous and solid species	Titration calculation that included iron and sulfide aqueous and solid species	C ₆ H ₁₀ O ₅ degradation set up as an irreversible reaction, calculation included iron and sulfide aqueous and solid species	C ₆ H ₁₀ O ₅ degradation set up as an irreversible reaction, calculation included iron and sulfide aqueous and solid species, tripled iron corrosion rate	C ₆ H ₁₀ O ₅ degradation set up as an irreversible reaction, calculation included iron and sulfide aqueous and solid species, C ₆ H ₁₀ O ₅ degradation rate set equal to zero
Final Solid Phases	Brucite, calcite, halite, magnesite, pirssonite, sylvite	Anhydrite, brucite, calcite, halite, magnesite, sylvite	Brucite, calcite, halite, magnesite, sylvite, troilite	Brucite, calcite, halite, magnesite, pirssonite, sylvite, troilite	Brucite, calcite, halite, iron, magnesite, pirssonite, sylvite, troilite	Brucite, calcite, halite, magnetite, portlandite, sylvite, troilite

Table B.1 Wolery and Sassani (2007) Modeling Results (continued)

Brine	GWB	GWB	GWB
Brine Volume (m ³)	1,045	1,045	1,045
Organic Ligands	None	None	None
EQ6 Output File	test.6o	1-gwb-04.6o	1-gwb-4x.6o
Suppressed Minerals	Dolomite, glauberite, polyhalite, pyrite	Dolomite, glauberite	Dolomite, glauberite, polyhalite
Salado Minerals (% DRZ)	49%	25%	25%
Final pH	6.82	11.3	7.32
X _i (moles)	66.0	33.4	33.4
Final log f _{CO2}	n.r.	n.r.	n.r.
Final Total Carbonate (m)	5.498 × 10 ⁻⁴	0.249	4.464 × 10 ⁻⁴
Notes	Titration calculation that included iron and sulfide aqueous and solid species	Reran unpublished titration calculation without iron or sulfides	Titration calculation that included sulfide aqueous and solid species
Final Solid Phases	Brucite, calcite, halite, iron, magnesite, sylvite, troilite	Brucite, calcite, halite, magnesite, pirssonite, sylvite	Anhydrite, brucite, calcite, halite, magnesite, oxychloride-Mg, sylvite

REFERENCES

Wolery, T.J., and D.C. Sassani. 2007. *Analysis of Sulfate Reduction Modeling by Brush et al. (2006)*. Prepared by Lawrence Livermore National Laboratory and Sandia National Laboratories, September 4, 2007.

APPENDIX C: AVAILABILITY OF SULFATE TO SUPPORT MICROBIAL DEGRADATION

In the 2005 Performance Assessment Baseline Calculation (PABC) it was assumed that the predominant mechanism for biodegradation of the cellulosics, plastics and rubber (CPR) in the WIPP repository was sulfate reduction. This was based on the presumption that adequate sulfate was available in the near field to provide the required oxyanions. However, a rigorous analysis was not conducted to verify availability of adequate sulfate to support biodegradation reactions. Because geochemical modeling simulations of CPR degradation in the WIPP repository have indicated that the brine pH may be sensitive to the amount of sulfate available for reaction, the following analysis provides this verification.

C.1 RATES OF MICROBIAL DEGRADATION OF CPR

Carbon dioxide is produced by the microbial degradation of CPR. Carbon dioxide gas generation rates used in the Compliance Certification Application (CCA), the Performance Assessment Verification Test (PAVT), and the Compliance Recertification Application (CRA)-2004 were based on experimental measurements of microbial degradation for time periods of up to 411 days for the maximum inundated rates and up to 1,034 days for the minimum inundated rates (Nemer et al. 2005). For the PABC, the gas generation rates were updated and revised to include experimental data for 10 years. The revised long-term rates are significantly lower, reflecting the fact that the gas generation from microbial degradation decreased with time, after an initial high rate. The two sets of data are summarized in Table C-1. It should be noted that the data for the maximum rate are based on cellulose degradation under inundated, anaerobic conditions with the solutions amended with nutrients and excess nitrate. Tests on unirradiated and electron-beam irradiated samples of rubber and plastics showed no significant gas generation for up to 840 days (Francis et al. 1997).

Table C-1. Inundated Reaction Rates Used in BRAGFLO for Various WIPP Performance Assessments (Nemer et al. 2005, Table 2)

Inundated Rate	CCA, PAVT, CRA-2004		PABC	
	(mole C/kg cellulose/yr)	(mole C/kg cellulose/sec)	(mole C/kg cellulose/yr)	(mole C/kg cellulose/sec)
Maximum inundated rate	0.30	9.5129×10^{-9}	1.757×10^{-2}	5.5692×10^{-10}
Mean inundated rate	0.15	4.915×10^{-9}	9.270×10^{-3}	2.9388×10^{-10}
Minimum inundated rate	0.010	3.1710×10^{-10}	9.727×10^{-4}	3.0827×10^{-11}

In Table C-1, the experimental measurements have been converted to units suitable for input to BRAGFLO and the mean values have been calculated based on an assumed uniform probability distribution between the minimum and maximum inundated rates.

It can be observed in Table C-1 that the mean reaction rate was an order of magnitude less for the PABC than for earlier performance assessments.

In a special performance assessment associated with DOE's request to dispose of Advanced Mixed Waste Treatment Project (AMWTP) waste, Kanney et al. (2004) examined BRAGFLO output files to determine the time at which CPR degradation was essentially complete. Inundated reaction rates were the same higher rates as used in the CCA, the PAVT, and the CRA. For all but a few of the vectors in this special performance assessment, the CPR had been consumed in less than 2,000 years for both S1 (undisturbed) and S2 (E1 intrusion at 350 years) scenarios (Kanney et al. 2004, Figures 4 and 5). This is a reasonable conclusion because, based on the mean CCA/CRA/PAVT inundated rate (Table C-1) and the equivalent mass of cellulose⁴ from the CRA of 2.89×10^7 kg (Table C-2) containing 1.09×10^9 moles of carbon (Table C-3), the rate of carbon generation from microbial degradation would be 4.34×10^6 moles of carbon per year (0.15 moles C/kg cellulose/yr $\times 2.89 \times 10^7$ kg cellulose). At that rate, all the CPR would be consumed in about 250 years (1.09×10^9 moles C/ 4.34×10^6 moles C/yr). However, based on the mean microbial degradation rate used in the PABC, about 4,000 years would be required to consume all of the CPR, assuming an equivalent cellulose mass of 3.25×10^7 kg (1.21×10^9 moles C/ $[9.270 \times 10^{-3}$ moles C/kg cellulose/yr $\times 3.25 \times 10^7$ kg cellulose]). CPR consumption based on the PABC inundated microbial degradation rates is shown in Figure C-1.

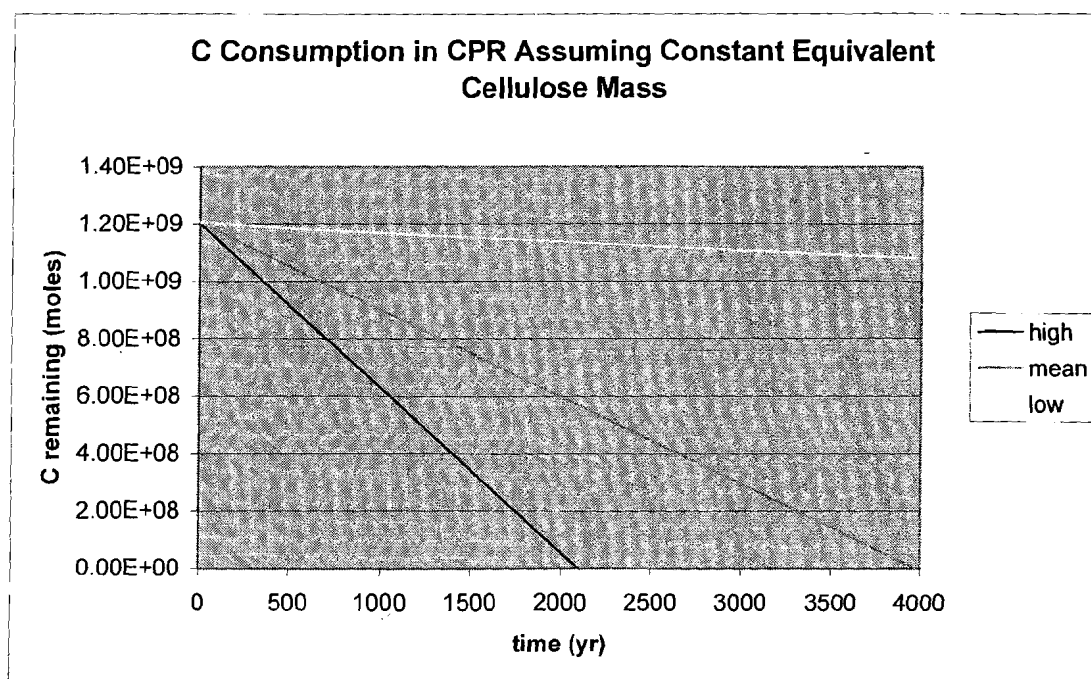


Figure C-1. Consumption of CPR by Microbial Degradation in PABC Based on Inundated Reaction Rates in Table C-1

⁴ To obtain the equivalent mass of cellulose, the moles of carbon in each non-cellulosic component are divided by the mass of component and multiplied by the molecular weight of cellulose and divided by 6 to reflect the moles of carbon in a mole of cellulose (see Wang and Brush 1996). Based on the mix of CPR materials assumed in performance assessments, the multiplier to convert the mass of rubber to the equivalent mass of cellulose is 1 and the multiplier for plastics is 1.7.

Table C-2. Mass of CPR and Equivalent Cellulose Used in CRA and PABC Performance Assessments

CPR Material	PABC	PABC	PABC	PABC	CRA	CRA	CRA	CRA
	Waste Material Density (kg/m ³)	Volume (m ³)	Mass (kg)	Equivalent Cellulose Mass (kg)	Waste Material Density (kg/m ³)	Volume (m ³)	Mass (kg)	Equivalent Cellulose Mass (kg)
CH								
Cellulose	60	168485	1.01×10^7	1.01×10^7	58	168485	9.77×10^6	9.77×10^6
Rubber	13	168485	2.19×10^6	2.19×10^6	14	168485	2.36×10^6	2.36×10^6
Plastic	43	168485	7.24×10^6	1.23×10^7	42	168485	7.08×10^6	1.20×10^7
Packaging (plastics/liners)	17	168485	2.86×10^6	4.87×10^6	16	168485	2.70×10^6	4.58×10^6
RH								
Cellulose	9.3	7079	6.58×10^4	6.58×10^4	4.5	7079	3.19×10^4	3.19×10^4
Rubber	6.7	7079	4.74×10^4	4.74×10^4	3.1	7079	2.19×10^4	2.19×10^4
Plastic	8.0	7079	5.66×10^4	9.63×10^4	4.9	7079	3.47×10^4	3.73×10^4
Packaging (plastics/liners)	3.1	7079	2.19×10^4	3.73×10^4	1.4	7079	9.91×10^3	5.90×10^4
Emplacement Material								
Cellulose			2.07×10^5	2.07×10^5			0.00	0.00
Plastic			1.48×10^6	2.52×10^6			0.00	0.00
TOTAL			2.43×10^7	3.25×10^7			2.20×10^7	2.89×10^7

Table C-3. Total Moles of Carbon in CPR for CRA and PABC Performance Assessments

Materials	PABC Mass (kg)	CRA Mass (kg)	Formula	Mol. Wt. (kg/mole)	PABC Moles C	CRA Moles C
Cellulosics	1.04×10^7	1.00×10^7	$C_6H_{10}O_5$	0.16214	3.84×10^8	3.72×10^8
Plastics	1.17×10^7	9.85×10^6				
PE (80%)	9.33×10^6	7.88×10^6	C_2H_4	0.02805	6.65×10^8	5.62×10^8
PVC (20%)	2.33×10^6	1.97×10^6	C_2H_3Cl	0.06250	7.47×10^7	6.30×10^7
Rubbers	2.24×10^6	2.41×10^6				
Hypalon (50%)	1.12×10^6	1.20×10^6	$(C_7H_{13}Cl)_{12}$ - $(CHSO_2Cl)_{17}$	3.50470	3.22×10^7	3.47×10^7
Neoprene (50%)	1.12×10^6	1.20×10^6	C_4H_5Cl	0.08854	5.05×10^7	5.44×10^7
Total	2.43×10^7	2.23×10^7			1.21×10^9	1.09×10^9

The estimates of the time required to consume all the CPR described above assume that the mass of cellulose (as a surrogate for CPR) remains constant and thus, not only the reaction rate expressed as moles C/kg cellulose/yr, but also the rate of carbon release expressed as moles C/yr are constant. However, the mass of CPR will decrease with time as microbial degradation progresses. This physical fact can be represented by assuming that the mass of CPR remaining decreases exponentially rather than linearly. Using this assumption and the mean inundated reaction rate for the PABC, the mass of CPR remaining at 10,000 years is 3.42×10^6 kg or about 14% of the original CPR mass. Even at the maximum (high) inundated rate for the PABC, a small amount of CPR remains. This situation is illustrated in Figure C-2.

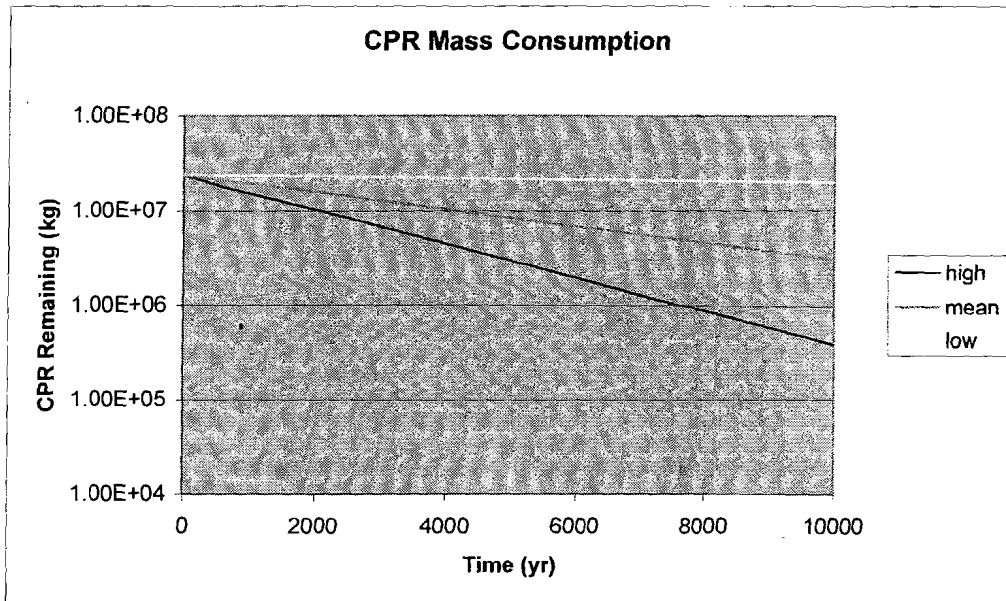
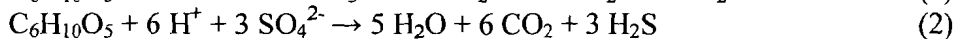
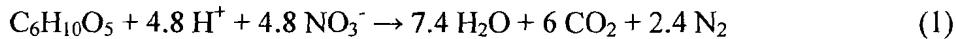


Figure C-2. CPR Consumption Based on Adjusting Inundated Microbial Degradation Rates for Continuous Reduction in CPR Mass

C.2 SULFATE REQUIREMENTS FOR MICROBIAL DEGRADATION

For the PABC, EPA required DOE to assume that all microbial degradation occurred by denitrification or sulfate reduction (reactions 1 and 2 below). Methanogenesis (reaction 3) was excluded on the presumption that adequate sulfate was available in the surrounding Salado Formation to support continuing sulfate reduction, which is energetically favored over methanogenesis.



Sulfate is present in the Salado and Castile brines, as well as in minerals present in the Salado Formation surrounding the repository, including anhydrite (CaSO_4), gypsum [$\text{CaSO}_4 \cdot 2\text{H}_2\text{O}$] and polyhalite [$\text{K}_2\text{MgCa}_2(\text{SO}_4)_4 \cdot 2\text{H}_2\text{O}$]. For sulfate to be available to participate in the microbial degradation process, it must be transported through the Salado to the CPR materials in the waste. For simplicity, we will assume here that the waste is inundated with brine and that once the sulfate ions have reached the brine they are immediately available for reaction with the CPR. Transport and mixing in the brine occur instantaneously.

If one makes the further simplifying assumption that all microbial degradation were to proceed according to reaction (2),⁵ 3 moles of sulfate would be required for each mole of cellulose (containing 6 moles of carbon). Based on the PABC value of 1.21×10^9 moles of carbon in the CPR or 2.02×10^8 moles of cellulosic equivalents, 6.06×10^8 moles of sulfate (or 5.82×10^7 kg) must be available to support the sulfate reduction reaction, if the CPR completely degrades within the repository lifetime. On a panel basis, 5.82×10^6 kg would be required for total CPR consumption.

Considerable uncertainty exists as to whether or not microbial degradation will occur in the WIPP and, if it does, to what extent will the cellulose, plastics, and rubber be consumed. For microbial degradation to occur, conditions that must be met include (Brush 2004):

- Presence of halophilic microbes that persist for thousands of years
- Presence and availability of sufficient nutrients
- Presence and availability of sufficient electron acceptors
- Presence of sufficient water

To account for this uncertainty, DOE assumed in the PABC that the probability of microbial degradation occurring was expressed by parameter (BIOGENFC) varying uniformly between 0 and 1. This uncertain parameter was used as a multiplier for the gas generation rates associated with microbial degradation of CPR. To account for uncertainty in the extent to which these reactions occur, it was assumed in the PABC that degradation of the cellulose occurs in all

⁵ Based on the nitrate content of the waste used in the PABC, denitrification results in degradation of only 4% of the CPR (Leigh et al. 2005a).

realizations and degradation of the plastics and rubber occurs in 25% of the realizations (Nemer and Stein 2005).

C.3 ADVECTIVE TRANSPORT OF SULFATE

Kanney et al. (2004) considered mechanisms and pathways for sulfate transport through the Salado Formation, including diffusion and advection. With regard to advection in the undisturbed repository, if the room pressure is less than lithostatic pressure, Kanney et al. (2004) concluded that any cracks in the salt strata in the back or the floor would heal in 50 to 100 years, isolating sulfate-bearing strata (e.g., Marker Bed 139) from advective flow. While healing of the DRZ in the rib area would take longer because of the stress distribution in the halite, cracks in this region would be parallel to the walls and thus not provide advective pathways for brine access. For conditions in the undisturbed repository where the room pressure exceeds lithostatic, fracturing of the adjacent rocks could occur. However, as long as the pressure in the fractures exceeds the far-field pressure of the interstitial brines, brine flow to the waste will be impeded. If this pressure decays, healing of the fractures will occur. Consequently, advective flow and sulfate transport should be limited for the undisturbed repository.⁶

Kanney et al. (2004) assumed that the maximum advective transport of sulfate would be associated with maximum brine inflow from an E1 intrusion. This inflow was $7.74 \times 10^4 \text{ m}^3$ into a panel for time periods of up to 2,000 years for the AMWTP performance assessment. However, based on the reduced CPR degradation rate used in the PABC, one should consider the full 10,000-year repository regulatory period. The maximum brine inflow into an intruded waste panel in the PABC was $3.19 \times 10^4 \text{ m}^3$ (Nemer and Stein 2005, Table 6-13). Values for the two performance assessments are compared in Table C-4.

Table C-4. Estimates of the Maximum Amount of Sulfate Advected into an Intruded Waste Panel by WIPP Brines

Time (yr)	Performance Assessment	Sulfate ⁻ (mole/L)	Maximum Brine Inflow (m ³)	Sulfate Advected in Brine	
				(moles)	(kg)
2,000	AMWTP	0.182 ^a	7.74×10^4	1.41×10^7	1.35×10^6
10,000	PABC	0.170 ^b	3.19×10^4	5.42×10^6	5.21×10^5

a – GWB after microbial reaction (Kanney et al. 2004)

b - ERDA-6 brine (Kanney et al. 2004)

It should be noted that the values in Table C-4 are per panel.

⁶ The maximum brine volume in an undisturbed waste panel in the PABC is $7,746 \text{ m}^3$ (Clayton 2006).

For the AMWTP performance assessment, the amount of advected sulfate available to participate in the sulfate reduction reaction in an intruded panel is about 23% of the 5.82×10^6 kg required for consumption of all CPR by sulfate reduction. Advected sulfate provides only about 9% of the amount required based on PABC assumptions. Clayton and Nemer (2006) performed a probability analysis using PABC vectors and determined that there was less than a 1% probability that enough sulfate would enter the “worst case” panel and consume 27% or more of the carbon by sulfate reduction. This supports the position presented in Table C-4 that sufficient sulfate is available in advected brines to support only limited microbial degradation based on the PABC.

C.4 DIFFUSIVE TRANSPORT OF SULFATE

Kanney et al. (2004) also examined diffusion from the surrounding Salado Formation rocks as a source of sulfate to support microbial degradation. They argued that, as sulfate is consumed by the waste, a concentration gradient would be established between sulfate in the brine contacting the waste and the brine in the DRZ pore water. This would create a driving force for continuing diffusion toward the waste. As sulfate is depleted from the DRZ pore water, it would be restored by dissolution of sulfate from the surrounding Salado rocks. The dissolution would also be diffusion-controlled. However, to develop a conservative bounding estimate, Kanney et al. (2004) assumed that dissolution of sulfate into the DRZ pore water was not a rate-limiting process. It should be emphasized that this model assumes that a continuous brine pathway exists to transport the sulfate from the DRZ to the waste.

For a bounding diffusion calculation, Kanney et al (2004) assumed an effective sulfate diffusion coefficient, D_{eff} , of 4.48×10^{-12} m²/sec. This diffusivity was based on modifying the free liquid diffusion coefficient for sulfate in sea water for porosity and tortuosity (using a cementation factor). Solving Fick’s Law for appropriate initial and boundary conditions yielded the following equation:

$$C_{\text{SO}_4} - C_0 / C_\infty - C_0 = \text{erf}(x / \sqrt{4D_{\text{eff}}t})$$

where x is the distance from the panel surface into the rock, t is time over which diffusion occurs, C_{SO_4} is the sulfate concentration as a function of x and t , C_0 is the sulfate concentration at the panel surface, and C_∞ is the initial bulk sulfate concentration (i.e., the far-field concentration). When the argument of the error function is unity, x is a characteristic length (L_{diff}) at which the sulfate concentration is 85% of the far-field value. Kanney et al. (2004) used a value of $t = 2,000$ years based on the fact that, in the AMWTP PA, all of the CPR had been degraded in less than that time for most PA vectors. Using this time, they calculated a value for L_{diff} of 1.06 m. Combining this value of L_{diff} , a panel surface area of 3.19×10^4 m², and an initial sulfate concentration of 69.799 kg/m³ in the DRZ rock, they calculated that 2.37×10^6 kg of sulfate diffused from the rock (Kanney et al. 2004, Table 9).

This approach is likely to significantly overestimate the available sulfate, since it is based on the initial concentration of sulfate in the Salado rocks and a rock volume defined by a characteristic diffusion length. The concentration at the characteristic diffusion length is 85% of the far-field concentration and falls to C_0 at the panel surface following a concentration/distance curve

defined by the error function. Thus, the calculated quantity of sulfate diffusing from the rock into the brine is overstated in Kanney et al. (2004). Figure C-3 shows the relative sulfate concentration as a function of distance from the panel surface for various times. In this figure, C_0 is zero and C_∞ is unity. It may be noted that, for the 2,000-yr curve at a distance of one meter, the concentration is about 85% of the far-field value, consistent with that reported in Kanney et al. (2004). It can also be seen that assuming that all sulfate is removed from the affected volume defined by the characteristic diffusion length at 2,000 years overstates the available sulfate significantly. It can be estimated from the 2,000-year curve in Figure C-3, that the average concentration remaining in a 1-m surface layer is about 45% of the far-field concentration. Thus, the amount available would be 1.30×10^6 kg (3.19×10^4 m² \times 1.06 m \times 69.799 kg/m³ \times (1 - 0.45)), rather than 2.37×10^6 kg proposed by Kanney et al. (2004).

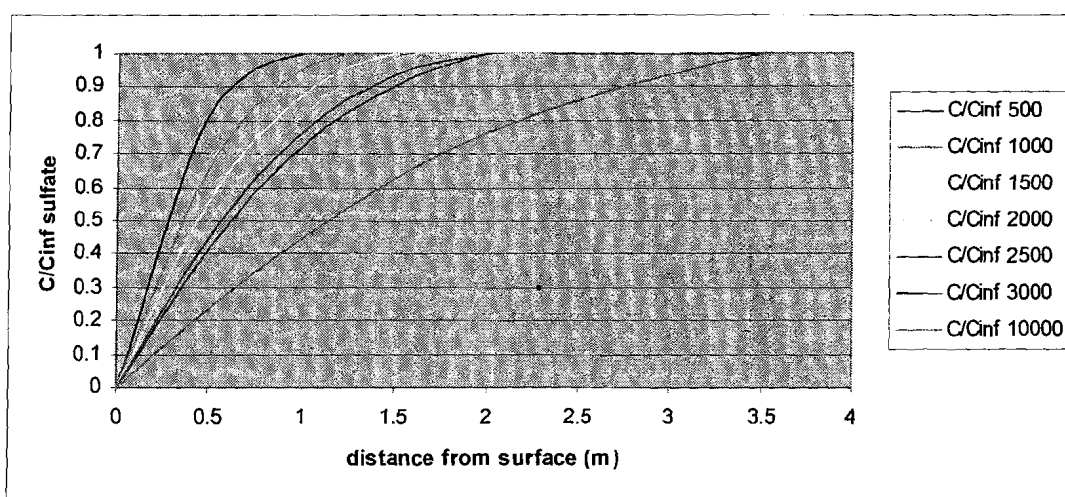


Figure C-3. Relative Sulfate Concentration in WIPP Panel Wall as Functions of Diffusion Time and Distance

For $t = 10,000$ yr, L_{diff} is 2.4 m. The total mass of sulfate contained in the volume defined by this thickness and the panel wall surface area is 5.34×10^6 kg (2.4 m \times 3.19×10^4 m² \times 69.799 kg/m³). From Figure C-3, it can be estimated that the average relative sulfate concentration remaining in the host rock is 0.5 for the thickness interval between 0 and 2.4 m. Thus, the amount of sulfate removed from the walls of a panel by diffusion is 2.67×10^6 kg (50% of 5.34×10^6 kg), and the amount of sulfate removed from the walls of 10 equivalent panels is 2.67×10^7 kg.

As noted above in the discussion of Figure C-2, 3.42×10^6 kg of CPR would remain at the mean degradation rate, assuming a continuously declining mass of CPR from biodegradation. Consequently, 2.09×10^7 kg of CPR would have been consumed (2.43×10^7 kg [see Table C-3] $-$ 3.42×10^6 kg = 2.09×10^7 kg). Assuming, for simplicity, that this mass of CPR has a chemical composition equivalent to cellulose, the moles of cellulose would require consumption of 3.86×10^8 moles of sulfate via reaction (2), which equals 3.71×10^7 kg. Since only 2.67×10^7 kg are available from diffusion, diffusion alone would not support sulfate reduction of 2.09×10^7 kg of CPR at the mean biodegradation rate. This conclusion is based on the assumptions that the

average sulfate content of the Salado rocks local to the repository horizon is 69.799 kg/m³ (Kanney et al. 2004, Section 3.1.2) and that the sulfate is uniformly distributed.

C.5 NON-UNIFORM SULFATE DISTRIBUTION

Based on the Salado stratigraphy, it can be argued that use of the average sulfate content of 69.799 kg/m³ might underestimate the sulfate content in the rock close to the waste panels due to the proximity of marker beds and other anhydrite layers. Table C-5 summarizes data on critical thicknesses and elevations of several sulfate-bearing stratigraphic horizons near the waste panels (Christian-Frear and Webb 1996, pp. C-3 and C-4).⁷ It is important to note that the back in Panels 3, 4, 5, 6, and 9 will be raised 2.4 m to Clay Seam G [which coincides with anhydrite layer *b*] at 386.88 m (DOE 2004, Appendix PA, Attachment MASS, MASS-2.5.1)]. While one DOE reference shows that Clay Seam G is removed but Anhydrite *b* remains (Stein and Zelinski 2003), a more recent presentation to EPA by Dr. W. A. Thompson of WRES–Golder Associates states categorically that for the raised panels “Anhydrite *b* is also removed” (Thompson 2004). It is assumed here that Anhydrite *b* is removed, because this approach is more conservative with respect to sulfate availability.

Table C-5. Location of Anhydrite Near Repository Horizon

Unit	Thickness (m)	Elevation at Unit Top (m amsl)
MB-138 (Clay K)	0.22	396.00
Anhydrite <i>a</i> (Clay K)	0.22	389.11
Anhydrite <i>b</i> (Clay G)	0.06	386.88
Panels 3,4,5,6,9	4.0	386.88
Panels 1,2,7,8,10	4.0	380.49+4.0 = 384.49
MB-139 (Clay E)	0.85	379.11

The top of the Anhydrite *a* layer is 389.11 m or about 2.2 m above the back for this group of raised panels. Thus, Anhydrite *a* could provide an above-average concentration of sulfate, at least for Panels 3, 4, 5, 6, and 9.

Using information from Stein (1985), it is possible to estimate the anhydrite content of selected stratigraphic elements. Stein examined drill core taken near the waste disposal area of the repository. Samples from the drill core were crushed and immersed in water, removing soluble components such as halite. The water-insoluble residue was then boiled in 0.25 M EDTA to dissolve anhydrite and any divalent carbonates. The remaining EDTA-insoluble residue contained species such as quartz, magnesite, and magnesium silicates. The dissolution results were supported by x-ray diffraction studies of the residues. It is assumed in this report that the material dissolved in EDTA was anhydrite. Stein’s results are summarized in Table C-6. Two samples (FH-202 and FH-224) were taken from the stratum containing Marker Bed 139 (MB-139), so the average of the results is used here.

⁷ Another DOE reference (Stein and Zelinski 2003) quotes the same thicknesses for the Anhydrites *a* and *b* and MB-139 as used here, but slightly different thicknesses for the intervening strata.

Table C-6. Anhydrite Content of Selected Stratigraphic Horizons^a

Sample No.	Sample Thickness (m)	Stratum	Water-Insoluble Residue (wt. %)	EDTA-Insoluble Residue (wt. %)	Estimated Anhydrite Content (wt. %)
FH-236	0.14	Anhydrite <i>a</i>	87.08	0.2	86.88
FH-231	0.06	Anhydrite <i>b</i>	28.32	0.03	28.29
FH-202	0.21	MB-139	34.35	0.17	34.18
FH-224	0.12	MB-139	61.14	0.92	60.22

a – Source: Stein (1985), Tables 2 and 3.

MB-139 lies below the repository floor, being about 3.8 m below the floor of Panels 3, 4, 5, 6, and 9 and 1.4 m below the floor in Panels 1, 2, 7, 8, and 10. MB-139 could be a source of sulfate for Panels 1, 2, 7, 8, and 10 and possibly for Panels 3, 4, 5, 6, and 9. MB-139 is 0.85 m thick and the panel footprint is $1.15 \times 10^4 \text{ m}^2$ (the panel volume is $4.61 \times 10^4 \text{ m}^3$ per Attachment PAR, Table PAR-45 and the panel height is 4 m per Christian-Frear and Webb 1996, Figure 9). Thus the volume of mineral in MB-139 underlying a panel is $9.8 \times 10^3 \text{ m}^3$. MB-139 contains 47 wt % anhydrite (average of samples FH-202 and FH-224 in Table C-6), with the water-soluble balance assumed to be halite. Using $2,970 \text{ kg/m}^3$ for the density of anhydrite and $2,160 \text{ kg/m}^3$ for the density of halite, the amount of the sulfate in MB-139 under a panel would be $8.26 \times 10^6 \text{ kg}$ ($[2,970 \text{ kg/m}^3 \times 0.47 + 2,160 \text{ kg/m}^3 \times 0.53] \times 9.8 \times 10^3 \text{ m}^3 \times 0.706 \text{ kg sulfate/kg anhydrite} \times 0.47 \text{ kg sulfate/kg mineral}$). Based on this estimated sulfate content, the mass of sulfate in the MB-139 anhydrite is sufficient to support complete degradation of all of the CPR by the sulfate reduction reaction, which requires $5.82 \times 10^6 \text{ kg}$ of sulfate for each of these five panels.

Anhydrite *b* lies about 2.3 m above the back of Panels 1, 2, 7, 8, and 10 and could also be a source of sulfate to promote CPR degradation in this group of panels. The volume of the Anhydrite *b* overlying each of these panels is 690 m^3 ($1.15 \times 10^4 \text{ m}^2 \times 0.06 \text{ m}$). Assuming that Anhydrite *b* contains 28% anhydrite, the amount of sulfate in Anhydrite *b* overlying each of these five panels is $3.26 \times 10^5 \text{ kg}$ of sulfate ($[2,970 \text{ kg/m}^3 \times 0.28 + 2,160 \text{ kg/m}^3 \times 0.72] \times 6.9 \times 10^2 \text{ m}^3 \times 0.706 \text{ kg sulfate/kg anhydrite} \times 0.28 \text{ kg sulfate/kg mineral}$).

Since Panels 3, 4, 5, 6, and 9 lie more distant from MB-139, Anhydrite *a* must be considered as a source of sulfate for these panels. According to Christian-Frear and Webb (1996), the thickness of Anhydrite *a* is 0.22 m. Anhydrite *a* would contain $4.44 \times 10^6 \text{ kg}$ of sulfate above each of these panels ($0.22 \text{ m} \times 1.15 \times 10^4 \text{ m}^2/\text{panel} \times [2,970 \text{ kg/m}^3 \times 0.87 + 2,160 \text{ kg/m}^3 \times 0.13] \times 0.706 \text{ kg sulfate/kg anhydrite} \times 0.87 \text{ kg sulfate/kg mineral}$).

In summary, it appears that sulfate from Anhydrite *a* is sufficient to support microbial degradation of 76% of the CPR in Panels 3, 4, 5, 6, and 9, and sulfate from MB-139 is sufficient to support microbial degradation of all of the CPR in Panels 1, 2, 7, 8, and 10. However, this sulfate must diffuse through the intervening halite to reach the waste and become available to promote the sulfate reduction reaction. The likelihood that this can occur is discussed subsequently.

Sulfate from Anhydrite *b* would also be available in the side walls around the periphery of the disposal rooms in Panels 3, 4, 5, 6, and 9. A repository room is 91 m long and 10.1 m wide (DOE 2004, Chapter 3, Section 3.2) and the repository contains 120.3 equivalent rooms (Clayton 2006). Since Anhydrite *b* is 0.06 m thick (Table C-5), the exposed area of Anhydrite *b* in the periphery of each of these panels would be 145 m^2 ($[2 \times 91 \text{ m} + 2 \times 10.1 \text{ m}] \times 120.3 \text{ rooms}/10 \text{ panels} \times 0.06 \text{ m}$). If anhydrite is available to a depth of 2.4 m into the side walls (for $t = 10,000 \text{ yr}$, L_{diff} is 2.4 m), $1.64 \times 10^5 \text{ kg}$ of sulfate would be contained in the peripheral volume in Anhydrite *b* around each panel ($2.4 \text{ m} \times 145 \text{ m}^2 \times [2,970 \text{ kg}/\text{m}^3 \times 0.28 + 2,160 \text{ kg}/\text{m}^3 \times 0.72] \times 0.706 \text{ kg sulfate}/\text{kg anhydrite} \times 0.28 \text{ kg sulfate}/\text{kg mineral}$). Of this, about 50% or $8.21 \times 10^4 \text{ kg}$ of sulfate would have diffused into each of Panels 3, 4, 5, 6, and 9 in 10,000 years (see Section C.4). These panels must be brine-filled to provide a transport pathway from this sulfate source.

As described above, there is a significant amount of sulfate in the marker beds and anhydrite layers near the repository horizon. The question is whether this material can diffuse at a rate sufficient to meet the sulfate requirements for microbial degradation of CPR based on a non-uniform sulfate distribution defined by near-field stratigraphy. Crank (1975) analyzed the case of diffusion in a plane sheet where the initial concentration at one surface was C_1 , the initial concentration in the sheet was C_0 , and the concentration at the other surface was C_2 . If one considers the Salado rock lying between an anhydrite layer and a waste panel surface as such a sheet with initial sulfate concentration C_0 , constant sulfate concentration at the anhydrite interface C_1 , and concentration at the waste panel surface as C_2 , the diffusion equation can be solved, but the solution is cumbersome. For the simplified case where C_0 and C_2 are zero, the solution is more manageable. Assuming that $C_2 = \text{zero}$ is consistent with the situation that sulfate reacts immediately with the CPR in the waste when sulfate ions arrive at the panel wall. Assuming that C_0 is zero is consistent with the assumption that most of the sulfate is present in the anhydrite layers, rather than uniformly distributed through the Salado rock. Crank (1975) provides in his Figure 4.2 a graphical solution to the diffusion equation plotting $Q_t/1C_1$ as the ordinate versus Dt/l^2 as the abscissa. This figure is reproduced here as Figure C-4. Q_t is the quantity of sulfate diffusing in time t through a sheet of thickness l with one surface at concentration C_1 . Steady state is achieved when Dt/l^2 is 0.45 and conditions are not far from steady state when $Dt/l^2 > 0.3$. It should be noted that C_1 is the product of the concentration density of the diffusing species (kg/m^3) and the surface area for diffusion (m^2).

DIFFUSION IN A PLANE SHEET

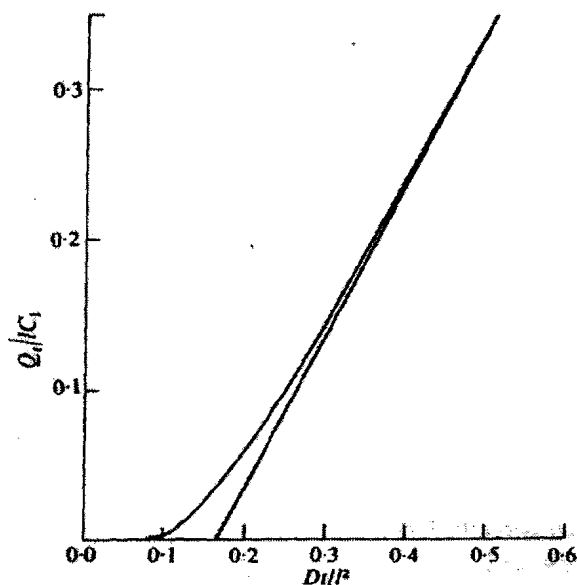


Figure C-4. Approach to steady-state flow through a plane sheet (Crank 1975, Figure 4.2)

If one assumes that l is 2.3 m (the distance from the top of Panels 1, 2, 7, 8, and 10 to the bottom of Anhydrite b), that D is $4.48 \times 10^{-12} \text{ m}^2/\text{sec}$, and that t is 10,000 years, then Dt/l^2 is 0.27. From Figure C-4 [Figure 4.2 in Crank (1975)], Q_t/IC_1 is about 0.11. If the panel footprint is $1.15 \times 10^4 \text{ m}^2$, and the sulfate concentration density is $4.72 \times 10^2 \text{ kg/m}^3$ [$2,970 \text{ kg/m}^3 \times 0.28 + 2,160 \text{ kg/m}^3 \times 0.72$] $\times 0.28$ weight fraction of anhydrite in mineral $\times 0.706$ molecular weight of SO_4 /molecular weight of CaSO_4), then Q_t , the amount of sulfate diffusing into a panel from Anhydrite b in 10,000 years, is $1.37 \times 10^6 \text{ kg}$ ($0.11 \times 4.72 \times 10^2 \text{ kg/m}^3 \times 1.15 \times 10^4 \text{ m}^2/\text{panel} \times 2.3 \text{ m}$). However, as described above, only $3.26 \times 10^5 \text{ kg}$ are available in this area of Anhydrite b to support diffusion, so all of the available sulfate could diffuse into the brine and support sulfate reduction.

Considering diffusion from MB-139 into these same panels, the bottom of the panels lies 1.4 m above MB-139. For this sulfate source, Dt/l^2 is 0.72. This value is outside the range included in Figure C-4 and, therefore, $Q_t/IC_1 > 0.35$. However, for long times, as t approaches infinity (e.g., 10,000 yr), $Q_t = DC_1/l \times (t - l^2/6D)$ (Crank 1975, Equation 4.25). For the five panels nearest to MB-139, the sulfate concentration density is 843 kg/m^3 [$2,970 \text{ kg/m}^3 \times 0.47 + 2,160 \text{ kg/m}^3 \times 0.53$] $\times 0.47$ weight fraction of anhydrite in mineral $\times 0.706$ molecular weight of SO_4 /molecular weight of CaSO_4) and $Q_t = 4.2 \times 10^6 \text{ kg}$. Since this is less than the total amount of sulfate underlying each of these five panels ($8.26 \times 10^6 \text{ kg}$), adequate sulfate is available to support the estimated quantity diffusing. Similarly, for diffusion from Anhydrite a into Panels 3, 4, 5, 6, and 9, where the bottom of Anhydrite a lies 2.2 m above the top of this group of panels, Dt/l^2 is 0.29 and Q_t/IC_1 is about 0.14. For Anhydrite a , the sulfate concentration density is $1,759 \text{ kg/m}^3$ [$2,970 \text{ kg/m}^3 \times 0.87 + 2,160 \text{ kg/m}^3 \times 0.13$] $\times 0.87$ weight fraction of anhydrite in mineral $\times 0.706$ molecular weight of SO_4 /molecular weight of CaSO_4). The amount of sulfate potentially diffusing into each of these five panels in 10,000 years is $6.23 \times 10^6 \text{ kg}$ ($0.14 \times 1.76 \times 10^3 \text{ kg/m}^3$

$\times 1.15 \times 10^4 \text{ m}^2 / \text{panel} \times 2.2 \text{ m}$). This quantity is greater than the total amount of sulfate in Anhydrite *a* overlying each of these panels ($4.44 \times 10^6 \text{ kg}$), so that all of the sulfate in that region could be consumed. The quantity of sulfate that could diffuse into these panels from Anhydrite *a* is sufficient to allow significant CPR degradation to occur via reaction (2).

MB-139 lies 3.8 m below the bottom of Panels 3, 4, 5, 6, and 9, so Dt/l^2 is 0.098 and Q_i/IC_1 is essentially zero. Thus, MB-139 would not be a significant source of sulfate for these panels.

It should also be noted that the DRZ is assumed to lie between MB-138 and MB-139, so that all of the projected sulfate diffusion would occur within disturbed rock.

C.6 CONSIDERATION OF REACTION RATES

An implicit assumption in the analysis in the preceding section (C.5) is that the rate of arrival of sulfate ions at reaction sites in the waste is adequate to support the rate of the sulfate reduction reaction (Equation 2). The validity of that assumption is examined here. Using the mean inundated reaction rate from the PABC of 2.94×10^{-10} mole C/kg cellulose/sec (Table C-1) and the total equivalent mass of cellulose of $3.26 \times 10^7 \text{ kg}$ (Table C-2), the rate of carbon release is 9.58×10^{-3} moles C/sec. Since each mole of cellulose contains 6 moles of carbon and, per Equation 2, each mole of cellulose requires three moles of sulfate to promote microbial degradation, 4.79×10^{-3} moles SO_4^{2-} /sec must arrive at the waste.

For the case of diffusion through a plane sheet described in Section C.5, the rate of arrival of sulfate per unit area is $-D(\partial C/\partial x)_{x=l}$ (Crank 1975, Section 4.3.3). For long times $C = C_1 - C_1 \times x/l$, and $(\partial C/\partial x)_{x=l} = C_1/l$, then the rate of sulfate arrival is $-DAC_1/l$ kg/sec where *A* is the surface area across which diffusion is occurring. For MB-139, $l = 1.4 \text{ m}$, $A = 1.15 \times 10^4 \text{ m}^2/\text{panel}$, and $C_1 = 843 \text{ kg SO}_4^{2-}/\text{m}^3$, the rate of sulfate arrival at a panel surface is $3.1 \times 10^{-5} \text{ kg/sec}$ ($4.48 \times 10^{-12} \text{ m}^2/\text{sec} \times 1.15 \times 10^4 \text{ m}^2/\text{panel} \times 843 \text{ kg SO}_4^{2-}/\text{m}^3/1.4 \text{ m}$). This is equivalent to 3.22×10^{-4} moles SO_4^{2-} /sec. For the entire repository the rate would be 3.22×10^{-3} moles SO_4^{2-} /sec. Thus the rate of sulfate arrival is about two-thirds of the rate needed to support the sulfate reduction reaction, if the mass of cellulose is assumed to remain constant.

However, as described in Section C.1, the mass of CPR or equivalent cellulose does not remain constant over the lifetime of the repository. From Figure C-2, it can be estimated that for the mean inundated reaction rate, the mass of CPR remaining after 10,000 years is $3.04 \times 10^6 \text{ kg}$ or $4.07 \times 10^6 \text{ kg}$ of cellulose equivalents. Thus, the average mass of cellulose equivalents over 10,000 years is $1.84 \times 10^7 \text{ kg}$ ($[3.26 \times 10^7 \text{ kg} + 4.07 \times 10^6 \text{ kg}]/2$). At the mean inundated reaction rate, the rate of carbon release for the repository is 5.41×10^{-3} moles C/sec (2.94×10^{-10} mole C/kg cellulose/sec $\times 1.84 \times 10^7 \text{ kg}$ cellulose equivalents). This would require that 2.70×10^{-3} moles SO_4^{2-} /sec arrive at the waste to support sulfate reduction of the cellulose. Since this value is less than the calculated rate of arrival (3.22×10^{-3} moles SO_4^{2-} /sec), diffusive transport should be sufficiently rapid to support the sulfate reduction reaction for the mean inundated reaction rate.

C.7 UNCERTAINTIES IN SULFATE DIFFUSIVITY

The preceding discussion used an adjusted value for diffusivity derived from the free liquid diffusion coefficient of sulfate in seawater ($D_0 = 9.84 \times 10^{-10} \text{ m}^2/\text{sec}$) (Kanney et al. 2004). Since the ionic strength of seawater is an order of magnitude lower than the ionic strength of the WIPP brines, diffusion of sulfate in seawater should be higher than diffusion in WIPP brines. Consequently, the free liquid diffusivity should represent a reasonable upper bound for possible values of diffusivity. Kanney et al. (2004) adjusted this measured value in seawater for the porosity and tortuosity (using a cementation factor) of the DRZ and obtained a value for D_{eff} of $4.48 \times 10^{-12} \text{ m}^2/\text{sec}$, which they used in their calculations and which was also used here.

Alternatively, one can assume that $D_{\text{eff}} \approx D_0 \Phi^2$ where D_0 is the free liquid diffusivity and Φ is the porosity (Kanney and Vugrin 2006). (Kanney et al. 2004 used a porosity of 0.05 which they described as the maximum allowable DRZ porosity (PHIMAX) in BRAGFLO.)

The DRZ initial porosity (Φ_0) is linked to the initial halite porosity (Φ_{OH}) by the equation:

$$\Phi_0 = \Phi_{\text{OH}} + 0.0029 \quad (\text{DOE 2004, Appendix PA, Equation 28}).$$

The initial halite porosity is assigned a cumulative distribution ranging from a low of 0.001 to a high of 0.03 with a median value of 0.01 and a mean value of 0.0128 (DOE 2004, Attachment PAR, Parameter 17). If one assumes that the minimum initial DRZ porosity provides a reasonable basis for estimating the lower bound for diffusivity, one would calculate a value of $1.44 \times 10^{-14} \text{ m}^2/\text{sec}$ ($[0.001 + 0.0029]^2 \times 9.48 \times 10^{-10}$). For this diffusivity, the characteristic diffusion length, L_{diff} , at $t = 10,000 \text{ yr}$, is 0.13 m, indicating that virtually no diffusion of sulfate occurs in 10,000 years, assuming a uniform distribution of sulfate in the rock. In such circumstances, methanogenesis would become the dominant biodegradation reaction.

C.8 STATE OF MOISTURE IN REPOSITORY

Microbial degradation can occur under both humid and inundated conditions in the repository waste disposal rooms. In PA modeling, the relative contributions between the two processes are defined by the following equation:

$$Q_{\text{rgm}} = (R_{\text{mi}} \times S_{\text{b,eff}} + R_{\text{mh}} \times S_{\text{g}}^*) \times K \quad (4)$$

where Q_{rgm} is the rate of microbial gas generation, R_{mi} is the inundated degradation rate, $S_{\text{b,eff}}$ is the effective brine saturation, R_{mh} is the humid degradation rate, S_{g}^* is a factor related to $S_{\text{b,eff}}$, and K is a conversion factor (DOE 2004, Appendix PA, PA-4.2.5). The effective brine saturation takes into account not only the actual brine saturation, S_{b} , but also the fact that some wicking of brine into the waste can occur, causing more of the waste to be subject to inundated conditions. When $S_{\text{b,eff}} = 0$, then $S_{\text{g}}^* = 0$; when $S_{\text{b,eff}} > 0$, then $S_{\text{g}}^* = 1 - S_{\text{b,eff}}$. Thus when no brine is present, no microbial degradation occurs, when some brine is present both humid and inundated degradation occur, and when the effective brine saturation is one, only inundated microbial degradation occurs.

The wicking saturation, S_w , is a sampled parameter varying uniformly from zero to one. The effective brine saturation is defined by the equations:

$$\begin{aligned} S_{b,\text{eff}} &= S_b + S_w \text{ for cases where } 0 < S_b < 1 - S_w \\ S_{b,\text{eff}} &= 0 \text{ when } S_b = 0 \\ S_{b,\text{eff}} &= 1 \text{ if } S_b > 1 - S_w. \end{aligned}$$

Therefore, wicking can, in some PA realizations, cause the effective brine saturation to be unity even though the actual brine saturation is low.

For the undisturbed repository, brine saturation increases very rapidly in the first few hundred years as brine flows in from the DRZ. This is promoted by a large pressure differential between the DRZ and the disposal rooms and initial high permeability in the DRZ. The brine inflow slows as pressures equalize and healing of the DRZ progresses. Anoxic corrosion may then consume water at a rate faster than the rate of inflow. Higher gas pressures in some PA scenarios may eventually drive brine out of the waste areas. Over time, the brine saturation in most scenarios declines after the initial peak. For the PABC, the maximum, average, and minimum values of brine saturation for the undisturbed repository are 0.959, 8.13×10^{-2} , and 1.01×10^{-6} , respectively (Nemer and Stein 2005). In only one vector of replicate R1 for the PABC does the brine saturation approach unity in the undisturbed repository (Nemer and Stein 2005, Figure 6-6a). In contrast, for the disturbed case scenario S2 (a drilling intrusion at 350 years which hits Castile brine), the average saturation for the R1 replicate of 100 realizations is 0.800 (Nemer and Stein 2005, Table 6-14). Thus for S2 scenarios, adequate brine should be available to support diffusive transport from the panel walls to the waste for most intrusion scenarios.

However, other factors may mitigate against extensive CPR degradation. For many PA realizations in the PABC, the cellulose or CPR are not fully consumed even for intrusion scenarios (S2) where a borehole encounters a Castile brine reservoir. Figure 6-49a of Nemer and Stein (2005) shows that some cellulose or CPR remain in 95 of 100 scenarios. Factors such as high iron corrosion, low wicking saturation, and only a 25% probability that microbial degradation of plastics and rubber will occur contribute to reduced biodegradation.

In summary, it is possible that in situations where humid degradation dominates (e.g., in some undisturbed repository scenarios), available sulfate may be limited to that in the waste since adequate brine may not be available to support advective and diffusive transport mechanisms to provide significant additional sulfate. Consequently, microbial degradation would occur by methanogenesis in such situations once the nitrate and sulfate in the waste are consumed. In the disturbed case scenarios, significantly more brine is generally available and sulfate transport by diffusion and advection can probably supply sufficient sulfate to support the sulfate reduction reaction for most PA realizations.

C.9 SUMMARY

Sulfate requirements to support biodegradation and sulfate availability to the waste are summarized in Table C-6. Data are presented based on five-panel groupings because the

different elevations of Panels 1, 2, 7, 8, and 10 compared to Panels 3, 4, 5, 6, and 9 create significantly different sulfate sources. Assuming that the sulfate is concentrated in anhydrite-rich layers rather than being uniformly distributed, there is adequate sulfate available to consume 87% of the CPR emplaced in each of the panels by the sulfate reduction reaction. The assumption that sulfate is concentrated in anhydrite beds is supported by the available characterization of the local stratigraphy (Stein 1985).

This amount of sulfate (5.08×10^6 kg) is sufficient to consume all of the cellulose, all of the rubber, and 80% of the plastics. Since the current baseline performance assessment assumes that degradation of plastics and rubber occurs in only 25% of the realizations, the impact of this sulfate deficit on PA should be minimal. Furthermore, if the exponential reduction of CPR in each panel is considered in the evaluation, sufficient sulfate is available for degradation of CPR at the mean rate for all panels (Table C-6).

These analyses assume that sufficient brine is available to transport the sulfate to the waste and the diffusivity of the sulfate in the Salado rocks is $\geq 4.48 \times 10^{-12}$ m²/sec.

Table C-6. Sulfate Mass Balance to Support Biodegradation In A Repository Panel

Sulfate Sources and Requirements	Sulfate Required (kg)	Sulfate Available for Panels 1, 2, 7, 8 and 10 (kg)	Sulfate Available for Panels 3, 4, 5, 6, and 9 (kg)
Mass of sulfate required for all CPR in each panel	5.82×10^6		
Mass of sulfate required at mean inundated biodegradation rate with exponential reduction in cellulose for each panel	3.72×10^6		
Mass of sulfate in waste		4.43×10^{4a}	4.43×10^{4a}
Mass of sulfate advected into waste (Table C-4)		5.21×10^5	5.21×10^5
Mass of sulfate diffusing from Anhydrite <i>b</i> in panel side walls			$8.21 \times 10^4^b$
Mass of sulfate diffusing from Salado rock assuming uniform distribution		$\{2.67 \times 10^6\}^c$	$\{2.67 \times 10^6\}^c$
Mass of sulfate diffusing from Anhydrite <i>b</i> assuming non-uniform distribution		3.26×10^{5c}	
Mass of sulfate diffusing from Anhydrite <i>a</i> assuming non-uniform distribution			4.44×10^{6d}
Mass of sulfate diffusing from MB-139 assuming non-uniform distribution		4.20×10^6	0
Total mass of sulfate available assuming non-uniform distribution		5.09×10^6	5.08×10^6

a – Leigh et al. 2005b, Section 4.5.2

b – For Panels 3, 4, 5, 6, and 9 only

c – For Panels 1, 2, 7, 8, and 10 only, limited by available mass in Anhydrite *b*.

d – For Panels 3, 4, 5, 6, and 9 only, limited by available mass in Anhydrite *a*

e – Not included in total mass

C.10 REFERENCES

Brush, L.H. 2004. *Implications of New (Post-CCA) Information for the Probability of Significant Microbial Activity in the WIPP*. Sandia National Laboratories, Carlsbad, New Mexico. ERMS 536205.

Brush, L.H., Y. Xiong, J.W. Garner, A. Ismail, and G.T. Roselle. 2006. *Consumption of Carbon Dioxide by Precipitation of Carbonate Minerals Resulting from Dissolution of Sulfate Minerals in the Salado Formation in Response to Microbial Sulfate Reduction in the WIPP*. Sandia National Laboratories, Carlsbad, New Mexico.

Christian-Frear, T.L. and S.W. Webb. 1996. *Effect of Explicit Representation of Detailed Stratigraphy on Brine and Gas Flow at the Waste Isolation Pilot Plant*. SAND94-3173. Sandia National Laboratories. April 1996.

Clayton, D. 2006. *Update of the Minimum Brine Volume for a Direct Brine Release and New Maximum Castile and Salado Brine Volumes in a Waste Panel*. Memorandum to L.H. Brush, Sandia National Laboratories, Carlsbad, New Mexico, October 11, 2006, ERMS 544453.

Clayton, D. and M. Nemer. 2006. *Normalized Moles of Castile Sulfate Entering the Repository and Fraction of MgO Lost Due to Brine Flow Out of the Repository*. Memorandum to E.D. Vugrin, Sandia National Laboratories, Carlsbad, New Mexico, October 9, 2006.

Crank, J. 1975. *The Mathematics of Diffusion*. 2nd Edition. Clarendon Press, Oxford.

DOE (U.S. Department of Energy). 2004. *Title 40 CFR 191 Parts B and C Compliance Recertification Application*, U.S. Department of Energy Field Office, March 2004. Docket A-98-49 Category II-B2.

Francis, A.J., M.R. Gillow, and M.R. Giles. 1997. *Microbial Gas Generation Under Expected Waste Isolation Pilot Plant Repository Conditions*. SAND96-2582. Sandia National Laboratories, Albuquerque, New Mexico. ERMS 244883.

Kanney, J.F. and E.D. Vugrin. 2006. *Updated Analysis of Characteristic Time and Length Scales for Mixing Processes in the WIPP Repository to Reflect the CRA-2004 PABC Technical Baseline and the Impact of Supercompacted Mixed Waste and Heterogeneous Waste Emplacement*. Memorandum to D.S. Kessel, Sandia National Laboratories, Carlsbad, New Mexico, August 31, 2006.

Kanney, J.F., A.C. Snider, T.W. Thompson, and L.H. Brush. 2004. *Effect of Naturally Occurring Sulfate on the MgO Safety Factor in the Presence of Supercompacted Waste and Heterogeneous Waste Emplacement*. Sandia National Laboratories, Carlsbad Programs Group, Carlsbad, New Mexico. March 5, 2004.

Leigh, C., J. Kanney, L. Brush, J. Garner, R. Kirkes, T. Lowry, M. Nemer, J. Stein, E. Vugrin, S. Wagner, and T. Kirchner. 2005a. *2004 Compliance Recertification Application Performance Assessment Baseline Calculation*. Sandia National Laboratories, Carlsbad, New Mexico, ERMS 541521.

Leigh, C., J. Trone, and B. Fox. 2005b. *TRU Waste Inventory for the 2004 Compliance Recertification Application Performance Assessment Baseline Calculation*. Sandia National Laboratories, Carlsbad, New Mexico, ERMS 541118.

Nemer, M. and J. Stein. 2005. *Analysis Package for BRAGFLO: 2004 Compliance Recertification Application Performance Assessment Baseline Calculation*. Sandia National Laboratories, Carlsbad, New Mexico, ERMS 540527.

Nemer, M., J. Stein, and W. Zelinski. 2005. *Analysis Report for BRAGFLO, Preliminary Modeling Based Upon Recent Experimental Results*. Sandia National Laboratories. ERMS 539437.

Stein, C.S. 1985. *Mineralogy in the Waste Isolation Pilot Plant (WIPP) Facility Stratigraphic Horizon*. SAND-85-0321, Sandia National Laboratories, Albuquerque, New Mexico, September 1985.

Stein, J. and W. Zelinski. 2003. *Analysis Plan for the Testing of a Proposed BRAGFLO Grid to be used for the Compliance Recertification Application Performance Assessment Calculations, AP-106*. Carlsbad, New Mexico: Sandia National Laboratories. ERMS 525236.

Thompson, B. 2004. *Changes to the Underground Facility*. Presentation to EPA, Washington DC, April 20, 2004. WRES-Golder Associates Inc.

Wang, Y. and LH. Brush. 1996. *Estimates of Gas-Generation Parameters for the Long-Term WIPP Performance Assessment*. Unpublished memorandum to M.S. Tierney, Sandia National Laboratories, Albuquerque, New Mexico, January 26, 1996, WPO 31943. ERMS 231943

Cooper, Andrea

From: Cooper, Andrea on behalf of Moody, Dave C. - DOE
Sent: Tuesday, February 03, 2009 4:31 PM
To: Daub, Vernon - DOE; Nelson, Roger - DOE; Gadbury, Casey - DOE; Galbraith, Don - DOE; Welton, Art; Holland, Ava; Scott, Gary - DOE
Subject: FW: Chemistry Conceptual Models Report & Correspondence
Attachments: Chemistry Letter FINAL 2309.pdf; FinalReport-Chem Concept Model-WA 4-02.pdf



Chemistry FinalReport-C
r FINAL 2309; Concept Moc

-----Original Message-----

From: Lee.Raymond@epamail.epa.gov [mailto:Lee.Raymond@epamail.epa.gov]
Sent: Tuesday, February 03, 2009 3:17 PM
To: Moody, Dave C. - DOE; Marcinowski, Frank; Harris, Alton; Patterson, Russ - DOE; Basabilvazo, George - DOE; Zappe, Steve
Cc: Edwards.Jonathan@epamail.epa.gov; Peake.Tom@epamail.epa.gov; Byrum.Charles@epamail.epa.gov; Eagle.Mike@epamail.epa.gov; Joglekar, Rajani; Feltcorn, Ed; Bender.Lindsey@epamail.epa.gov; Ghose.Shankar@epamail.epa.gov; Stone, Nick; Puskin.Jerome@epamail.epa.gov
Subject: Chemistry Conceptual Models Report & Correspondence

Hello,

Attached you will find a letter transmitting EPA's report entitled, "Verification of the Waste Isolation Pilot Plant Chemistry Conceptual Models." Should you have any problems opening the .pdf, please let me know.

Sincerely,

Ray Lee
Radiation Protection Division
Center for Radiation Information & Outreach
(202) 343-9463

(See attached file: Chemistry Letter FINAL 2309.pdf) (See attached file: FinalReport-Chem Concept Model-WA 4-02.pdf)

MAIL ROOM COPY

Cooper, Andrea

From: Lee.Raymond@epamail.epa.gov
Sent: Tuesday, February 03, 2009 3:17 PM
To: Moody, Dave C. - DOE; Marcinowski, Frank; Harris, Alton; Patterson, Russ - DOE; Basabilvazo, George - DOE; Zappe, Steve
Cc: Edwards.Jonathan@epamail.epa.gov; Peake.Tom@epamail.epa.gov; Byrum.Charles@epamail.epa.gov; Eagle.Mike@epamail.epa.gov; Joglekar, Rajani; Feltcorn, Ed; Bender.Lindsey@epamail.epa.gov; Ghose.Shankar@epamail.epa.gov; Stone, Nick; Puskin.Jerome@epamail.epa.gov
Subject: Chemistry Conceptual Models Report & Correspondence
Attachments: Chemistry Letter FINAL 2309.pdf; FinalReport-Chem Concept Model-WA 4-02.pdf



Chemistry FinalReport-C
r FINAL 2309; Concept Moc

Hello,

Attached you will find a letter transmitting EPA's report entitled, "Verification of the Waste Isolation Pilot Plant Chemistry Conceptual Models." Should you have any problems opening the .pdf, please let me know.

Sincerely,

Ray Lee
Radiation Protection Division
Center for Radiation Information & Outreach
(202) 343-9463

(See attached file: Chemistry Letter FINAL 2309.pdf) (See attached
file: FinalReport-Chem Concept Model-WA 4-02.pdf)